CHARACTERIZING THE FUNCTION OF GAS1 IN MUSCLE STEM CELLS AGING

by

Liangji Li

A dissertation submitted to The Johns Hopkins University in conformity with the requirements for the degree of Doctor of Philosophy

Baltimore, Maryland

August, 2019

ABSTRACT

Muscle undergoes progressive weakening and regenerative dysfunction with age due in part to the functional decline of skeletal muscle stem cells (MuSCs). MuSCs are heterogeneous but whether their gene expression changes with age and the implication of such changes are unclear. Here I show that in mice, the membrane protein Growth arrest-specific gene 1 (Gas1) is expressed in a small subset of young MuSCs with its expression progressively increasing in larger fractions of MuSCs later in life. I present genetic evidence that Gas1 reduces the quiescence and self-renewal capacity of MuSCs, via over-expression of Gas1 in young MuSCs and inactivation of Gas1 in aged MuSCs. I further show that Gas1 reduces Ret signaling, which is required for MuSC quiescence and self-renewal. I demonstrate that the Ret ligand, Glial Cell-Derived Neurotrophic Factor (GDNF), can counteract Gas1 by stimulating Ret signaling and enhancing MuSC self-renewal and regeneration, thus improving muscle function. I propose that strategies aimed to target this pathway can be exploited to improve the regenerative decline of muscle stem cells.

Primary Reader and Advisor: Chen-Ming Fan, Ph.D.

Second Reader: Yixian Zheng, Ph.D.

Committee Members: Allan C. Spradling, Ph.D.

Mark B. Lewandoski, Ph.D.

ACKNOWLEDGEMENTS

First and foremost, I would like to thank my advisor Dr. Chen-Ming Fan. Through his cordial mentoring and guidance, I have learned tremendously during my graduate work. I learnt how to ask the right scientific questions, how to address questions by designing correct experiments and how to face difficulties and cope with them. I am truly grateful to Fan for letting me take an adventurous research direction for my dissertation work, and will always be inspired by his meticulous and enthusiastic scientific attitudes.

Next, I would like to thank my thesis committee, Allan Spradling, Yixian Zheng and Mark Lewandoski for their insightful advice over the years and selflessness for donating their time to assist my graduate career. I also thank numerous other professors in the Johns Hopkins Biology Department and Carnegie Institution: Steven Farber, Marnie Halpern, Alex Bortvin, Rejji Kuruvilla, Xin Chen, and Haiqing Zhao. They not only gave me great lectures on various courses, but also provided valuable advice generously. And I thank our collaborators: Jordan Kreidberg at Harvard University and Florian Bentzinger at University of Sherbrooke.

Furthermore, I would like to thank the members of in Fan lab from past to present including: David Martinelli, Christoph Lepper, Michelle Rozo, Lydia Li, Tyler Harvey and Yun Bai. I also thank other colleagues and staffs working in the Johns Hopkins Biology Department and Carnegie Institution: Eugenia Dikovsky, Sibiao Yue, Xiaobin Zheng, Frederick Tan, and Joan Miller.

Finally, I would like to thank my parents for their endless care, love and supports during my time in graduate school even though I was thousands miles away from home.

TABLE OF CONTENTS

ABSTRACT ii

ACKNOWLEDGMENTS iii

TABLE OF CONTENTS iv

INDEX OF FIGURES vi

CHAPTER 1: Introduction 1

CHAPTER 2: Characterizing Gas1's Function in Muscle Stem Cell Aging 10

INTRODUCTION 11

RESULTS 14

DISCUSSION 42

MATERIALS AND METHODS 45

CHAPTER 3: Cellular/Molecular Mechanism of Gas1 in Muscle Stem Cell Aging 50

INTRODUCTION 51

RESULTS 52

DISCUSSION 66

MATERIALS AND METHODS 69

CHAPTER 4: Ret-GDNF Signaling in Muscle Stem Cell Aging 73

INTRODUCTION 74

RESULTS 76

DISCUSSION 102

MATERIALS AND METHODS 104

CHAPTER 5: Targeting β1-integrin signaling enhances regeneration in aged and dystrophic muscle in mice 111

INTRODUCTION 112

RESULTS 114

DISCUSSION.....131
MATERIALS AND METHODS 133
REFERENCES.....138
CURRICULUM VITAE.....154

INDEX OF FIGURES

Figure 2.1. Single-cell RNA-seq of young and aged MuSCs. 14

Figure 2.2. Single-Cell RNA-seq reveals changes in heterogeneity of MuSCs during aging. 17

Figure 2.3. Single-Cell RNA-Seq reveals up-regulated genes cohorts in aged MuSCs. 20

Figure 2.4. Gas1 is expressed in wild type adult MuSCs. 22

Figure 2.5. Gas1 expression does not match MuSCs quiescence establishment. 24

Figure 2.6. Gas1 is expressed heterogeneously in young MuSCs. 26

Figure 2.7. Pan-expression of Gas1 in young MuSCs impairs regeneration.....29

Figure 2.8. Pan-expression of Gas1 triggers young MuSCs activation and differentiation.....32

Figure 2.9. Inactivation of Gas1 improves aged MuSCs.....36

Figure 2.10. Gas1-expression negatively impacts MuSC renewal and regenerative muscle function. 40

Figure 3.1. Isolating MuSCs based on 4 surface marker and Pax7 (YFP). 53

Figure 3.2. RNA-sequencing of Yng Ctrl and Aged Ctrl MuSCs. 55

Figure 3.3. ChIP-sequencing of Yng Ctrl and Aged Ctrl MuSCs. 58

Figure 3.4. Gas1 mouse models display age-associated molecular signatures of MuSCs. 60

Figure 3.5. Single cell RNA-seq from young and aged MuSCs revealed Gas1 is associated with stress-genes. 64

Figure 4.1. Ret is downstream of Gas1. 76

Figure 4.2. Ret is required for MuSC self-renewal. 81

Figure 4.3. Ret is activated in young MuSCs and its signaling is dampened in aged

MuSCs. 83
Figure 4.4. Gas1 binds Ret and inhibits its signaling. 86
Figure 4.5. GDNF can improve MuSCs self-renewal 88
Figure 4.6. GDNF enhances muscle regeneration in Yng Gas1EX mice....91
Figure 4.7. GDNF does not alter MuSCs self-renewal and muscle regeneration in young RetKO Mice 93
Figure 4.8. GDNF enhances MuSCs self-renewal and muscle regeneration in aged Mice 95
Figure 4.9. Dysregulated p-p38 signaling is correlated to the defects in young Gas1EX MuSCs 98
Figure 4.10. GDNF could rescue the dysregulated p-p38 signaling in Aged Ctrl and Yng Gas1EX MuSCs....101
Figure 5.1. *Itgb1*$^{-/-}$ cells show defective expression of polarity marker Par3 115
Figure 5.2. *Itgb1*$^{-/-}$ MuSCs show a compromised response to FGF-2 that can be partially restored by exogenous FGF-2 117
Figure 5.3. Distribution of β1-integrin in aged and dystrophic MuSCs....120
Figure 5.4. TS2/16 and FGF-2 increase the fraction of aged MuSCs displaying polarized pp38....123
Figure 5.5. Activating β1-integrin in aged MuSCs enhances FGF signaling to promote MuSC expansion 125
Figure 5.6. Activating β1-integrin in mdx mice ameliorates dystrophic pathology and restores muscle strength 128

Chapter 1

Introduction

Muscle stem cell and skeletal muscle regeneration

Skeletal muscle is the most abundant tissue of the body, generating forces required for daily locomotion and other physical activities including interactions with the environment. The striated muscle tissue is composed of multinucleated muscle fibers. Under normal conditions, adult mammalian skeletal muscle is maintained at a stable status, whereas upon damages induced by injury or degenerative diseases such as muscular dystrophy, it possesses potent regenerative ability to repair damaged muscles (Carlson, 1973). This capacity for regeneration depends on the myogenic stem cells to be activated and differentiate into new myofibers (Bentzinger et al., 2012). The myogenic muscle stem cells are also called 'satellite cells' for their anatomical location: they are mononuclear cells adjacent to basal lamina that surrounds the muscle fibers (Mauro, 1961). They are thought to be the major contributors to the postnatal growth as well as regeneration of skeletal muscle after damage. Muscle stem cells are present in healthy adult mammalian skeletal muscle tissues in a quiescent state. The quiescence could be switched to an activated status by muscle injury, in which the muscle stem cells undergo transient amplification and generate substantial amounts of new myofibers within a short period of times (Whalen et al., 1990).

Mouse muscle stem cells in quiescent states are mainly marked by transcription factor paired box 7 (Pax7) (Zammit et al., 2006, Lepper et al., 2009). Many other marker have also been identified, such as Vcam-1, syndecan-4, and α7 integrin (Rosen et al., 1992; Cornelison et al., 2001; Blanco-Bose et al., 2001). Some of the identified surface markers are particularly useful for isolating muscle stem cell by fluorescence activated cell sorting (FACS). Usually a combination of different makers are used aiming for obtaining pure muscle stem cells. As alternative options, mice expressing fluorescent reporters specifically in muscle stem cells are also commonly

used, such as mice expressing a GFP reporter driven by Pax7-Cre or expressing ZsGreen under the control of Pax7 regulatory elements (Bosnakovski et al., 2008).

Reacting to the muscle injury, muscle stem cells become activated and trigger myogenic program to expand and differentiate (Dhawan et al., 2005). The myogenic program is coordinated by critical transcription factors that direct the changes of cellular states from activation and proliferation to differentiation and self-renewal of muscle stem cells (Yin et al., 2013). These activated muscle stem cells are also referred to as myoblasts. After activation, the myoblasts first down-regulate the expression of Pax7. Myogenic regulatory factor 5 (Myf5) and myogenic differentiation 1 (MyoD) mainly control the advancement of activated myoblast toward differentiation, followed by subsequent myogenic programs including fusion of the differentiated myoblasts to form regenerated muscle fibers. It has been suggested that a proportion of $Pax7^{+}/MyoD^{+}$ proliferating cells are able to return to a $Pax7^{+}/MyoD^{-}$ status and return to quiescence after the cessation of regeneration. These cells are considered to be the self-renewed population.

Stem cell aging

Adult stem cells are crucial for maintaining tissue homeostasis and responsible for repair in response to tissue damage. Under normal conditions, the adult stem cells are maintained at a stable status, relying on their self-renewal capacity to replenish the stem cell pool. However, they are not able to sustain full fitness and function endlessly. Their role for tissue repair declines during the progression of aging. Age-related alterations that impact adult stem cells are multilayered and the exhaustion of stem cells is a comprehensive outcome of various sources of aging-associated damages, ranging from systemic to cell intrinsic factors (Jung et al., 2014).

Corresponding to the tissues they are located, adult stem cells have different properties. Nonetheless, they also share some basic attributes. For instance, they can exist in quiescent or activated state, undergo symmetric as well as asymmetric cell division, and can be greatly influenced by their local microenvironment. These common features change during aging along with the tissues they reside in, which give rise to defective outcomes for the stem cell per se as well as for the long-term tissue homeostasis (Oh et al., 2014).

For skeletal muscle, the regeneration capacity is also reduced in aged animals, mainly as a result of the dysfunction of muscle stem cells (Chakkalakal et al., 2012; Sousa-Victor et al., 2014). In aged muscle, the muscle stem cells number is declined, with accompanying functional defects, including inability for proper activation and proliferation, and aberrant lineage commitment. Healthy adult stem cell function requires appropriate extrinsic signals from the systemic factors and microenvironment (i.e. stem cell niche). This proposition holds true for muscle stem cells. Parabiosis assay demonstrates that muscle repair is regulated by the soluble factors in the serum (Conboy et al., 2005). Based on this, changes in the circulating factors were thought to be the main cause for muscle stem cells becoming defective in repair during aging. In addition, it has been reported that, during aging, niche compositions are altered and unable to provide appropriate supports for muscle stem cell function, thus causing inferior regeneration (Rozo et al., 2016; Lukjanenko et al., 2016). On the other hand, inflammatory response, which increases in the aging circulation, also has negative influence on muscle stem cell functions (Smythe et al., 2008; Shavlakadze et al., 2010). However, more recent studies utilizing transplantation of purified aged muscle stem cells into young muscles reveals that cell-intrinsic factors also contribute to their dysfunctions in the process of aging, which are not be reversed by placing them in the

young tissue environment (Bernet et al., 2014, Cosgrove et al., 2014).

Muscle stem cell heterogeneity

Muscle stem cells were thought to be a homogenous cell population comprised of uniform myogenic progenitors. However, more and more data suggest that muscle stem cells bear diverse properties in nature in terms of gene expression, myogenic propensity, and stem cell function. For gene expression, muscle stem cells were known to express Pax7. Yet, through experiments using Pax3-LacZ reporter mice, Buckingham's group first noticed that some muscle stem cells express Pax3, a transcriptional regulator and a paralog to Pax7, and they were limited to a subset of muscle groups, including the diaphragm, most trunk muscles, and selective limb muscles (Montarras et al., 2005). In addition, Zammit's group reported that CD34, an established marker of hematopoietic stem cells, and Myf5, the earliest marker of myogenic commitment, could be used as markers for muscle stem cells. However, via β-Gal reporter assay, they found that these two proteins are not expressed by a subpopulation of muscle stem cells (Beauchamp et al., 2000). The single cell transplantation study reported by Blau's group has investigated the expression of Pax7, Pax3, Myf5, and MyoD in 40 single muscle stem cells. They observed that these cells all express Pax7 and Myf5, but varied in the expression of Pax3 and MyoD (Sacco et al., 2008).

The gene expression diversity within a cell group may result in functional differences. Muscle stem cells from different sources or have different gene expression have also been reported to have different myogenic potentials. Morgan's group performed transplantation experiments using muscle stem cells isolated from different skeletal muscle sources (Collins et al., 2005), and found that the regenerated fibers

formed by tibialis anterior (TA) myofiber grafts were significantly fewer than those originated from extensor digitorum longus (EDL) or soleus muscle. These findings imply that there exist inherent variations in proliferation and differentiation propensity of muscle stem cell populations in different muscle types. Moreover, using Pax7-nGFP transgenic mice, Tajbakhsh's group observed that muscle stem cells expressing the highest levels of nGFP (by inference, the highest levels of Pax7 or Pax7-high) are less primed for differentiation and have a lower metabolic activity compared to those expressing the lowest levels of nGFP (i.e. the lowest level of Pax7, Pax7-low) (Rocheteau et al., 2012). They showed that Pax7-high cells represent a reversible dormant stem cell state resembling a quiescent status, and generating distinct daughter cell fates by asymmetrically segregating template DNA strands when activated, thus implied that a small subpopulation of muscle stem cells are the true stem cells, differed from the more committed myogenic progenitor subpopulations.

Although the aforementioned lines of evidence illustrate that muscle stem cells represent a heterogeneous population, many questions remain to be solved. For example, even though different markers could separate the muscle stem cells into subpopulations, it is still not fully understood what their complete gene expression differences are, what controls their differential gene expression, and of those differences, what underlies their function differences in muscle regeneration. Further investigation to reveal molecular and functional differences of a specific subpopulation should shed light on the mechanisms underlying the origin and transition between various muscle stem cell subpopulations. It will be also interesting to explore the changes of muscle stem cell heterogeneity during different biological processes or under different environmental influences, including diseases and aging.

The Gas1 gene

Growth arrest-specific gene 1 (Gas1) is a glycosylphosphatidylinositol (GPI)-anchored protein and was first discovered to be up-regulated in NIH3T3 mouse fibroblast cell line that was blocked at G0 stage of the cell cycle via serum starvation (Schneider et al., 1988). Expression of Gas1 is sufficient to arrest NIH3T3 at G0, and this function of Gas1 has been reported to be dependent on the tumor suppressor gene p53 (Ruaro et al., 1997). Based on these findings, it has been proposed that Gas1 plays a role in tumor suppression. In line with this, Segovia's group showed that expression of Gas1 decreased glia proliferation and induced apoptosis in C6 glioma cell line by inducing protease Caspase 3 activity (Zamorano et al., 2003). Furthermore, Green's group reported that, from a genome-wide shRNA screening, Gas1 was identified as a novel melanoma metastasis suppressor gene that promotes apoptosis (Gobeil et al., 2008). Nonetheless, its role as a tumor suppressor needs to be further substantiated in vivo, given that Gas1 germline knockout mice do not give rise to overall increased cell division or show increased tumor formation (Seppala et al., 2007). Moreover, it has been report that Gas1 can have reverse effects: ectopic expression of Gas1 in endothelial or HEK293 cells leads to reduced apoptosis without impact on cell proliferation (Spagnuolo et al., 2004). In addition to the presumed anti-tumor activity, it is also shown that Gas1 is structurally homologous to glial cell-derived neurotrophic factor (GDNF) family receptor α (GFRα) and it can alter downstream signaling effectors of GDNF via interactions with the receptor tyrosine kinase (RTK) Ret (Cabrera et al., 2006). These data suggests that Gas1 is a multi-functional protein in vitro and its function varies in different cellular contexts.

The multi-functional nature of Gas1 has been demonstrated in different tissues and cell types in vivo. For instance, it's been reported by our lab that interaction

between Gas1 and sonic hedgehog (Shh) promotes the signaling activity of this pathway during embryogenesis (Martinelli et al., 2007a). Our lab showed that Gas1 positively regulates Shh signaling by binding directly to Shh, indicating that Gas1 is part of the Shh reception machinery. Importantly, Gas1 deficient mice exhibit phenotypes resembling those in Shh deficient mice. Another example of Gas1 regulating Shh signaling is the enteric neuron axons. Our lab reported that the exclusion of enteric central projections towards the gut epithelium by Shh depends on its binding to Gas1 (Jin et al., 2015). In other tissues, Gas1 appears to play a role in regulating FGF signaling. Our collaborator Kreidberg showed that transcription factor Wilms' tumor suppressor 1 (WT1) modulates FGF signaling in the developing kidney by activating Gas1 (Kann et al., 2015). Loss of function of Gas1 leads to hypoplastic kidneys with reduced nephron mass due to premature depletion of nephron progenitor cells, correlating with a phenotype caused by reduced FGF signaling. In addition, our lab also showed that, in the developing limb, Gas1 is required in the mesenchyme to maintain the regulatory loop between Fgf10 in the mesenchyme and Fgf8 in the apical ectodermal ridge, which is essential to drive limb outgrowth (Liu et al., 2002). Taken together, these data indicate that Gas1 has various functions and its diverse roles are cell-type specific.

Overview of thesis research

My thesis work primarily focuses on the role of Gas1 in muscle stem cells. I show that Gas1 is expressed in a small fraction of young muscle stem cells, and gradually becomes expressed in most of these cells in aged mice. The young Gas1-expressing muscle stem cells share cellular and molecular properties with aged ones (Chapter 2). Pan-expression of Gas1 in young muscle stem cells in vivo reduces

regenerative function and increases expression of aging hallmark genes (Chapter 3). By contrast, inactivation of Gas1 in aged muscle stem cells rejuvenates regeneration and gene expression profile. These complementary results support that Gas1 is a molecular determinant for muscle stem cells aging. Furthermore, I define two mechanisms by which Gas1 directs muscle stem cells aging via reducing the activity of Ret, a receptor tyrosine kinase needed for robust renewal of muscle stem cells (Chapter 4). I also uncover a competitive antagonism between Gas1 and the Ret-ligand, GDNF, which tunes Ret activity in the muscle stem cells. By exploiting this antagonism, I show that GDNF can boost Ret activity, enhance stem cells renewal, and strengthen the function of the regenerated muscle in aged mice. Together, I provide evidence that Gas1 regulates aging, and suggest that the temporal increase of Gas1-expressing muscle stem cells, from heterogeneous to homogeneous, drives the muscle stem cell populations into a repressed state of Ret signaling and dysfunction.

In addition to my study about Gas1 in MuSCs aging, I also described my work as a co-author of a published paper demonstrating how β1-integrin acts as a muscle stem cell niche sensor and how it regulates MuSCs functions in the context of aging and musclular dystrophy (Chapter 5).

CHAPTER 2

Characterizing Gas1's Function in Muscle Stem Cell Aging

INTRODUCTION

Muscle stem cells/satellite cells (MuSCs) are essential for the growth, maintenance, and repair of skeletal muscle (Tedesco et al., 2010; Yin et al., 2013). Cell-lineage tracing in adult mice thus far has identified two stem/progenitor cell origins marked by the expression of Pax7 and Twist2 (Lepper et al., 2009; Liu et al., 2017). They likely arise from different developmental origins, and they occupy distinct compartments in the adult skeletal muscle: $Pax7^+$ cells are the classical satellite cells located in the sublaminal niche attached to the muscle fiber (Mauro, 1961), whereas $Twist2^+$ cells reside in the interstitial space between muscle fibers. Cell ablation studies conclude that the $Pax7^+$ population is indispensable for general muscle regeneration (Lepper et al., 2011; Murphy et al., 2011; McCarthy et al., 2011; Sambasivan et al., 2011). On the other hand, the $Twist2^+$-lineage contributes exclusively to type IIb/x myofibers (Liu et al., 2017). Heterogeneous composition of adult MuSCs/muscle progenitors has also been characterized by various combinations of surface markers (Sherwood et al., 2004; Gilbert et al., 2010; Cheung et al., 2012), and those with different marker combinations display different myogenic properties in vitro (Sherwood et al., 2004). In addition, MuSCs expressing high versus low levels of a Pax7 reporter (Pax7:nGFP) are functionally distinct (Rocheteau et al., 2012). These heterogeneous features of MuSCs in juvenile and young adult mice reflect a diversified functional composition, and are presumed advantageous to maintain the homeostasis of muscles and MuSCs.

During aging, the number of MuSCs progressively decreases, with a concomitant decline in regenerative property (Sousa-Victor et al., 2015; Brack and Munoz-Canoves, 2016). Probing for changes in systemic factors and niche environment has yielded valuable insights into MuSC aging. Increased levels of Wnt and Tgfβ1

ligands in the sera of aged mice are thought to compromise MuSC function (Brack et al., 2007; Carlson et al., 2009). Elevated levels of FGF2 at the MuSC niche are detected in old mice, associated with MuSC quiescence-break and loss (Chakkalakal et al., 2012). Reduced levels of the extra cellular matrix protein fibronectin and diminished activity of integrins have also been implicated to weaken niche interaction by aged MuSCs (Lukjanenko et al., 2016; Rozo et al., 2016). Furthermore, elevated stress, a general systemic aging factor, is associated with MuSC aging (Schworer et al., 2016). Aged MuSCs, compared to the young, have lower proliferation capacity and higher propensity for differentiation in culture (Chakkalakal et al., 2012; Cosgrove et al., 2014), indicating intrinsic changes. Microarrays and ChIP-seq have been used to assess the intrinsic differences between young and aged MuSCs (Liu et al., 2013; Price et al, 2014). Age-specific differences detected by these population-based assays predict that the heterogeneous composition of MuSCs in the young is likely also distinct from that in the aged, a perspective that should be explored.

Because heterogeneity is thought to be biologically advantageous for functional diversification in a cell population, and is an intrinsic characteristic of young MuSCs, I asked how the aged MuSCs are different from the young in heterogeneity by producing and analyzing single cell RNA sequencing (scRNA-seq) data. I identified genes that are expressed in a small fraction of young MuSCs and expanded to a larger fraction of aged MuSCs. Of them, I interrogated the role of Growth arrest-specific gene 1, Gas1, which encodes a GPI-anchored plasma membrane protein (Martinelli and Fan, 2007a). In this chapter, I present evidence that functional decline of MuSCs is caused by homogenized expression of Gas1. Specifically, targeted pan-expression of Gas1 in vivo revealed that Gas1 caused aging-like phenotypes in young MuSCs. Conversely, conditional knock-out of Gas1 in aged MuSCs rejuvenate their regenerative response.

Additional in vitro assays substantiate the negative impact of Gas1 on MuSC renewal. All together, my results support a model that Gas1 expression, from heterogeneous to homogeneous in the MuSC population over time, represents a critical change that underlies the functional decline of aged MuSCs.

RESULTS

Heterogeneous composition of MuSCs changes with age

To assess heterogeneous compositions of young versus aged MuSCs, I performed scRNA-seq for 4037 and 3670 MuSCs isolated from 2 month (m) and 20 m old mice, respectively, using the method by Liu et al. 2013. Young and aged MuSCs are distributed as adjacent clusters, presented on t-SNE (Figure 2.1A) and principal component analysis (Figure 2.1B) plots, with a fraction of overlap. Unsupervised clustering by Cell Ranger assigned these young and aged cells into 5 clusters (Figure 2.1C and D): among them, 91% of the young MuSCs are distributed into three clusters (clusters 2-4), whereas 93% aged MuSCs belong to one cluster (cluster 1).

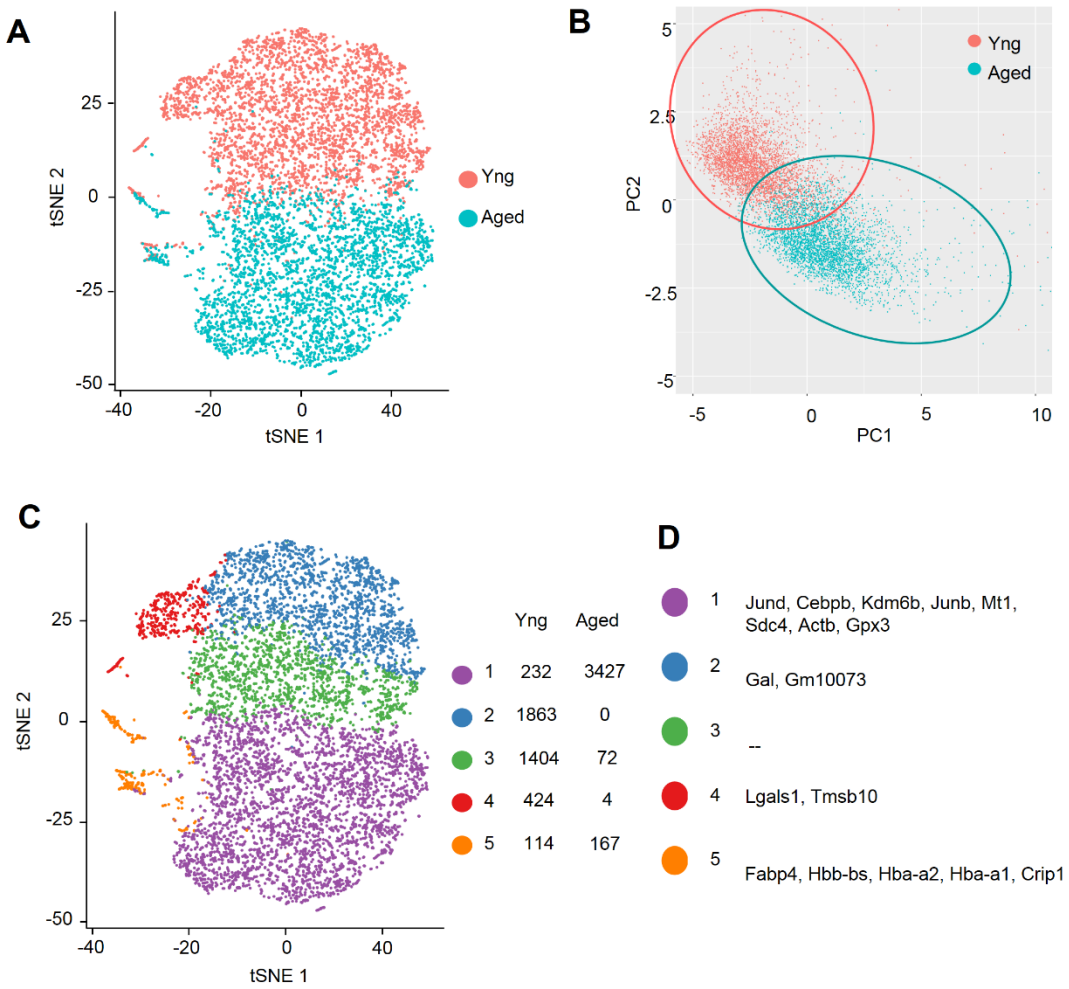

Figure 2.1. Single-cell RNA-seq of young and aged MuSCs.

(A) Transcriptome of individual MuSCs isolated from young (Yng, 2 month (m) of age) and aged (Aged, 20 m) mice. Each cell is represented as a dot and plotted on the t-SNE graph.

(B) Principal component analysis of individual young and aged MuSCs isolated from young (Yng, 2-month-old) and aged (Aged, 20-month-old) WT mice, using data in (A). Each cell is represented as a dot.

(C) Unbiased clustering of the scRNA-seq transcriptomes from the data in (A). Each cell is represented as a dot, assigned to a cluster by Cell Ranger, and plotted on the t-SNE graph. Cell numbers in each cluster are indicated.

(D) Genes enriched in each of the clusters in (C) by Cell Ranger.

By Monocle 2 pseudotime, a fraction of young cells displayed a trajectory along with aged cells (Figure 2.2A). It therefore appears that young MuSCs are more heterogeneous than the aged, and some young MuSCs have aged characteristics. Comparison of cells in early (left to node 1 in Figure 2.2A) versus late (right to node 2) states identified 292 genes expressed in a larger cell fraction in the late states; 43 of them topped the list with > 2-fold increase (Table S1). Gene ontology and KEGG analyses using the 292 differentially expressed gene lists revealed enrichment for MAPK cascade/pathway and cell/focal adhesion (Figure 2.2B and C), likely reflecting changes in FGF2 (Chakkalakal et al., 2012) and integrin signaling (Rozo et al., 2016) relevant to MuSC aging. I also noted that the increase of Fos, Jun, Junb, and Socs3 (some of them included in MAPK and focal adhesion) expressing cells in late states were used to indicate enriched TNF signaling, and these genes were also reported to reflect enriched Jak/Stat signaling in aged MuSCs (Price et al., 2014). Thus, scRNA-seq is useful to probe for genes and pathways associated with MuSC aging.

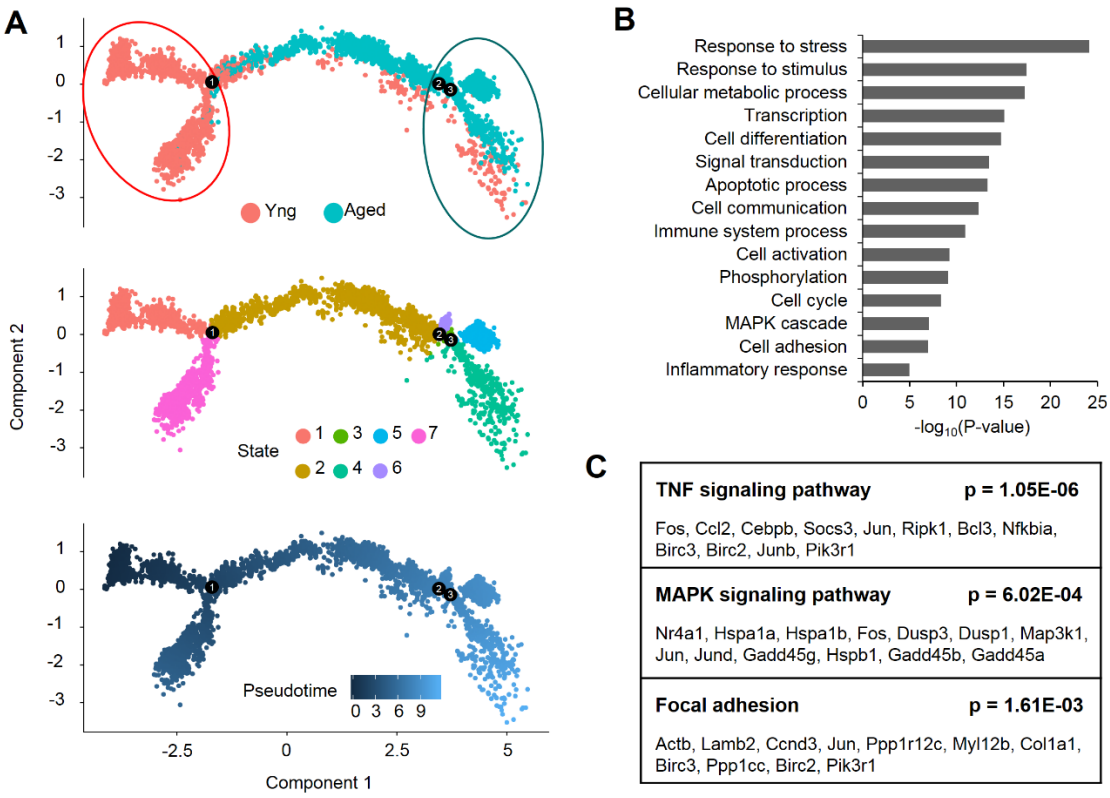

Figure 2.2. Single-Cell RNA-seq reveals changes in heterogeneity of MuSCs during aging.

(A) Trajectory analysis of the sc RNA-seq transcriptomes from the data in (A). Results are presented by young (pink) and aged (cyan) group (upper panel), unbiased clustering (middle panel), and by pseudotemporal ordering (lower panel) by Monocle 2.

(B) Gene ontology analysis of 292 genes expressed in increase fraction of Aged MuSCs by single-cell RNA-seq transcriptomes, using DAVID 6.8.

(C) KEGG pathway analysis of 292 genes expressed in increase fraction of Aged MuSCs genes Aged MuSCs by single-cell RNA-seq transcriptomes, using DAVID 6.8.

Table 2.1. 43 Genes Expressed in Increase Fraction (≥ 2 fold) of Aged MuSCs by Single-Cell RNA-Seq Transcriptomes,

Official Gene Symbol	q value	# total cells	# early cells	# late cells	normalized ratio	Ensembl ID
Cebpb	0	2435	522	819	3.08796956	ENSMUSG00000056501
Jund	0	2035	234	817	6.87172564	ENSMUSG00000071076
Gm26917	3.00E-282	2473	639	773	2.38088406	ENSMUSG00000097971
Sik1	1.31E-152	1081	326	399	2.40887857	ENSMUSG00000024042
Plau	3.45E-119	478	106	214	3.97344788	ENSMUSG00000021822
Fos	2.16E-111	893	256	307	2.36025009	ENSMUSG00000021250
Fosb	8.03E-106	1023	240	338	2.7718203	ENSMUSG00000003545
Comt	8.67E-94	942	237	306	2.54116399	ENSMUSG00000000326
Ccl19	2.21E-90	407	79	151	3.76191924	ENSMUSG00000071005
Ankrd1	3.49E-90	703	162	217	2.63635768	ENSMUSG00000024803
Pnrc1	8.10E-73	681	181	229	2.49009846	ENSMUSG00000040128
Gm42418	3.87E-70	655	114	216	3.72913849	ENSMUSG00000098178
Dcn	5.16E-70	258	71	102	2.82749233	ENSMUSG00000019929
Jun	6.90E-68	618	178	217	2.39938171	ENSMUSG00000052684
Ccl2	5.92E-65	302	65	119	3.60324022	ENSMUSG00000035385
Rhoh	2.49E-62	519	107	170	3.1269775	ENSMUSG00000029204
Socs3	2.72E-62	332	47	142	5.94634494	ENSMUSG00000053113
Maff	1.98E-58	554	117	183	3.07839851	ENSMUSG00000042622
Gm42726	4.21E-56	853	244	260	2.09721586	ENSMUSG00000107102
Insig1	9.05E-52	523	179	194	2.13308573	ENSMUSG00000045294
Hspa1a	2.55E-48	380	84	146	3.42084331	ENSMUSG00000091971
Dusp1	1.42E-43	596	176	183	2.04643537	ENSMUSG00000024190
Dcaf17	3.96E-42	472	111	150	2.65967084	ENSMUSG00000041966
Hdac1	4.49E-36	403	104	134	2.53589385	ENSMUSG00000028800
Hspa1b	1.81E-35	255	47	101	4.22944253	ENSMUSG00000090877
Gadd45g	2.22E-33	177	53	85	3.15647728	ENSMUSG00000021453
H2-Q4	1.42E-32	496	142	152	2.10675899	ENSMUSG00000035929
Crlf1	1.08E-27	433	105	112	2.09936685	ENSMUSG00000007888
Chpt1	2.83E-27	372	106	110	2.04242648	ENSMUSG00000060002
Syt11	9.90E-24	239	47	80	3.35005349	ENSMUSG00000068923

Gja1	2.25E-23	157	36	75	4.10032588	ENSMUSG00000050953
Bhlhe40	5.31E-19	204	56	72	2.53048683	ENSMUSG00000030103
Casp4	2.01E-18	176	39	60	3.02793296	ENSMUSG00000033538
Nr4a3	9.19E-18	207	60	73	2.39459032	ENSMUSG00000028341
Pecam1	1.74E-17	179	48	68	2.7882216	ENSMUSG00000020717
Lox	1.54E-16	140	43	55	2.51740938	ENSMUSG00000024529
Gm12216	1.96E-15	119	41	53	2.54420221	ENSMUSG00000081769
Vps8	2.73E-14	205	54	67	2.44197186	ENSMUSG00000033653
Gas1	4.44E-13	151	40	52	2.55860335	ENSMUSG00000052957
Gas6	3.64E-12	194	54	58	2.11394579	ENSMUSG00000031451
Birc3	1.25E-10	152	44	49	2.19181056	ENSMUSG00000032000
Map3k1	3.83E-09	150	41	54	2.59220602	ENSMUSG00000021754
Plpp3	2.53E-06	122	43	44	2.0139275	ENSMUSG00000028517

I next checked the top list for lesser studied genes with clues to MuSC aging, and I was intrigued by Gas1: It was found dramatically up-regulated in serum-starved NIH3T3 cells (Schneider et al., 1988), able to induce G0 quiescence in cell lines upon forced expression (Del Sal et al., 1992), and up-regulated in quiescent MuSCs by microarray (Fukada et al., 2007). Although Gas1 showed similar pseudotime trajectory as others on the gene list (Figure 2.3), it was not in the most enriched KEGG pathways (Figure 2.2C). I therefore decided to test the hypothesis that Gas1 plays a role in MuSC quiescence and aging via a pathway previously uncharacterized in the MuSCs.

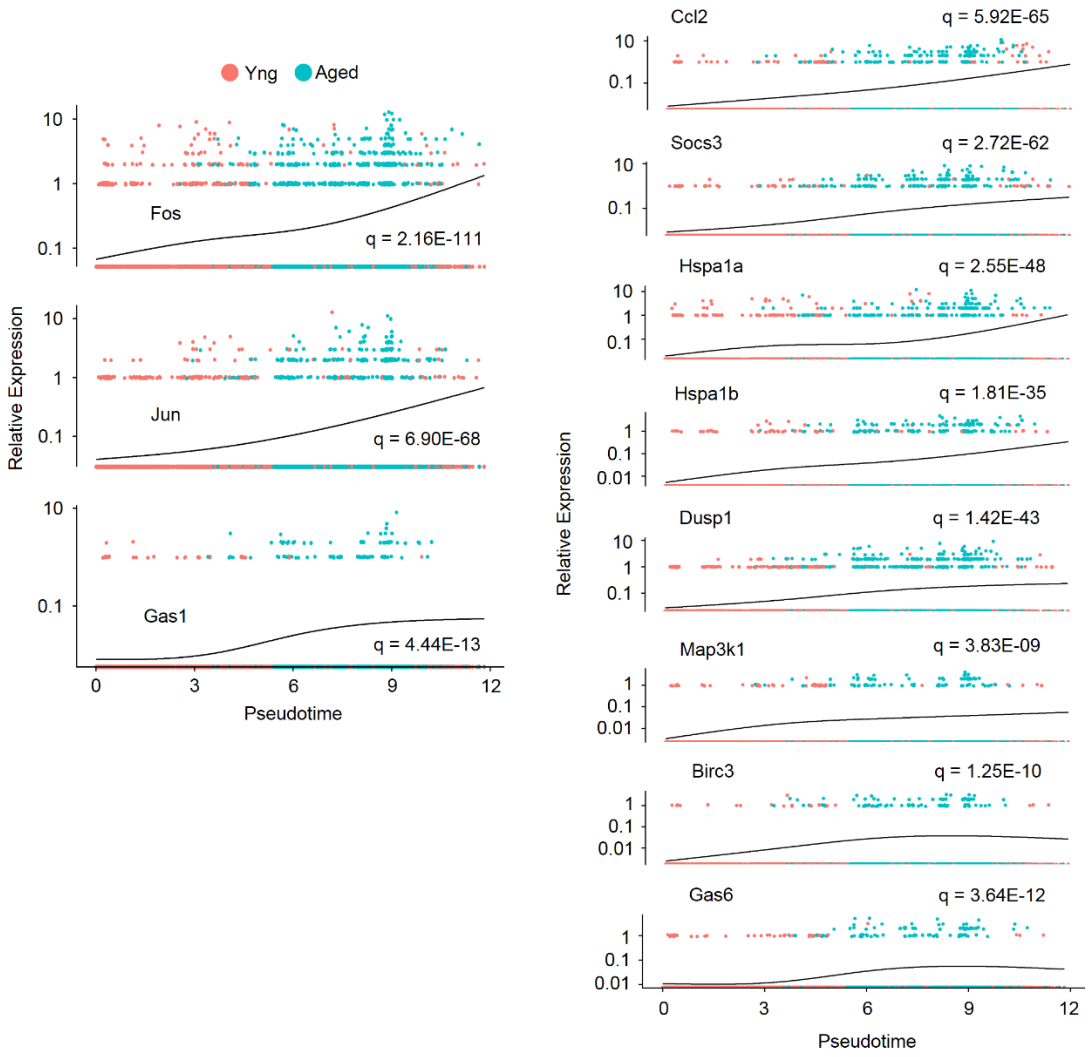

Figure 2.3. Single-Cell RNA-Seq reveals up-regulated genes cohorts in aged

MuSCs.

Trajectory analysis of the sc RNA-seq transcriptomes from the data in (Figure 2.1A). Results are presented by young (pink) and aged (cyan) group (upper panel), unbiased clustering (middle panel), and by pseudotemporal ordering (lower panel) by Monocle 2.

Functional heterogeneity is associated with Gas1 expression in young MuSCs

The expression of *Gas1*, which encodes a GPI-anchored plasma membrane protein, has been reported to be enriched in quiescent MuSC population (Fukada et al., 2007). I first performed immunostaining to confirm the Gas1 expression in MuSCs. Using Tibialis Anterior (TA) muscle sections from 6-months-old wild-type mice, Gas1 could be detected in the cells positive for Pax7, which is a quiescent MuSC marker (Figure 2.4).

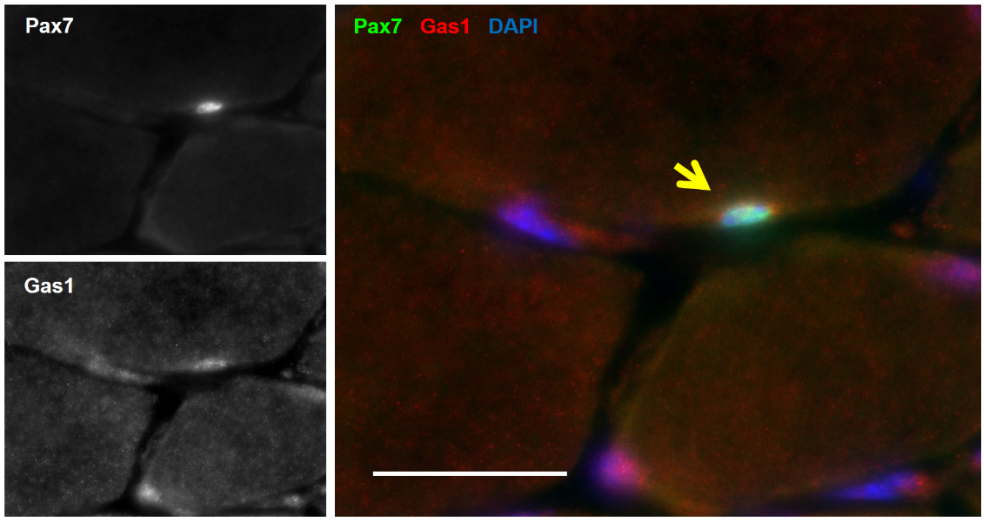

Figure 2.4. Gas1 is expressed in wild type adult MuSCs.

Representative images of MuSCs stained for Pax7 (green) and Gas1 (red) in TA muscle sections of wild type mice at 6 m of age; arrowheads, $Pax7^{+}Gas1^{+}$ MuSCs. Scale bar, 25 μm.

Given that Gas1 is a G0 indicator and can inhibit S phase entry when over-expressed in cell lines (Martinelli et al, 2007b), I surmised that it might contribute to establishing MuSC quiescence, which may in part explained its expression in increased fraction of aged MuSCs. To address this question, pulse experiment by EdU (5-ethynyl-2'-deoxyuridine) was carried out for assessing the induction of MuSC quiescence. The result showed that neonatal mice have a substantial proportion of MuSCs that are proliferating (7 day after birth) (Figure 2.5A). At around 1 month of age (28 postnatal day), most MuSCs became non-dividing and no EdU positive $Pax7^{+}$ cells was detected in the 2-month-old TA muscles. However, this timing of MuSC quiescence does not match the expression of Gas1: at 2 month of age when most MuSCs are quiescent, only ~40% of them express Gas1, based on the β-Gal signal using a *LacZ* knock-in reporter allele for Gas1 ($Gas1^{LacZ}$; Martinelli, D. C., 2007a) (Figure 2.5B and C). Also, by immunostaining of MuSCs in 2-month-old $Gas1^{LacZ}$ mice with β-Gal and Ki67, a cellular marker for proliferation, ~40% of MuSCs are $Gas1^{+}Ki67^{-}$ and ~60% are $Gas1^{-}Ki67^{-}$, consistent with the EdU pulse assay (Figure 2.5B and C). These data suggest that Gas1 expression does not exactly reflect the quiescent status of the MuSC and Gas1 may not play a role in establishing MuSC quiescence.

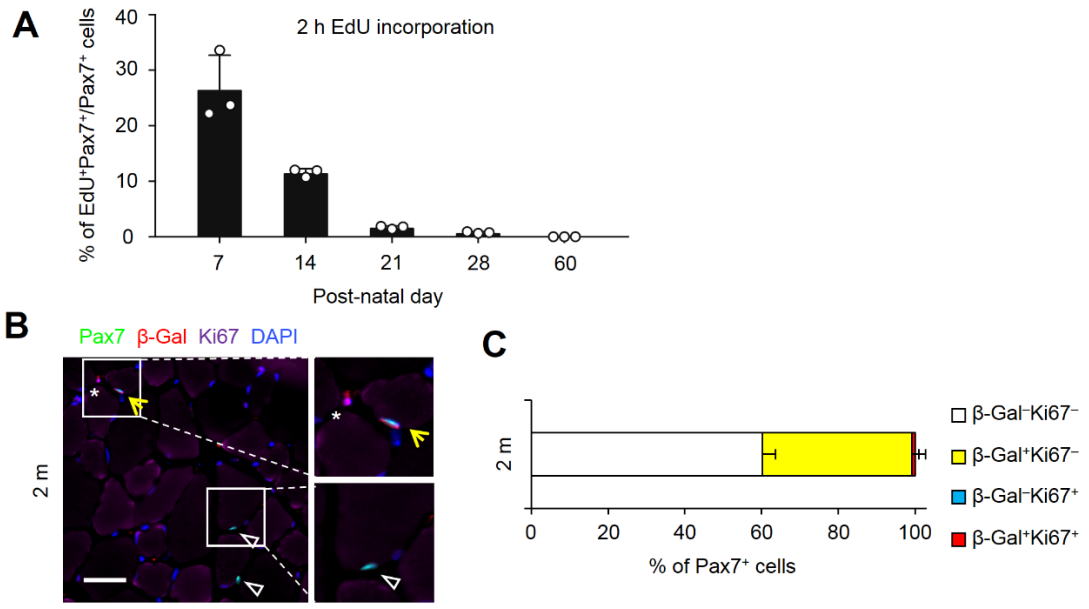

Figure 2.5. Gas1 expression does not match MuSCs quiescence establishment.

(A) Percentages of EdU^+Pax7^+ in total $Pax7^+$ MuSCs of TA muscles (from wild type mice) at specified ages (n = 3 animals per group, > 340 cells per age). EdU (5 mg/gram body weight) was pulsed for 2 h.

(B) Representative images for Ki67 (purple) staining in 2 m *Gas1*^{LacZ} TA muscle sections, co-stained for Pax7 (green), β-Gal (red) and DAPI (blue). Arrowhead, $Pax7^+$β-Gal^+Ki67^- cell; Arrows: $Pax7^+$β-Gal^-Ki67^- cells; asterisk: $Pax7^-$β-Gal^-Ki67^+ cell. Scale bar, 50 μm

(C) Quantification for percentages of indicated cell population using data in (B) (n = 3 animals, ten sections per animal).

To character Gas1's function in MuSCs, I further surveyed Gas1 expression using *Gas1*^{LacZ} reporter allele and obtained the time course expression profile of Gas1 in Pax7^{+} MuSCs throughout the lifespan of mice. β-Gal reporter present in a small fraction of young Pax7^{+} MuSCs (around 10% in 1-month-old mice) and increasing gradually with age (Figure 2.6A and B). Fluorescent activated cell sorting (FACS) confirmed the young-heterogeneous versus aged-homogenous composition of Gas1^{+} (and correspondingly, β-Gal^{+}) MuSCs (Figure 2.6C and D).

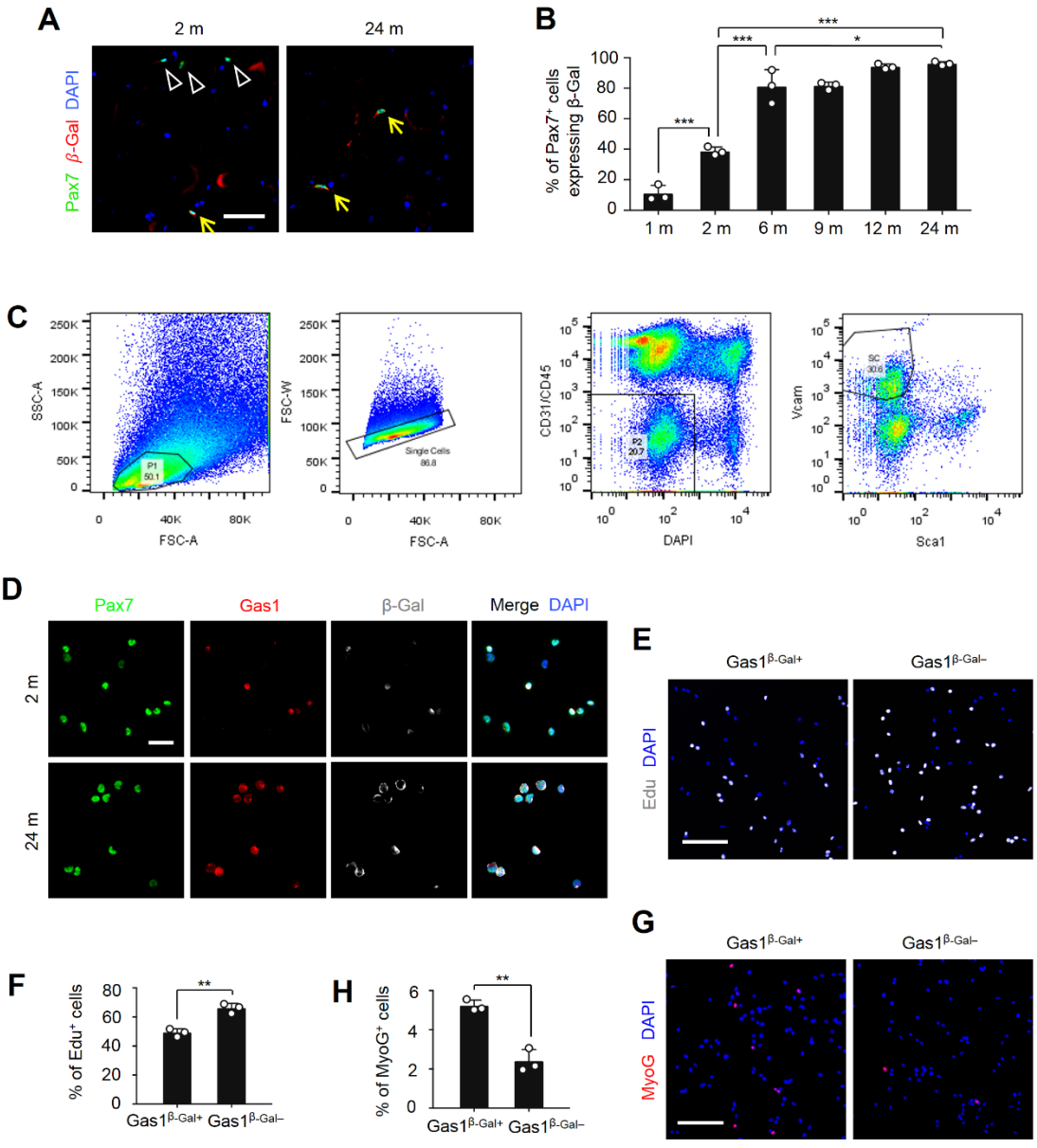

Figure 2.6. Gas1 is expressed heterogeneously in young MuSCs.

(A) Representative images of MuSCs stained for Pax7 (green) and β-Gal (red) in TA muscle sections of *Gas1*$^{LacZ/+}$ mice at 2 m and 24 m of age; open arrowheads, β-Gal^{-} MuSCs; arrows, β-Gal^{+} MuSCs. Scale bar, 25 μm.

(B) Percentages of β-Gal^{+}Pax7^{+} in total Pax7^{+} MuSCs in *Gas1* $^{LacZ/+}$ TA muscles at specified ages (*n* = 3 animals per group, ten sections per animal).

(C) Representative FACS plots for purifying MuSCs by 4 surface markers (CD45^{-} CD31^{-}Sca1^{-}Vcam^{+}).

(D) Freshly isolated MuSCs (by FACS) from 2 m and 24 m Gas1$^{LacZ/+}$ mice stained for Pax7 (green), Pax7 (red) and β-Gal (gray), and merged with DAPI (blue). Scale bar, 25 mm.

(E and F) β-Gal^{+} and β-Gal^{-} MuSCs were isolated from 2 m *Pax7*$^{Avi\text{-}2A\text{-}GFP}$*;Gas1*$^{LacZ/+}$ mice by FACS, cultured, pulsed by 2.5 h EdU (10 mM), stained (F) and quantified (G) for EdU incorporation (n = 3 animals, ≥200 cells per condition). Scale bars, 50 mm.

(G and H) The same isolated MuSCs as in (F and G) cultured, stained (H) and quantified (I) for MyoG expression (n = 3 animals, ≥200 cells per condition). Scale bars, 50 mm.

Data are mean ± s.d.; ** $P < 0.01$; by two-sided unpaired t-test (F, H).

The heterogeneity of Gas1 expression may manifest the functional heterogeneity of young MuSCs and contribute to MuSCs aging. To test this idea, β-Gal^{+} and β-Gal$^{–}$ MuSCs were differentiated by live β-Gal staining and isolated by FACS from 2-months-old *Gas1*^{LacZ} mice and subjected to cell culture assay in vitro for examining cell proliferation and differentiation. After the isolated MuSCs have been expended, they were pulsed by EdU for assessing proliferation. β-Gal^{+} fraction displayed lower proliferation index indicated by lower percentage of EdU incorporated cells, compared with non-expressing (β-Gal$^{–}$) fraction (Figure 2.6E and F). Also, this β-Gal^{+} population showed higher propensity to differentiate in culture, based on the higher proportion of cells expressing Myogenin (MyoG), a MuSC differentiation marker (Figure 2.6G and H). Thus, these data indicated that after activation, Gas1 inhibit proliferation and trigger precocious differentiation. Due to functional decline, naturally aged MuSCs also proliferate less and are more prone to differentiation over self-renewal in cell culture condition. Thus, young Gas1^{+} MuSCs display cellular properties known for aged MuSCs.

Pan-expression of Gas1 in young MuSCs impairs regeneration

The heterogeneous expression of Gas1 in young MuSCs and their functional differences in vitro led me to test whether the forced expression of Gas1 in the entire young MuSC population would change stem cell function and regeneration capability in vivo. To address this question, I generated a new conditional pan-expression allele of Gas1, Rosa26^{CAGGas1}, in order to express Gas1 in all MuSCs.

The targeting construct was generated on the basis of the Rosa26 targeting vector Ai32 (Madisen et al., 2012). First, in order to differentiate the ectopic Gas1 from endogenous one, an Avi-tag, a 15 amino acid peptide that enables biotinylation by BirA

biotin ligase and detection by avidin or streptavidin (Howarth et al., 2005), was inserted into a wildtype mouse Gas1 sequence. The Avi-Gas1 fragment was then cloned into the Ai32 plasmid (Rosa26-pCAGLSL-EYFP-WPRE-bGHpA-PGK-neo-pA), replacing its original EYFP sequence (Figure 2.7A). The inserted Avi-Gas1 was located between the LSL and WPRE sequence. And the LSL sequence contains specifically loxP-Stop codons-3x SV40 polyA-loxP, which allows for recombination between the loxP sites when Cre recombinase is expressed by specific Cre-driver and the ensuing expression of Avi-Gas1 driven by CAG promotor.

The final targeting vector for Gas1 pan-expression Rosa26-pCAGLSL-Avi-Gas1-WPRE-bGHpA-PGK-neo-pA was linearized by restriction enzyme digest and transfected into R1 embryonic stem (ES) cells by electroporation. ES cells were then cultured in selection media containing G418 until colonies were visible. G418-resistant ES clones were then subjected to screening by PCR using primers spanning the 5' homology arm. Positive ES clones were used to produce chimeric mice by morula aggregation. Chimeric mice were bred with C57BL/6J mice to obtain germline transmitted F1 mice with the Rosa26-CAGLSL-Gas1 ($R^{CAGGas1}$) transgene, determined by PCR.

To determine whether homogenized *Gas1* expression can cause dysfunction of young MuSCs in vivo, I used a $Pax7^{Cre\text{-}ERT2}$ ($Pax7^{CE}$)-driven, tamoxifen (Tmx)-inducible strategy (Lepper, C., 2009) for pan-expression of Gas1 via the $R^{CAGGas1}$ allele in young MuSCs. First, $R^{CAGGas1}$ was crossed with $Pax7^{CE/+}$;R^{YFP} to obtain the compound $Pax7^{CE/+}$;$R^{CAGGas1/YFP}$ (Gas1EX) mice (Figure 2.7B). To determine whether Cre-mediated loxP recombination at Rosa26 locus indeed led to Gas1 expression in MuSCs, Tmx were administered for 5 consecutive days. Single myofibers from the extensor digitorum longus (EDL) muscles were harvested 1 month after the first of five

tamoxifen injections, following by detection of Gas1 by immunofluorescence (Figure 2.7C). The result showed apparent expression of Gas1 on almost all young Pax7^{+} cells from Gas1EX muscles, while the control young mice without Tmx injection had only a fraction of Pax7^{+} cells expressing Gas1 as previously determined. Thus, Gas1 protein is efficiently induced by Tmx in Gas1EX MuSCs.

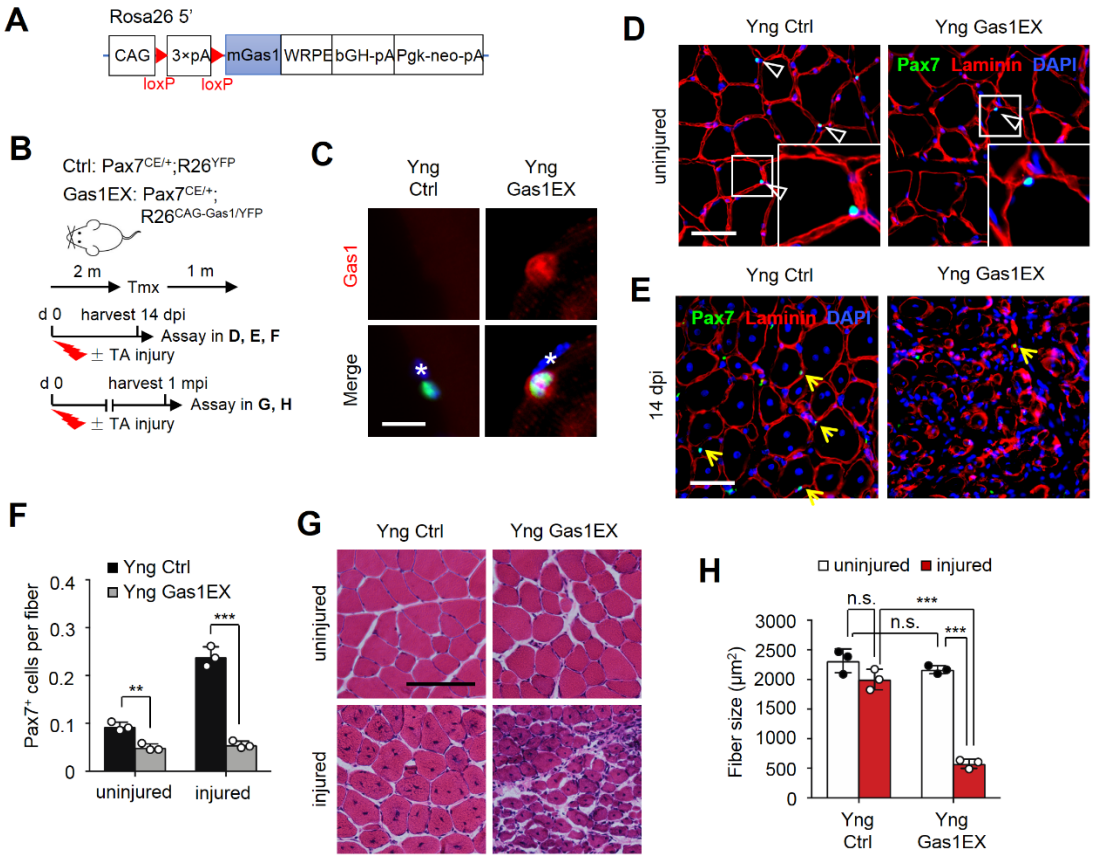

Figure 2.7. Pan-expression of Gas1 in young MuSCs impairs regeneration

(A) Diagram of the Gas1 pan-expression (EX) cassette knocked into the *Rosa26* locus. (B) Experimental schemes for young control and Gas1 pan-expression Gas1EX mice by *Pax7*^{CE}-directed, Tmx-induced expression; + and – indicate with and without injury, respectively, to the TA muscle. The *R26*^{YFP} reporter allele was included for cell marking. (C) Representative images for Gas1 (red) staining of MuSCs merged with Pax7 (green) and DAPI (blue) on single myofiber (SM) immediately after isolation from young (Yng)

control (Ctrl) and Yng Gas1 pan-expression (Gas1EX) mice. (n = 3 mice per group; ≥ 20 myofibers per condition). Scale bar, 50 μm.

(D and E) Representative images of Pax7 (green) and Laminin (red) staining of Yng Ctrl and Gas1EX TA muscle sections under uninjured (D) and 14 days post injury (dpi) (E) status as specified in (B). Scale bar, 50 μm.

(F) Averaged $Pax7^{+}$ MuSCs per fiber for uninjured and injured muscle sections as specified in (D and E) (n = 3 mice per group, 10 sections per mouse).

(G) Representative H&E stained images of TA muscle sections from Yng Ctrl and Gas1EX mice, as specified in (B). Scale bar, 150 μm.

(H) Averaged fiber sizes from data in (G) (n = 3 mice per group, 10 sections per mouse). Data are mean ± s.d.; ***$P < 0.001$; n.s., not significant, by multiple t-test (F) and two-way ANOVA (H).

To examine the phenotype of Gas1 pan-expression in MuSCs, I first quantified the number of $Pax7^+$ cells in Gas1EX mice 1 month after Tmx regimen and observed a diminished stem cell pool (Figure 2.7D and F). Young Gas1EX mice have substantially less $Pax7^+$ MuSCs, compared to control. The efficient and robust regeneration of myofibers after injury relies on stable stem cell ($Pax7^+$ MuSCs) pool. To investigate how the stem cell pool is reduced, I injected EdU daily after Tmx regimen and assessed MuSC behavior. In normal adult mice, MuSCs in resting limb skeletal muscle fibers are mostly under quiescent status (Schultz et al., 1978). As such, without any acute environmental or internal stimuli such as trauma or disease, the overall turnover of MuSC population is predicted to be very low. However, 14 days after Tmx treatment, Gas1EX MuSCs showed increased EdU incorporation, suggesting a spurious activation of stem cells in sedentary muscle (Figure 2.8A and B). Also, by immunofluorescent staining with differentiation marker MyoG, muscles from Gas1EX mice showed more MyoG ectopically expressing cells, indicating they are more inclined to differentiate (Figure 2.8C and D). YFP positive myofibers scattered in the uninjured muscles suggest that the Gas1EX differentiation cells eventually incorporate into muscle fibers (data not shown).

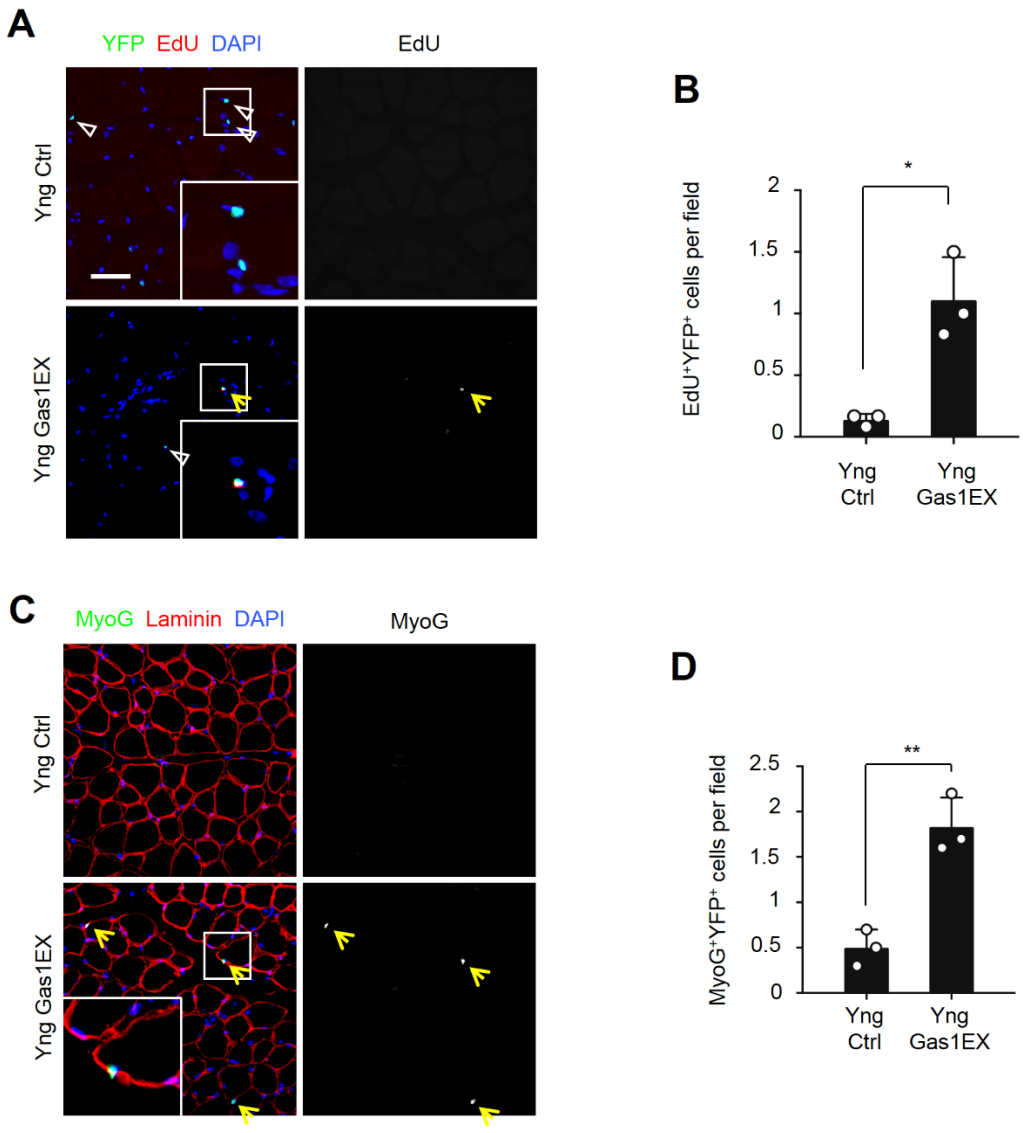

Figure 2.8. Pan-expression of Gas1 triggers young MuSCs activation and differentiation

(A and B) Representative images of EdU (red) labeling in Yng Ctrl and Gas1EX TA muscle sections, co-stained with YFP (green) and DAPI (blue) at 7 d post Tmx without injury and with EdU injection daily (A) and quantified for averaged EdU^+YFP^+ cells per field (1.074 mm^2) (B) (n = 3 mice per group, 10 sections per mouse). Note that R26YFP reporter was included in control and Gas1EX mice; open arrowheads, EdU^-YFP^+ cells; arrow, EdU^+YFP^+ cell. Scale bar, 50 μm.

(C and D) Same samples in (A) stained for MyoG (gren), Laminin (red) and DAPI (blue) and quantified for averaged $MyoG^+YFP^+$ cells per field (D) (n = 3 mice per group, 10 sections per mouse); arrows, $MyoG^+$ cells. Scale bar, 50 μm.

Data are mean ± s.d.; **P* < 0.05; ***P* < 0.01; by two-sided unpaired t-test (B and D).

I then injured the tibialis anterior (TA) muscles of Gas1EX mice by cardiotoxin (CTX) and assayed for regeneration at 14 days post injury (dpi). Regenerated myofibers could be readily distinguished from uninjured area in skeletal muscle cross sections by their centrally located myonuclei (Figure 2.7E). Normal young muscles are competent to regenerate robustly by virtue of the fully functional MuSCs. One month post injury by CTX, the regenerative myofiber sizes of young control mice had recovered to be equivalent to those in uninjured young control. Notably, Gas1EX MuSCs gave rise to smaller regenerative myofibers, compared to those in age matched controls (Figure 2.7G and H). The deficient regeneration was accompanied by a reduction of $Pax7^{+}$ cells, suggesting a self-renewal defect (Figure 2.7E and F). Therefore, targeted force expression of Gas1 in young MuSC population results in quiescence breaking, stem cell loss, defective regeneration, and compromised self-renewal, a phenotype reminiscent of aged satellite cell.

Inactivation of Gas1 improves MuSC number and function in aged mice

The aging-like features of Gas1EX MuSCs may reflect a gain-of-function phenotype. To test the idea that increased proportion of Gas1-expressing MuSCs during aging contributed to decreased stemness and regenerative function, I next examined whether removing Gas1 function in MuSCs would enhance their regeneration capacity in aged mice. For this, I bred the conditional knock-out mice for Tmx-induced deletion of Gas1 selectively in $Pax7^{+}$ MuSCs (Lepper et al., 2009) by crossing mice carrying the $Pax7^{CE}$ *allele* with mice carrying a Cre-conditional allele of Gas1, $Gas1^{flox}$ (Jin et al., 2015). The compound conditional Gas1 knock-out mice $Pax7^{CE/+}Gas1^{flox/flox}R^{YFP}$ (hereafter referred to as Gas1KO) were obtained. To assess if Cre-mediated loxP recombination at $Gas1^{flox}$ generate a Gas1 null allele, Tmx were administered for 5 consecutive days.

Single myofibers were harvested 1 month or 18 month after the first of five tamoxifen injections, following by immunofluorescent staining for Gas1 (Figure 2.9A). The result revealed that no Gas1 signal could be detected on any adult or aged $Pax7^+$ cells from the Gas1KO mice (Figure 2.9B), indicating that Gas1 protein on MuSCs is efficiently eliminated after Tmx regimen.

Next I used this Gas1KO mouse model to investigate the effects of eliminating Gas1 function in MuSCs during aging. Short-term deletion (1 month after Tmx regimen) of Gas1 in young MuSCs did not have impact on stem cell behavior or function, based on the normal regenerative myofiber sizes (data not shown). On the other hand, long-term Gas1 deletion experiments were performed using Gas1KO and control mice with Tmx administered at 2 months of age and stem cell behavior/function and analyzed 18 months later. In contrast to young Gas1EX mice, targeted inactivation of *Gas1* in MuSCs throughout adult life helped to retain the stem cell pool in aged mice under sedentary condition (Figure 2.9C and E). To examine how the stem cell pool was maintained in aged Gas1KO mice, a long-term BrdU labeling assay was used. Aged control and Gas1KO mice were fed with BrdU containing water daily for 6 weeks before harvest of TA muscles. Aging MuSCs have been reported to break quiescence erroneously (Chakkalakal, J. V., et al., 2012), leading to diminished stem cell pool in aged muscles. Consistent with the published data, BrdU signal could be detected in a certain percentage of $Pax7^+$ MuSCs from aged control animals. Aged Gas1KO mice, however, have fewer BrdU incorporated MuSC populations (Figure 2.9F and G), suggesting that these MuSCs are less prone to break quiescence, by which the stem cell pool is retained.

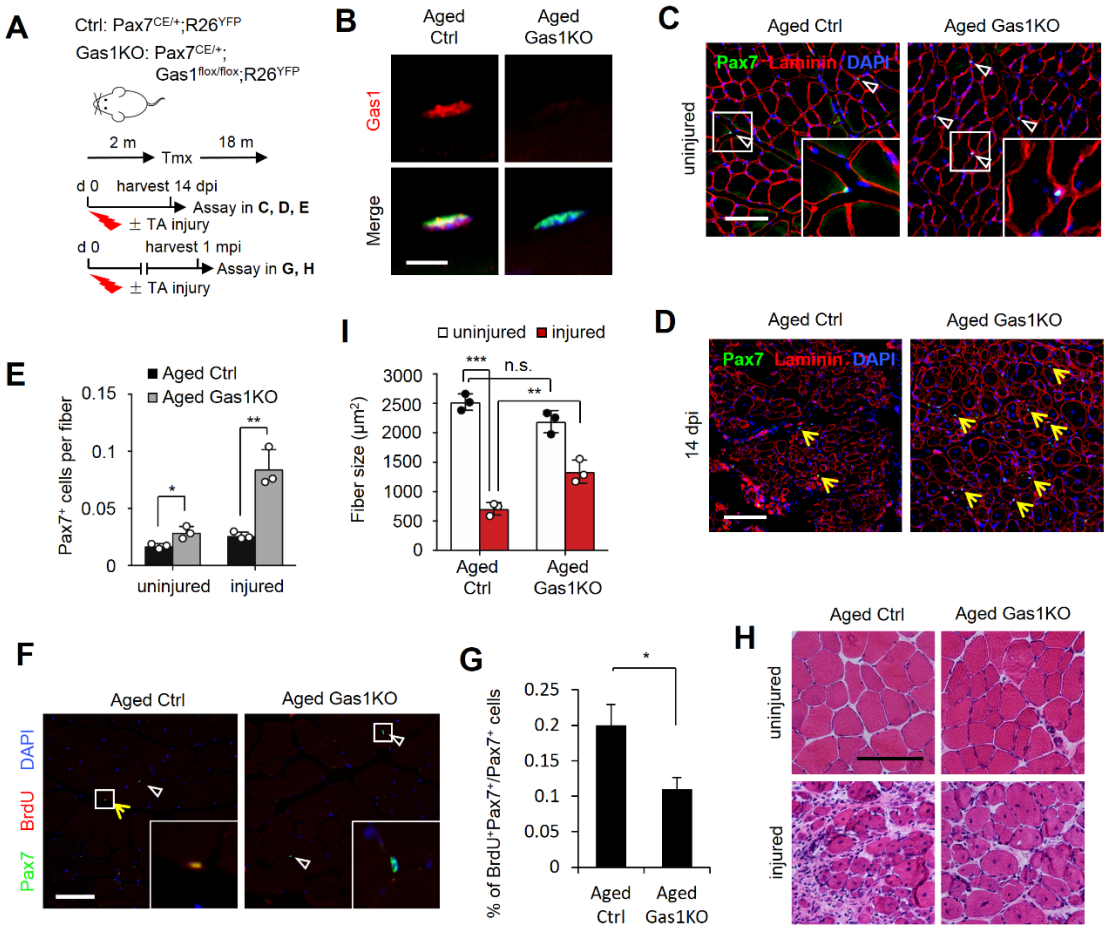

Figure 2.9. Inactivation of Gas1 improves aged MuSCs.

(A) Experimental schemes for aged (Aged) Ctrl and Gas1 knockout (KO) mice by $Pax7^{CE}$-directed, Tmx-induced expression; + and – indicate with and without injury, respectively, to the TA muscle. The $R26^{YFP}$ reporter allele was included for cell marking.

(B) Representative images for Gas1 (red) staining of MuSCs merged with Pax7 (green) and DAPI (blue) on single myofiber (SM) immediately after isolation from Aged Ctrl and Aged Gas1KO mice. (n = 3 mice per group; ≥ 20 myofibers per condition). Scale bar, 50 μm.

(C and D) Representative images of Pax7 (green) and Laminin (red) staining of Aged Ctrl and Gas1KO TA muscle sections under uninjured (C) and 14 days post injury (dpi) (D) status as specified in (A). Scale bar, 50 μm (C); 100 μm (D).

(E) Averaged $Pax7^+$ MuSCs per fiber for uninjured and injured muscle sections as specified in (C and D) (n = 3 mice per group, 10 sections per mouse).

(F and G) Immunostainig image of BrdU (red) labeling in Aged Ctrl and Gas1KO TA muscle sections, co-stained with Pax7 (green) and DAPI (blue) with 6 weeks of BrdU treatment (G) and quantified for averaged percentage of $BrdU^+Pax7^+/Pax7^+$ cells (n = 3 mice per group, 10 sections per mouse). Scale bar, 50 μm.

(H) Representative H&E stained images of TA muscle sections from Aged Ctrl and Gas1KO mice, as specified in (A). Scale bar, 150 μm.

(I) Averaged fiber sizes from data in (H) (n = 3 mice per group, 10 sections per mouse). Data are mean ± s.d.; $*P < 0.05$; $**P < 0.01$; $***P < 0.001$; n.s., not significant, by multiple t-test (E), two-sided unpaired t-test (G) and two-way ANOVA (I).

I then asked whether the increased MuSCs achieved by Gas1 disruption during aging could help to enhance regenerative capacity. Aged Gas1KO and control mice were subjected to TA muscle injury and left to recover for 14 or 30 days. Aged control muscle showed limited regeneration based on smaller muscle fiber size and increased fibrotic area. Compared to aged controls, Gas1KO muscles showed better regeneration, i.e. larger regenerated muscle fibers (Figure 2.9H and I). Importantly, increased $Pax7^{+}$ MuSC number was also found after regeneration (Figure 2.9D and E), indicating that MuSC self-renewal is also improved in Gas1KO mice.

Gas1-expression negatively impacts MuSC renewal and regenerative muscle function

Both the Gas1EX and Gas1KO models display effects on MuSC number prior to injury as well as on regenerated myofiber size, which makes it difficult to conclude whether the observed regeneration outcomes were solely caused by intrinsic changes in MuSC properties. To address this, I performed single myofiber culture assay (Zammit et al., 2004), in which aged Gas1KO or young Gas1EX MuSCs were associated with intact wild type fibers, in order to analyze myogenic cell fates ex vivo. A culture paradigm of 96 hours after myofiber isolation was used. After culture, the single myofibers were collected and subjected to immunostaining for Pax7 and MyoD. Quiescent MuSCs are characterized by their expression of Pax7 (Seale et al., 2000). Upon activation, they transcribe MyoD and begin proliferating (referred to as myoblasts) and execute the myogenic program (Parker et al., 2003; Zhao and Hoffman, 2004). Following proliferation, myoblasts begin differentiation by downregulating Pax7. After the transit amplifying stage, a portion of the activated cells return to quiescence to maintain the stem cell pool and regain the expression of Pax7 (Yin et al, 2013).

According to the myogenic program of MuSCs, the myogenic cell populations after ex vivo culture expressing only Pax7 ($Pax7^{+}MyoD^{-}$), both Pax7 and MyoD ($Pax7^{+}MyoD^{+}$), and only MyoD ($Pax7^{-}MyoD^{+}$) represent the self-renewed, proliferating, and differentiating populations, respectively.

On single myofibers cultured for 96 hours, aged control MuSCs gave rise to more $Pax7^{-}MyoD^{+}$ differentiating cells and fewer $Pax7^{+}MyoD^{-}$ self-renewed cells, compared to young control MuSCs (Figure 2.10A, B and C). This ex vivo data is consistent with the reported declined function of aged MuSCs in vivo. As for the experimental groups, aged Gas1KO MuSCs increased $Pax7^{+}MyoD^{-}$ self-renewed fraction, compared with aged controls (Figure 2.10A, B and C). Also, similar to aged controls, young Gas1EX MuSCs resulted in a larger $Pax7^{-}MyoD^{+}$ differentiation-committed fraction compared with young controls (Figure 2.10A, B and C). These data corroborated with the in vivo data that Gas1 expression in MuSCs is negatively associated with self-renewal.

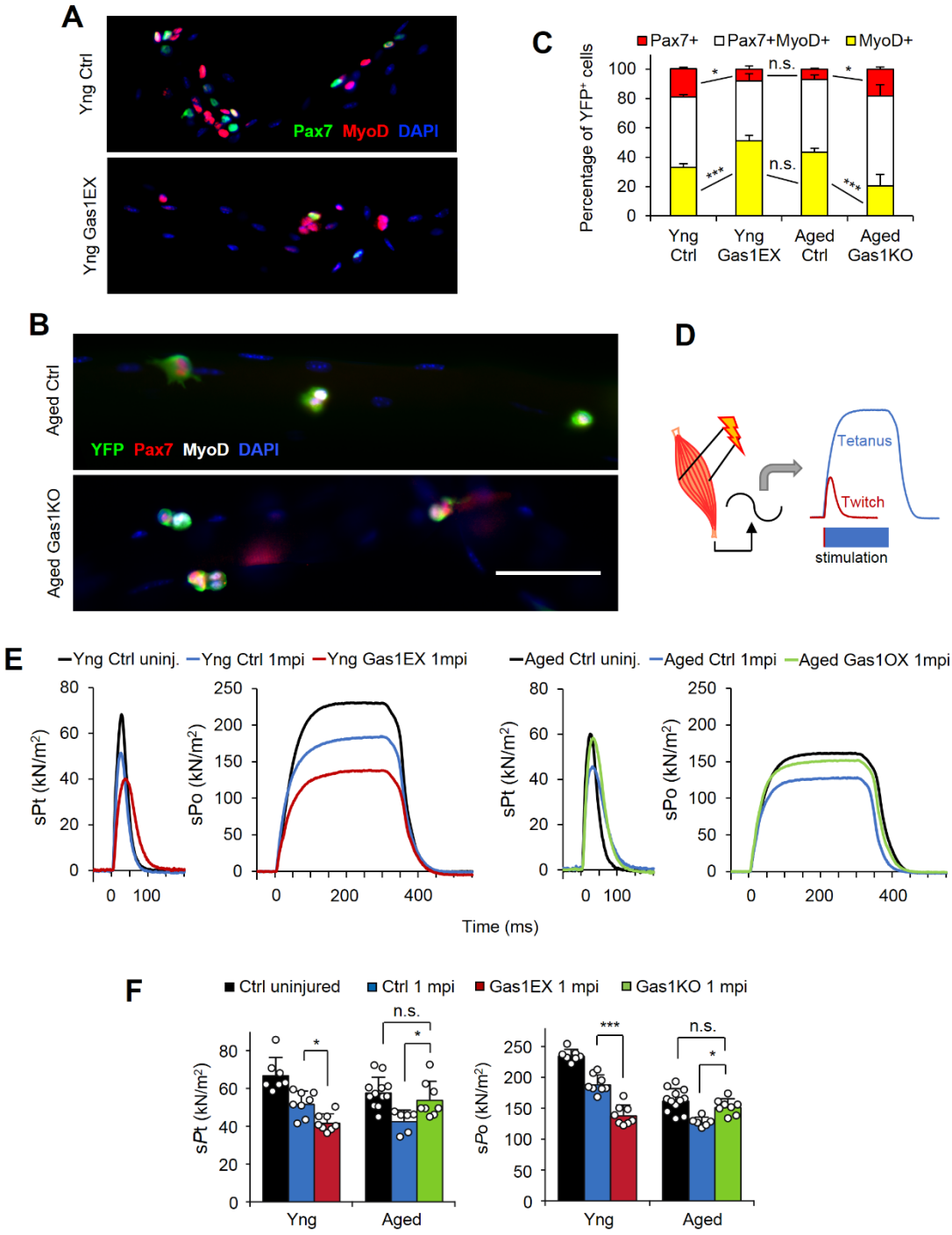

Figure 2.10. Gas1-expression negatively impacts MuSC renewal and regenerative muscle function.

(A and B) Representative images for single myofiber isolated from Yng Ctrl and Yng Gas1EX (A) or Aged Ctrl and Aged Gas1KO (B) mice, cultured for 96 h, and stain for

Pax7 and MyoD (n = 3 mice per group; ≥ 20 myofibers per mouse).

(C) Distribution of self-renewed ($Pax7^+$), proliferating ($Pax7^+MyoD^+$), and differentiated ($MyoD^+$) fractions in single myofiber cultures after 96 h using data in (A) and (B); myogenic cells are lineage-marked by YFP.

(D) Diagram for measuring specific twitch force (s*P*t) and specific maximum tetanic forces (s*P*o) of TA muscles in situ.

(E) Representative traces of normalized *sPt* and *sPo* (g) of TA muscles from specified groups (n ≥ 6 per condition).

(F) Normalized s*P*t and s*P*o of specified groups using data in (E).

Data are mean ± s.d.; **P* < 0.05; ****P* < 0.001; n.s., not significant; by two-way ANOVA (C) and one-way ANOVA (F).

I further assessed how changes in *Gas1* expression affected regenerated muscle function in young Gas1EX and aged Gas1KO mice by measuring single-twitch and tetanus forces in situ at 1 month post injury (1 mpi; Figure 2.10D). Correlating with histological data (Figure 2.7G and H; Figure 2.9H and I), regenerated young Gas1EX muscles showed marked diminution in both twitch and tetanus forces, relative to young controls (Figure 2.10E and F). By contrast, regenerated muscles of aged Gas1KO mice showed enhanced forces relative to age matched controls. Taken together, my results support that temporal spread of *Gas1* expression to the entire MuSC population contributes to their functional decline with age.

DISCUSSION

Every tissue of an organism is influenced by aging, a global complicated process. The speed of aging may be different in various species and tissues, but this process inevitably results in the reduction of health and vulnerability to diseases. Aging is the most hazardous factor for various kind of chronic diseases but the underlying causes of aging are still not well understood. Nonetheless, basic hallmarks and fundamental mechanisms of aging over various species have been proposed (Lopez-Otin et al., 2013). These include cell autonomous changes connected to epigenetic modifications, genomic instability caused by macromolecular deterioration, as well as gradual loss of proteostasis. The accumulated malignant cell intrinsic alterations lead to not only the damage of cell-cell interactions that help to counteract tissue damage (Neves et al., 2015), but also the systemic dysregulation that perturbs normal metabolism and beneficial inflammatory response (Franceschi et al., 2000).

A global impairment of regenerative capacity with age has been observed in various organisms. Adult stem cells, residing in most mammalian tissues, play a key

role in regulating tissue homeostasis and mediating repair after injury. Stem cell functions are influenced at different levels, from cell intrinsic regulation to environmental changes (Brack and Munoz-Canoves, 2016). The decline of stem cell properties associated with aging process, or the deleterious changes of stem cell environment, could contribute to the reduced tissue homeostasis and declined regenerative ability. For skeletal muscle, the MuSC is quiescent at normal condition, but can be activated to execute myogenic program to trigger stem cell proliferation and differentiation in response to injury. During aging, MuSCs number are declined, as well as intrinsic stem cell function (Chakkalakal et al., 2012). However, the aging-related cell intrinsic changes of MuSCs are not well studied. Thus, the underlying mechanism of MuSC aging remains to be explored.

Cell-to-cell differences always exist to some extent in any cell population, and the behaviors as a group of a specific cell population may not reflect the behaviors of any particular cell (Altschuler and Wu, 2010). Heterogeneity has been conceptualized and hypothesized to be an elementary feature of cellular systems (Elsasser, 1984). It is thought to be beneficial to a tissue or organ because heterogeneity creates diversity and thus larger capacity to enable elastic adaptation to environmental conditions. My data highlight a temporal dimension to the evolving heterogeneity in a stem cell population for tissue rebuilding. Here, I showed that young MuSCs preserve the elementary feature of heterogeneity for Gas1, not because $Gas1^{+}$ and $Gas1^{-}$ cells together offer diverse advantages, but rather $Gas1^{-}$ cells are free of disadvantage for robust regeneration. Other genes that help define the heterogeneous states of young MuSCs likely contribute to the robustness in $Gas1^{-}$ cells, and possibly also to counter the aging phenotype of $Gas1^{+}$ cells during the intermediate age. Conversely, homogeneity is inferred to limit functional elasticity and reduce adaptive response, such

as homeostasis and regeneration, which is observed for Gas1EX and aged MuSCs.

Here I provide complementary lines of genetic evidence that Gas1 drives MuSC aging. My results formulate a model in which heterogeneous expression of Gas1 in young MuSCs permits robust regeneration owing to the Gas1 non-expressing subpopulation. As Gas1-expressing MuSCs become a homogeneous population over time, the regeneration capacity wanes. Gas1 expression clusters with stress-response genes in young MuSCs and forced Gas1 expression can induce cell cycle arrest in cultured cells (Martinelli et al., 2007b), making me to speculate that it belongs to a stress-response circuit (see Chapter 3 and 4). In response to increased cellular stresses, aging MuSCs may therefore inadvertently turn on Gas1, with an unfavorable consequence. If so, the stress signal(s) that leads to the gradual spread of Gas1 expression to the majority of cells in the MuSC population with age is of curiosity. Whatever the stress signal(s) may be, the temporal heterogeneity of Gas1 reflects the progressive nature of aging, and suggests that stem cell aging is initiated in youth.

The increase of $Gas1^+$ MuSCs to a near-homogenous population precedes the timing of known MuSC aging. I suggest that in young and intermediate age, $Gas1^-$ MuSCs and other factors can overcome the presence of $Gas1^+$ MuSCs in vivo. It seems equally plausible that opposite to the Gas1 expression trend, there exists a youth-maintenance gene(s) with homogeneous-to-heterogeneous expression tempo during MuSC aging. A priori, either mode of expression changes in temporal heterogeneity is sufficient to drive aging. Both mechanisms likely exist to orchestrate ‘normal’ aging program, as a singular loss of youthful program may be permissive to uncontrolled pathological over ride. The aging driver may serve the role to prevent uncontrolled pathology due to loss of youthful program.

MATERIALS AND METHODS

Mice

The *Gas1*^{LacZ} mice (Martinelli and Fan, 2007a), *Pax7*$^{\text{cre-ERT2}}$ (referred to as *Pax7*^{CE} in legends; B6;129-*Pax7*$^{\text{tm2.1(cre/ERT2)}}$*Fan*/J) mice (Lepper et al., 2009), and *Gas1*^{flox} mice (Jin et al., 2015) have been described. The *R26*$^{\text{YFP}}$ (B6.129X1-*Gt*(*ROSA*)*26Sor*$^{\text{tm1(EYFP)}}$*Cos*/J) mice (Srinivas et al., 2001) was obtained from the Jackson Laboratory (JAX). Whenever YFP was included for assay, the *R26*$^{\text{YFP}}$ allele was included in the background for Pax7^{+} MuSC lineage marking. The Gas1 conditional pan-expression (Gas1EX) allele, *R26*$^{\text{CAG-Gas1}}$, is generated for this work. The Pax7-GFP knock-in allele, *Pax7* $^{\text{Avi-2A-GFP}}$ will be described by C. Lepper in a separate study. C57BL/6 mice were used as wild-type (WT) mice.

For young versus aged comparisons, mice were used at 2–3 month of age (young) or 18–24 month of age (aged). Sex was mixed. Animal experiments in this study were performed following the ethical regulations by Office of Laboratory Animal Welfare (OLAW), and in accordance with protocols approved by the Institutional Animal Care and Use Committee (IACUC) of the Carnegie Institution for Science (Permit number A3861-01).

Tamoxifen regimen, muscle injury, EdU and BrdU administration

Mice were given tamoxifen (Tmx, 20 mg/ml in corn oil; Sigma) at 4 mg per 40 g body weight intraperitoneally for 5 consecutive days. For young groups, unless noted otherwise, assays were conducted 1 m after Tmx regimen. For aged groups, assays were conducted 18 m after Tmx regimen.

For muscle injury, experimental and corresponding control mice were anaesthetized with isoflurane, their tibialis anterior (TA) muscle was injected with 50

μl of 10 μM cardiotoxin (CTX; Sigma) using an insulin syringe (U-100; Becton Dickinson), and harvested at post injury (pi) time points (stipulated as 'd' for day and 'm', for month) stated in the text and legends.

For short-term daily in vivo proliferation, 5-ethynyl-2′-deoxyuridine (EdU; Life Technologies) was given by intraperitoneal injection at 0.1 mg per 20 g bodyweight per injection and muscle harvested as specified in legends.

For long-term daily in vivo proliferation, Bromodeoxyuridine (EdU; Sigma) was administered by drinking water at 0.8 mg/ml for 6 weeks before the harvesting the TA muscles.

Muscle sample processing

TA muscles were harvested, fixed for 10 min in ice cold 4% paraformaldehyde (EMS) in PBS, sequentially changed through 10%, 20% and 30% sucrose/PBS overnight, embedded in OCT, frozen in isopentane (Sigma)/liquid nitrogen, and stored at –80 °C freezer until cryo-sectioning. Cross-sections (10 μm) of the muscle mid-belly region were stained with Hematoxylin and Eosin (H&E; Surgipath), or used for immunostaining and EdU reactions (see below).

MuSC isolation by FACS and myoblast culture

MuSCs were isolated following the previously described protocol (Liu et al., 2015) with slight modifications. For MuSC preparation, skeletal muscles were dissected and incubated in 0.2% Collagenase Type I (Thermo Fisher Scientific) in Ham's F-10 Nutrient Mix (F-10; Gibco) at 37 °C with gentle shaking for 1.5 h followed by centrifugation and wash. Tissues were then incubated in 0.2% Dispase (Gibco) in F-10 at 37 °C with gentle shaking for 0.5 h. Cells were then gone through 20-gauge

needles for dissociation and filtered through 40 μm cell strainer (VWR) and wash.

For surface maker labeling, cell were incubated with DAPI and fluorophore-conjugated antibodies against CD45, CD31, Sca-1 and Vcam, at 4 °C for 0.5 h. After wash, cells were subjected to fluorescence-activated cell sorting (FACS) using the ARIA III (BD Biosciences). Isolated mononuclear MuSCs were transferred to MuSC culture medium (20% Fetal Bovine Serum (FBS), 5% HS, 1% Pen/Strep, 1% Glutamax (Gibco), 0.1% chick embryo extract (MP biomedicals) in DMEM (Gibco)) for culture. They were plated on Matrigel-coated dishes (Corning, 354248; 30 min at 37 °C), and cultured at 37 °C in tissue culture incubators with 5% CO_2.

For live detection of β-Gal activity, cells were subjected to reaction using in vivo lacZ β-Galactosidase Intracellular Detection Kit (MarkerGene) following the manufacturer's guidelines and FACS isolated. For EdU labeling, EdU (10 μM) was added to MuSC culture medium for 2.5 h before harvesting for assay.

For single-cell RNA-seq, cells were collected in F-10 nutrient mix with 10% HS and subjected to 10X genomics single cell sequencing platform immediately (see below: Single cell RNA-seq and analyses)

Single myofiber (SM) isolation and culture

SMs with associated MuSCs were isolated from extensor digitorum longus (EDL) muscles (Zammit et al., 2004) by 1.5 h digestion in 0.2% Collagenase Type I in DMEM at 37 °C. The digested EDL muscle was then transferred to petri dishes containing DMEM, 1% Pen/Strep, and 1% Glutamax for mechanical dissociation to release individual myofibers. Isolated myofibers were subjected to direct fixation for immunostaining, or transferred to serum-coated Petri dishes for culture (SM culture medium: 10% FBS, 1% Pen/Strep, 1% Glutamax in DMEM).

Immunostaining

TA muscle sections, SMs or cytospun MuSCs were fixed for 10 min in 4% paraformaldehyde, permeabilized with 0.1% Triton X-100 (Sigma)/PBS for 10 min at room temperature (RT), rinsed with wash buffer (0.05% Triton-X 100/PBS), treated with blocking buffer (10% Normal Goat Serum (Genetex) and 1× carbo-free blocking solution(Vector)) for 1 h, prior to incubation with primary antibodies (see Supplementary Table) diluted in blocking buffer overnight at 4 °C. Samples were then washed with wash buffer and incubated with appropriate Alexa-Fluor-conjugated secondary antibodies (1:1,000, Life Technologies) and in blocking buffer for 1 h at RT. After wash and incubation with 4′,6-diamidino-2-phenylindole
(DAPI) at1 μg/ml for 5 min, samples were mounted with Fluoromount-G (SouthernBiotech) and coverslip (VWR). For EdU detection, the Click-iT reaction kit (Life Technologies) was used prior to incubation in DAPI according to manufacturer's recommendations.

Force measurement

In situ force measurements of TA muscles were conducted as previously described (Hakim et al., 2013, Rozo et al., 2016), and the data were analyzed using the 1300A Whole Animal System (Aurora Scientific). Mice were anaesthetized with isoflurane and placed on isothermal stage. Intact TA muscles were dissected and constantly immersed in Ringer's solution (homemade). Single twitch or tetanic contractions were elicited with electrical stimulations applied by two electrodes placed on either side of the muscle. In all experiments 0.2 ms pulses at 10 V supramaximal voltage were used. Muscle optimal length (Lo) that allows a maximum isometric twitch

force (*P*t) was determined by a series of twitch contractions with small variations of the muscle tension. To obtain maximum isometric tetanic force (*P*o), muscles were stimulated for 300 ms at different frequencies from 50 to 200 Hz. A 1 min recovery period was allowed between stimulations. Muscle wet weight and Lo were used to calculate the cross-sectional area (CSA) of the TA muscle for normalization to obtain specific isometric twitch force s*P*t (kN/mm^2) and s*P*o (kN/mm^2).

Single cell RNA-seq and analyses

Immediately following FACS isolation, young and aged MuSCs were counted by Countess II Automated Cell Counter (Thermo Fisher Scientific) and by hemocytometer manually for confirmation. GEMs were made using the Chromium Controller and libraries were made using the Chromium™ Single Cell 3' v2 Reagent Kit (10X Genomics) and sequenced on an Illumina NextSeq 500. The young and aged MuSCs were sequenced to a depth of 111 k reads/cell and 145 k reads/cell, respectively. Cell Ranger (v2.0.2) identified a median of 336 genes per cell and 716 UMIs per cell for the young MuSCs, and 175 genes per cell and 286 UMIs per cell for the aged MuSCs. Monocle (v2.6.3) (Qiu et al., 2017) was used for pseudotime analyses. The 292 genes that showed significant increase in cell fraction in late versus early MuSCs were generated by comparing cells in states right to node 2 versus those left to node 1, respectively, in Figure 2.2A. The 43 genes with more than 2-fold increase in cell fraction of late stages are in Table S1. DAVID 6.8 was used to perform gene ontology and KEGG pathway analyses using the 292 genes.

CHAPTER 3

Cellular/Molecular Mechanism of Gas1 in Muscle Stem Cell Aging

INTRODUCTION

The progress in high-throughput sequencing technology over the past ten years has made deep analysis of transcriptome possible for any tissue or cell type, which greatly advanced our knowledge in gene expression regulation of various biological processes. With the advanced deep sequencing techonolgy, many efforts have been made in the field of stem cell biology to decipher the mechanisms that govern important biological processes, including metabolism, development, and aging. For example, Rando's group used gene expression microarray analysis to elucidate the transcriptional profile of quiescent MuSCs and compared how it changes when stem cells activate during muscle regeneration after an acute injury (Liu et al, 2013). They also used ChIP-seq approach to obtain global epigenetic profiles of quiescent MuSCs and found epigenetic changes accumulate during aging and may lead to a functional decline. Rudnicki's group used microarray to compare the transcriptional profile of young and aged MuSCs and discovered that JAK-STAT signaling pathway is enriched in aged cells and the inhibition of this signaling could rescue the proliferation defect and ameliorates the engraftment potential of aged stem cells (Price et al, 2014). Also, by comparing the RNA-sequencing data from young and aged activated MuSCss, Rudolph's group showed that muscle stem-cell aging is induced by epigenetic stress responses via Hoxa9 developmental signals (Schworer et al, 2016).

Despite much progress towards understanding the myogenic programs of MuSCs has been made, the molecular pathways that regulate age-associated evolution of MuSC population remain incomplete. Here, I combined the comparison of overall transcriptome profiling and epigenetic profiling of H3K4 tri-methylation (H3K4me3) marks, which represent transcriptional activation, between young and aged quiescent MuSCs from control mice as well as from Gas1 gene-manipulated mice, i.e. young

Gas1EX and aged Gas1KO mice. My RNA-seq datasets provide another platform to visualize MuSC aging with regards to elucidating the molecular mechanism underlying age-associated stem cell intrinsic alterations. Importantly, I found that the transcriptional and H3K4me3 epigenetic landscape in young Gas1 pan-expressing MuSCs shows remarkable similarity to that in the naturally aged control MuSCs. Together with the stem cell property and functional phenotypes observed upon Gas1 pan-expression and depletion described in Chapter 2, these results indicate that increasing $Gas1^+$ MuSCs in young mice accelerates age-related transcriptome and epigenome changes that ultimately lead to functional decline.

RESULTS

Transcriptome and epigenome analyses reveal Gas1 as a driver for MuSC aging

MuSCs display transcriptome and epigenome changes during aging (Liu et al., 2013). However, previously reported transcriptome profiling data were mostly performed by microarray, and the data generated by different groups usually varied. In order to obtain a better understanding of the molecular mechanism underlying age-associated MuSC functional changes and investigate the role of Gas1 during the aging process, I independently performed mRNA sequencing (RNA-seq) supplemented with H3K4me3 ChIP sequencing (ChIP-seq) using MuSCs isolated by FACS. RNA-seq instead of microarray was used for generating transcriptome profiling because the former technique provides higher specificity and sensitivity, allowing for detection of transcripts low in abundance.

To gain an overall picture of natural MuSC aging, I first applied RNA-seq using young and aged control MuSCs FACS sorted based on four surface markers ($CD31^-$ $CD45^-Sca1^-Vcam^+$) and YFP reporter for Pax7 expression (Figure 3.1A). This gating

strategy is more stringent with the addition of the Pax7 reporter, and more relevant as a control for the following experimental groups that also used YFP as a reporter. Immunostaining after cytospin confirmed the purity of FACS sorted MuSCs (> 95%) (Figure 3.1B).

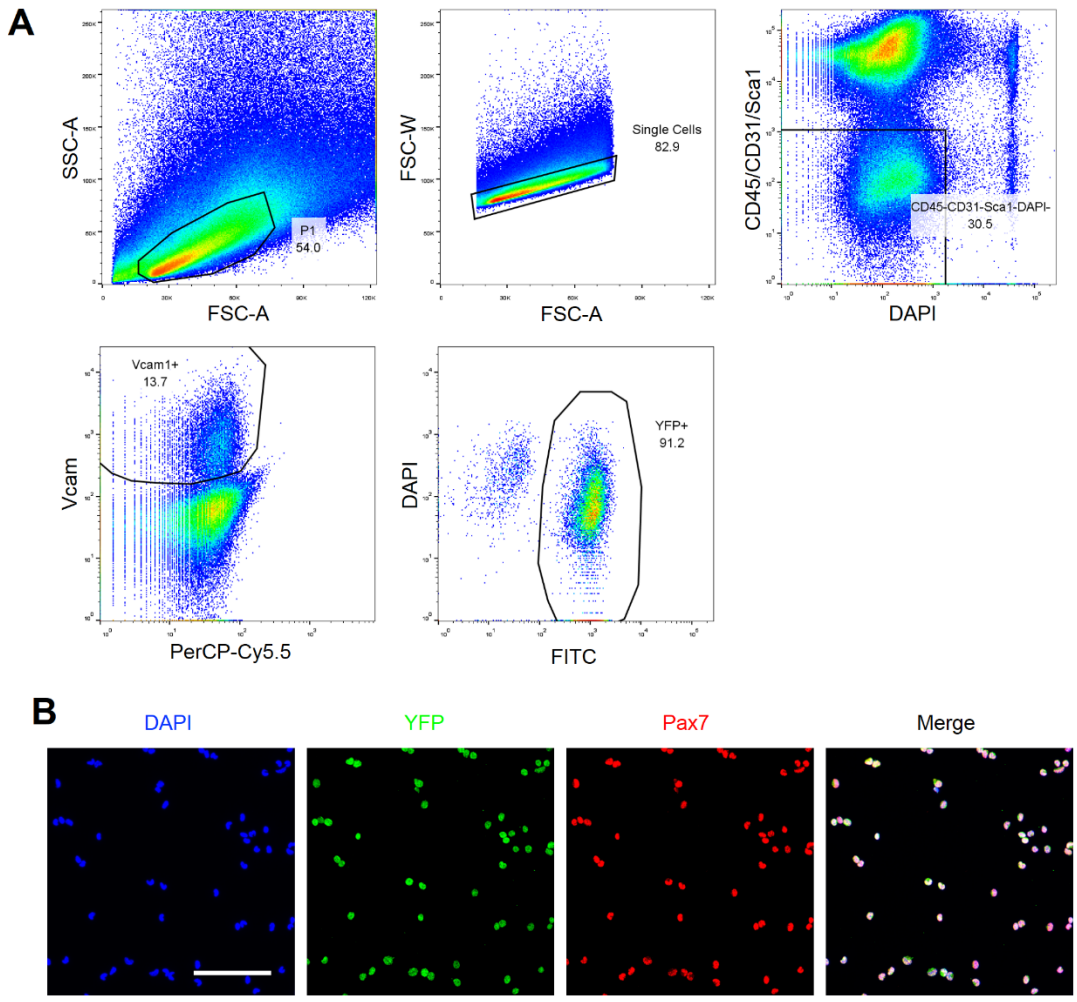

Figure 3.1. Isolating MuSCs based on 4 surface marker and Pax7 (YFP).

(A) FACS purification of MuSCs based on 4 surface markers ($CD45^{-}CD31^{-}Sca1^{-}Vcam^{+}$) and $R26^{YFP}$ reporter expression directed by $Pax7^{CE}$ and Tmx regimen. Representative FACS plots from Yng Ctrl MuSCs are shown. This sorting strategy is specifically used for RNA-seq and H3K4me3 ChIP-seq for Yng Ctrl, Yng Gas1EX,

Aged Ctrl and Aged Gas1KO MuSCs.

(B) Representative images for these sorted cells after cyto-spin and staining for Pax7 and YFP; ≥ 95% sorted single mononucleated cells are $Pax7^{+}YFP^{+}$ (n = 3 mice per group). Scale bars, 50μm.

RNA was isolated from freshly sorted cells of each group and then subjected to poly-A selection and RNA-seq cDNA library preparation. The RNA-seq results from three biological replicates of young and aged control MuSCs were obtained via sequencing the libraries at an average of 30 million read pairs. For each annotated gene in the dataset, RPKM of young and aged control MuSCs were compared. Most transcripts were expressed at equal levels, leading to a diagonal distribution in the plot (Figure 3.2A). I next determined which genes were differentially expressed between young and aged control MuSCs. There were 1,556 differentially transcribed genes with at least a 2-fold change. Of these, 854 were higher in the young control profile and 702 were higher in the aged control profile (Figure 3.2B), with adjusted false discovery rate (FDR) < 0.05 and p value < 0.05. These differentially expressed (DE) genes were subjected to unsupervised hierarchical clustering and resulted in two major clusters (Figure 3.2C). Visualized pathway network using data generated by gene set enrichment analysis (GSEA) showed that there was a high enrichment in the aged control group for transcripts whose products are involved in inflammatory response. In contrast, the most enriched down-regulated pathways in the aged control group are centered on cell cycle regulation (Figure 3.2D). These data fit well with previously reported observations that aged cells are featured by dysfunction in cell cycle checkpoints (which leads to cellular senescence) and increased inflammatory reactions (inflamm-aging). Overall, the differential gene expression between aged and young control MuSCs should serve as MuSCs aging-related gene sets.

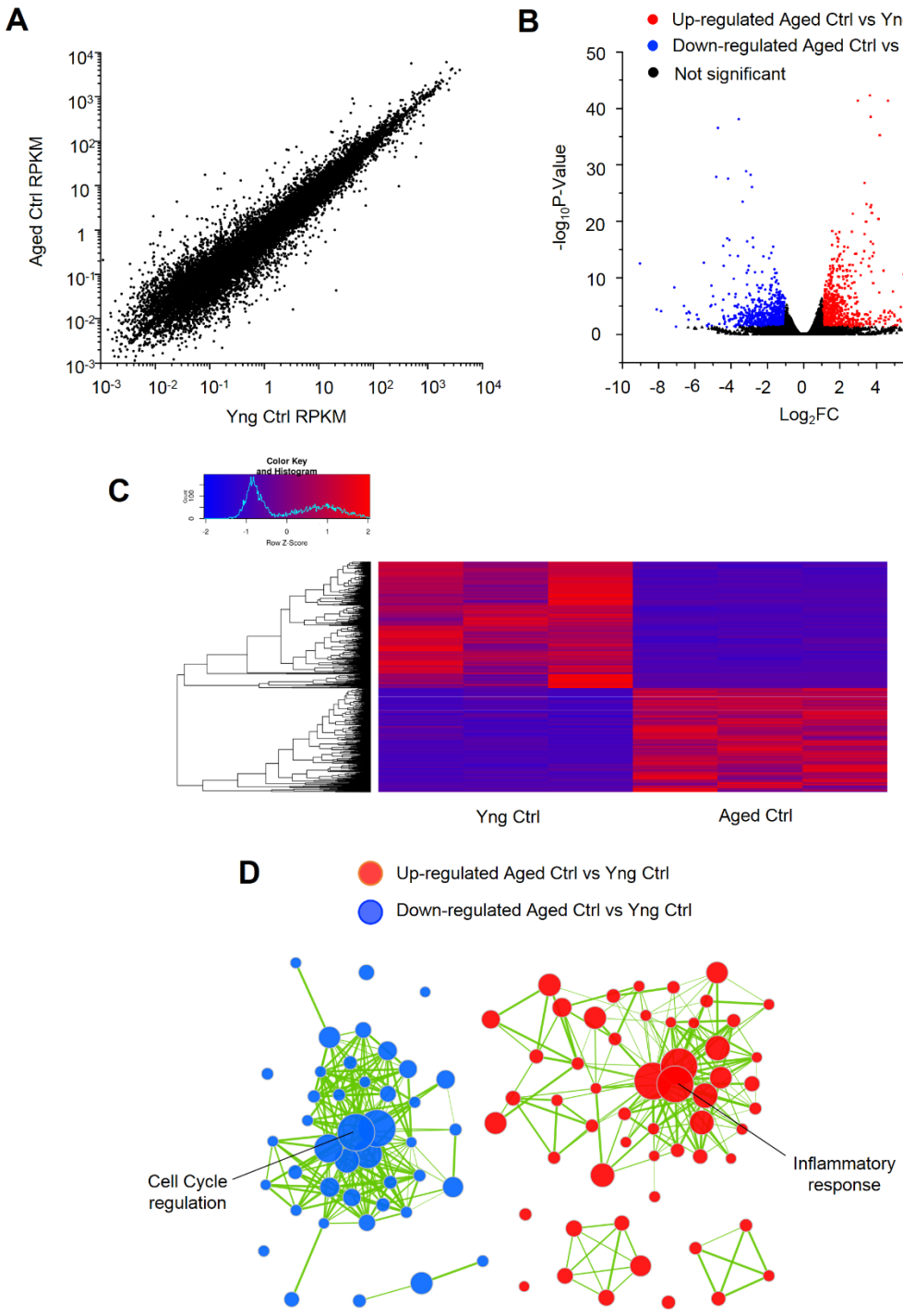

Figure 3.2. RNA-sequencing of Yng Ctrl and Aged Ctrl MuSCs.

(A) Scatterplot comparing the expression level of mRNA from Yng Ctrl to Aged Ctrl MuSCs. The average expression from three biological replicates is shown for each gene. (B) Volcano plot comparing Yng Ctrl and Aged Ctrl MuSCs transcriptomes. Each dot

represents a gene. Red dots represent genes that are more highly expressed in the Aged Ctrl transcriptome, while blue dots represent genes that are significantly higher in the Yng Ctrl transcriptome (FDR < 0.01 and log2 fold change ±2).

(C) Clustered heatmap of the gene expression profiles of Yng Ctrl and Aged Ctrl MuSCs. Three replicates were used for each sample.

(D) Plots displaying gene set enrichment. Differentially expressed genes (B) from Yng Ctrl and Aged Ctrl MuSCs were subjected to pathway analysis by gene set enrichment analysis (GSEA). The GSEA results are clustered by functional similarity and presented by scatterplot showing the visualized functional correlation using Cytoscape. Red circles represent pathways that are up-regulated in Aged Ctrl MuSCs, whicle blue circles represent pathways that are down-regulated in Aged Ctrl MuSCs.

The development of ChIP-seq technology in recent years boosted our understanding of the epigenome of various cell types (Mikkelsen et al., 2007). Epigenetic integrity is an essential factor to maintain normal stem cell function during aging (Liu and Rando, 2011). I therefore assayed for the histone modification profiles of MuSCs and to assess whether the functional decline of MuSCs with age could be attributed to changes in the epigenome. In order to compare the epigenetic profiles of active promoter marker H3K4me3 between MuSCs in young and aged mice, I isolated MuSCs from young and aged control mice in the same way as described before in the RNA-seq section to perform ChIP-seq analysis. The data showed similar result to the reported feature: most genes that were marked by H3K4me3 at their transcription start sites (TSSs) in MuSCs from young control mice retained the mark with age. There is a general down-regulation of the normalized H3K4me3 marker intensity around TSSs (Figure 3.3A and B). By comparing the H3K4me3 ChIP-seq results to the RNA-seq data in aged MuSCs, the up-regulated gene groups had increased H3K4me3 levels at their respective promoters, while the down-regulated gene groups had decreased levels (Figure 3.3C); an example for the *Ret* locus is shown (Figure 3.3D). For those DE genes that show no corresponding changes between H3K4me3 and expression levels, post-transcriptional regulation is likely at play.

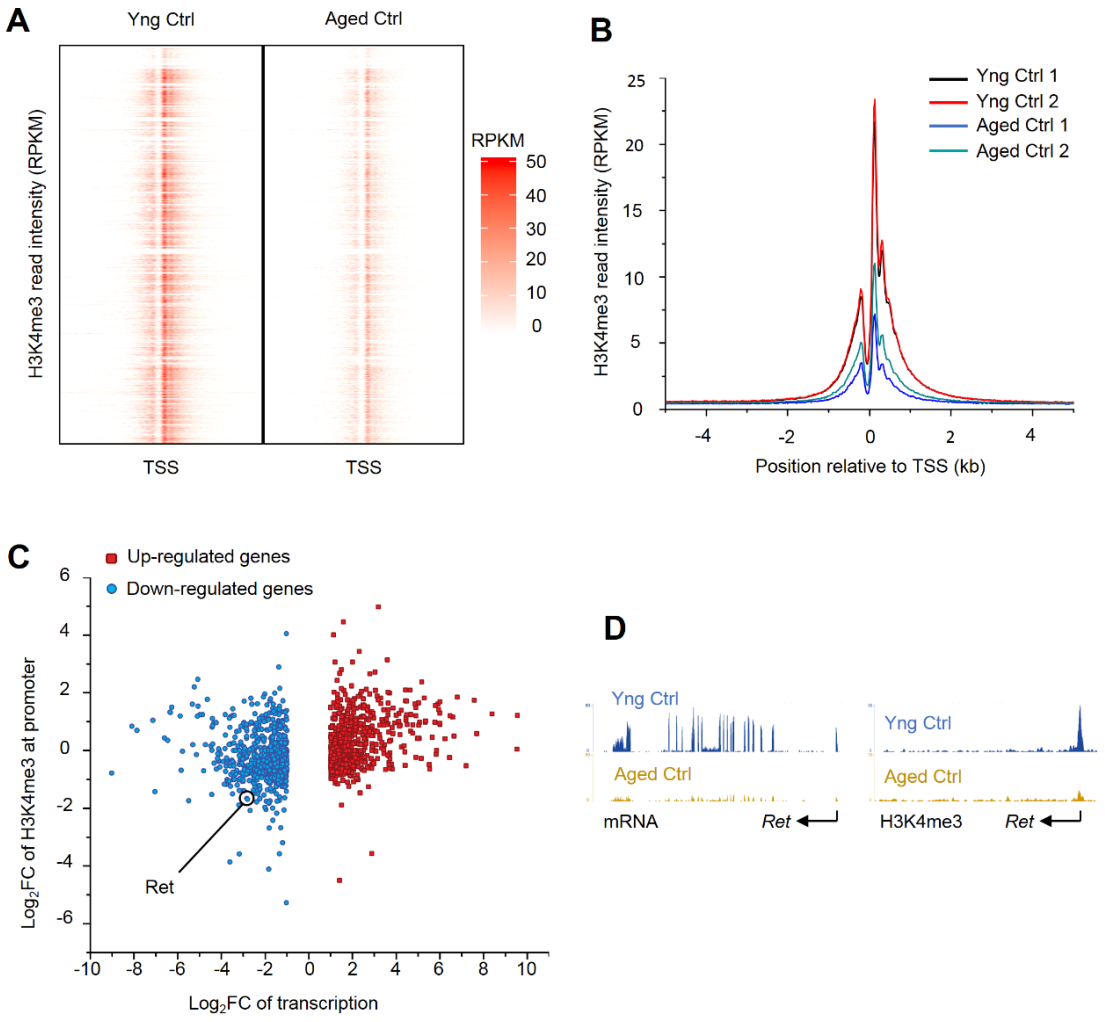

Figure 3.3. ChIP-sequencing of Yng Ctrl and Aged Ctrl MuSCs.

(A) Represented H3K4me3 intensity plot at TSSs in Yng and Aged Ctrl MuSCs across the entire genome.

(B) Averaged H3K4me3 read intensity at TSSs in Yng and Aged Ctrl MuSCs. Two replicates were shown for each group.

(C) Volcano plots for association between changes in transcription and promoter H3K4me3 mark in Aged and Yng Ctrl MuSCs, derived from means of three RNA-seq and two ChIP-seq biological replicates.

(D) RNA-seq (left) and H3K4me3 ChIP-seq (right) tracks from Yng Ctrl and Aged Ctrl MuSCs at the *Ret* locus.

In order to investigate the gene expression changes underlying the functional alterations in young Gas1EX and aged Gas1KO MuSCs, I applied the same FACS-purification strategy using MuSCs of these experimental groups and performed RNA-seq profiling to examine whether the transcriptomes of young Gas1EX and aged Gas1KO MuSCs show aging and rejuvenating signatures, respectively. Multidimensional scaling (MDS) segregates young and aged control MuSC transcriptomes far apart. Whereas, the MuSC transcriptomes from young Gas1EX and aged Gas1KO mice are grouped between the young and aged controls along the x-axis, but separated from each other along the y-axis (Figure 3.4A). Significantly, 93 of 120 up-regulated genes and 131 of 158 down-regulated genes in young Gas1EX MuSCs (compared to the young control) overlap with the aging-related DE gene sets (Figure 3.4B), supporting the similarity between young Gas1EX and aged MuSCs. When aged control is compared to aged Gas1KO, the overlap with aging-related gene set is also significant, supporting that Gas1KO transcriptome is of younger signature. Given that young Gas1EX and aged Gas1KO MuSCs encounter niche environment and physiological parameters that differ from the aged and young control MuSCs, respectively, their incomplete transcriptome transformation is not surprising.

I found a strong correlation between young Gas1EX and aged control MuSCs by GSEA (Figure 3.4C). In particular, as the two of the most featured differentially regulated pathways in young and aged control groups, inflammatory response genes associated with aging were found to be enriched in young Gas1EX MuSCs; dysregulation of cell cycle genes was also found. Next, I classified DE analysis into categories that are hallmarks of aging (Lopez-Otin et al., 2013) (Figure 3.4D) and found many MuSC aging-related genes overlapping with those altered in young Gas1EX and/or aged Gas1KO MuSCs. In addition to inflammation and cell cycle categories,

genes in the extracellular signaling, nutrient sensing, and cell adhesion categories are represented. Several genes or pathways previously implicated in systemic or MuSC aging were found, e.g. IGF1 (Holzenberger et al., 2003) and Fibronectin (Fn1) (Lukjanenko et al., 2016). Thus, pan-expression of Gas1 in young MuSCs replicates aspects of molecular signature of naturally aged MuSCs.

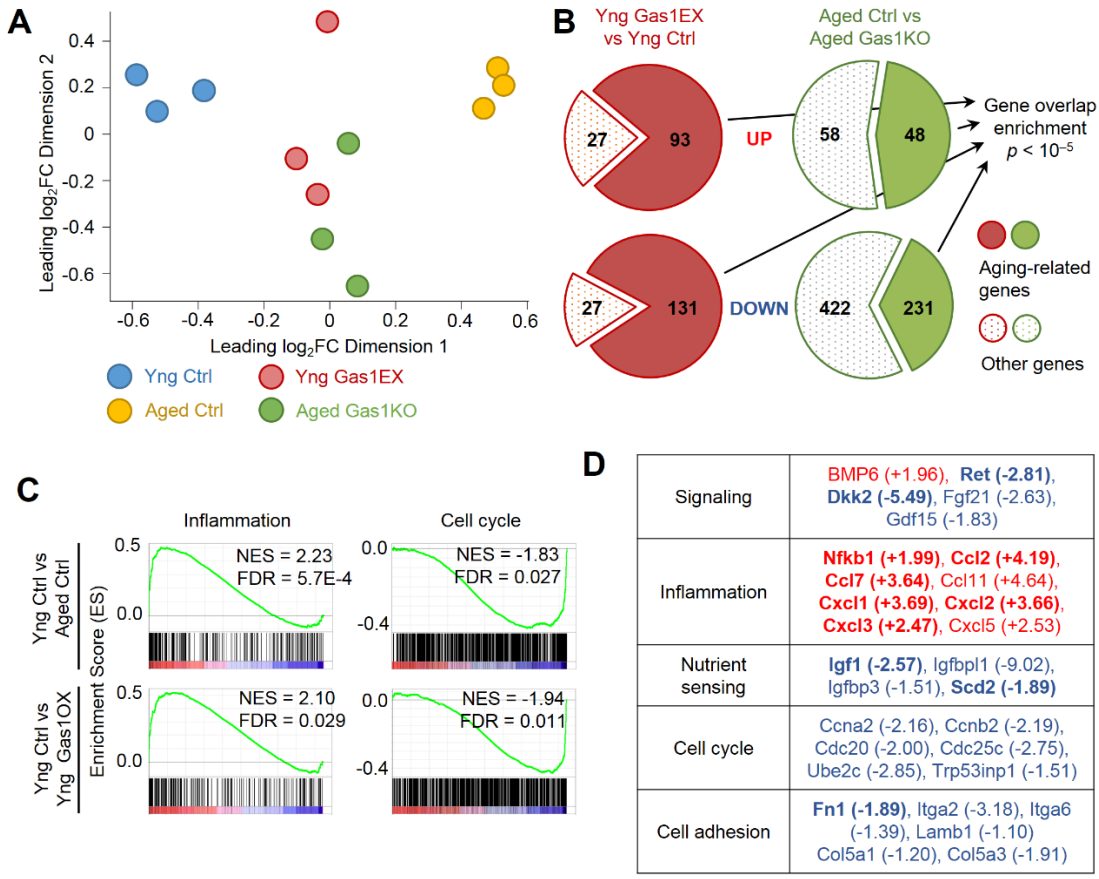

Figure 3.4. Gas1 mouse models display age-associated molecular signatures of MuSCs.

(A) Multidimensional scaling (MDS) plot of transcriptomes of Yng Ctrl, Aged Ctrl, Yng Gas1EX, and Aged Gas1KO MuSCs.

(B) Pie charts for Yng Gas1EX versus Yng Ctrl and Aged Ctrl versus Aged Gas1KO summarize up and down DE genes; aging-related genes in darker shades. Aging-related genes were derived from comparison of Aged Ctrl versus Yng Ctrl. Data were derived

from mean of 3 biological replicates; $P < 10^{-5}$; hypergeometric test.

(C) Enrichment for inflammation and cell cycle gene sets by GSEA comparison of Yng Ctrl to Aged Ctrl (top) and Yng Ctrl to Yng Gas1EX MuSCs (bottom).

(D) Aging hallmark categories for selected DE genes in Aged Ctrl versus Yng Ctrl MuSCs. Log_2FCs are indicated; up-regulated in red and down-regulated in blue. DE genes in bold overlap with both Yng Gas1EX versus Yng Ctrl and Aged Ctrl versus Aged Gas1KO comparisons. Genes not in bold overlap with one of the above two comparisons.

Single-cell RNA-sequencing data can be used to define Gas1-co-regulated genes during aging

One of the major challenges in biological science is to map the genotype to phenotypes. Conducting transcriptional profiling analysis provides great insights for addressing this question. Although every cell in an organism share identical genotypes, transciptome profile in any particular cell may only reflect the activation of a subpopulation of genes. Conventional bulk population sequencing, however, could only present the average expression profiling of an ensemble of cells. But there are increasing evidence suggesting that gene expression is heterogeneous, even for an overall homogeneous cell population. The subtle differences in a heterogeneous cell population may be important to determine the biological process, like cell fate decisions and adaptability to environmental changes. In order to further understand the stochastic biological processes, establishing the transcriptome profiles for each individual cells may provide more details and unveil subtle diversities of gene expression, which could be critical to promote advantageous or detrimental status of the entire cell population.

Single-cell RNA sequencing (scRNA-seq), a novel RNA-seq technique that focused on demonstrating transcriptional profiles of individual cells, shed new light on revealing the regulatory relationships between genes in complex cell populations (Patel et al., 2014). To better understand the heterogeneous to homogeneous Gas1 expression in MuSCs during aging, I sought to find genes whose temporal expression matches Gas1 using the 10X Genomics scRNA-seq platform. To obtain a gene set that covaries with Gas1, I leveraged heterogeneous Gas1 expression in young MuSCs to train the data set by Monocle 2 supervised machine learning (Figure 3.5A). A cohort of 18 genes was uncovered to parse young MuSCs into 7 states – with one state highly enriched for Gas1. This cohort was used to order aged MuSCs and Gas1 was found in all aged states.

Fos and Hspb1 in this cohort are expressed in more aged MuSCs (Figure 3.5A to D), and indeed they have been suggested as indicators for MuSC activation (Price, F. D., et al., 2014) and aging (Cosgrove, B.D., et al., 2014), respectively. While they are not as ubiquitously expressed in aged MuSCs as Gas1, their increases likely reflect the propensity for breaking quiescence of aged MuSCs. Thus, the scRNA-seq data can be used to parse out a Gas1-cohort whose expression trends towards a larger proportion in aged MuSC population. These genes may be collectively used as aging indicators for MuSC, with Gas1 expression prefiguring and becoming homogeneous in aged MuSCs. Also, of the cohort, Fos^{+} and $Hspb1^{+}$ MuSC fractions increase not only in aged, but also in Gas1EX mice (Figure 3.5E to G), lending support to the latter as models for MuSC aging.

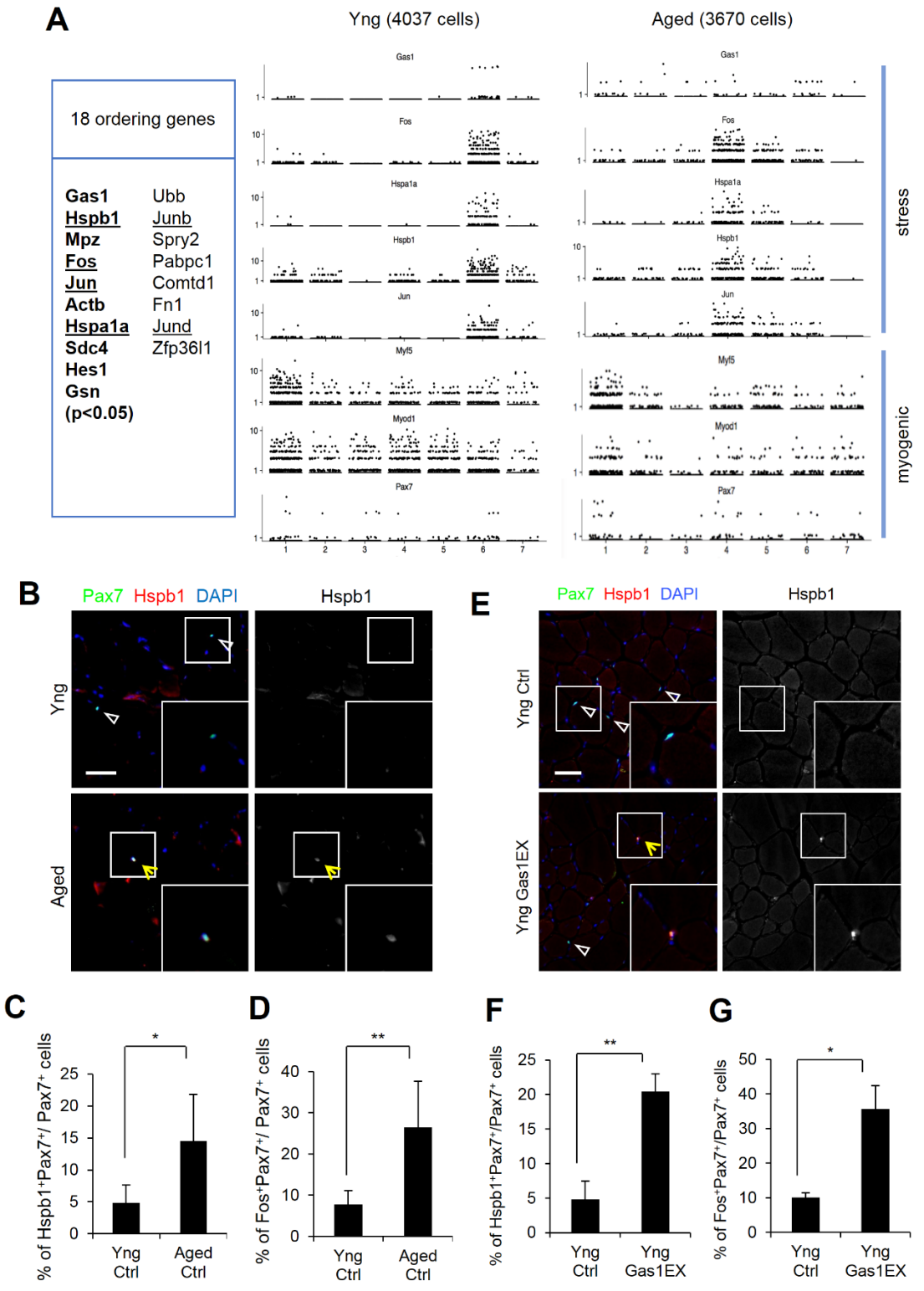

Figure 3.5. Single cell RNA-seq from young and aged MuSCs revealed Gas1 is associated with stress-genes.

(A) Single cell RNA-seq was performed using young or aged FACS sorted MuSCs. Left: List of 18 ordering genes from young Gas1-expression ($Gas1^+$) enriched cluster; right: sub-populations from young and aged MuSC demonstrating the expressions of Gas1, stress-related genes, and myogenic genes. Machine learning analysis in aged samples was based on the same criteria from young ones using the 18 ordering genes. Representative result from two independent replicates is shown.

(B) Staining of Yng and Aged wild-type TA muscle sections for Hspb1. Scale bars, 50 μm.

(C) Percentages of $Hspb1^+Pax7^+$ in total $Pax7^+$ MuSCs from Yng and Aged wild-type TA muscles using data (B) (n = 3 animals per group, ten sections per animal).

(D) Percentages of Fos^+Pax7^+ in total $Pax7^+$ MuSCs from Yng and Aged wild-type TA muscles (n = 3 animals per group, ten sections per animal).

(E) Staining of Yng and Yng Gas1EX TA muscle sections for Hspb1. Scale bars, 50 μm.

(F) Percentages of $Hspb1^+Pax7^+$ in total $Pax7^+$ MuSCs from Yng and Yng Gas1EX TA muscles using data (E) (n = 3 animals per group, ten sections per animal).

(G) Percentages of Fos^+Pax7^+ in total $Pax7^+$ MuSCs from Yng and Yng Gas1EX TA muscles (n = 3 animals per group, ten sections per animal).

Data are mean ± s.d.; $*P < 0.05$; $**P < 0.01$; two-sided unpaired t-test (C, D, F and G).

DISCUSSION

In this chapter, I present genome-wide transcriptome and H3K4me3 epigenome profiling for MuSCs from young and aged control as well as Gas1 manipulated mouse models. The FACS sorting strategy combining four surface markers and the Pax7 driven YFP enabled a stringent isolation of pure MuSCs and also ensured the expression of Cre-driven Gas1 gene manipulations. The comparison of the global transcriptional comparison between young and aged control samples provided informative datasets for discovering genes differentially expressed in muscles stem cells influenced by aging. Further comparison by incorporating Gas1 pan-expressing and knock-out datasets helped to narrow down the altered genes that plays a role in MuSC aging and correlated to Gas1's function. The GSEA pathway analysis revealed a significant enrichment of up-regulated inflammatory response and down-regulated cell cycle regulation in naturally aged MuSCs. These are consistent with previous findings in the field (Smythe et al., 2008; Shavlakadze et al., 2010; Lopez-Otin et al., 2013). In addition to these two major changes, I was also intrigued by the transcriptional and epigenetic changes of the receptor tyrosine kinase proto-oncogene *Ret*. It is a known receptor for neurotrophic factor GDNF and its function has been illustrated in neural system as well as other tissues or cell types, such as hematopoietic stem cells (Fonseca-Pereira et al., 2014), but it's not clear whether it plays a role in regulating MuSCs. According to the findings from my deep sequencing analysis, I next utilized conditional knock-out mouse model, combined with biochemistry and in vitro/ex vivo assays to investigate the function of Ret in MuSCs and elucidate its relationship to Gas1 in Chapter 4.

Single cell RNA-sequencing technology offers new avenues for discovering cellular and systemic compositional distinctions of a complex cell group. In addition to

tackling the spatial diversity, it is also tempting to utilize this approach to unveil the temporal alterations within a relatively similar population. Here I used scRNA-seq to investigate the changes of MuSCs that occur during aging, and found that Gas1 and its co-regulated gene cohort (e.g Fos) likely form a molecular basis for the dynamic heterogeneity that links to aging tendency. I showed that, consisting with my in vivo and ex vivo immunostaining data, Gas1 expressing cells increased in aged MuSCs populations, compared with young ones. Of note, my bulk RNA-seq data did not reveal Gas1's changes between young and aged MuSCs, likely due to the overall relatively low expression in the aged MuSCs, albeit the expression becomes homogenous. It is intriguing that the differential expressed genes do not necessarily overlap between sc- and bulk RNA-seq data, suggesting that some subtle differences may be averaged out when using the whole population as input. Meanwhile, due to the relative shallow sequencing depths, some overall dissimilitude may not be able to be captured when generating transcriptomes at single cell level. Combining both approaches provide a more comprehensive view of changes in a relatively kindred population like MuSCs.

The progressive increase of $Gas1^{+}$ MuSCs reflects the protracted nature of aging, and indicates that stem cell aging is initiated in youth. As Gas1-expressing MuSCs become a homogeneous population over time, the muscle regeneration capacity wanes. Curiously, many genes, e.g. Gas1, Fos and Jun, whose expression was detected in more aged MuSCs by scRNA-seq did not show up-regulated levels in my bulk RNA-seq data. Whereas, Ret showed decreased expression in aged MuSCs by RNA-seq, but was not detected by scRNA-seq in MuSCs of either age. The lists of up-regulated genes during MuSC aging between published microarrays (Liu et al, 2012, Price et al., 2014) and my bulk RNA-seq also show differences. While each platform has pros and cons, they are together powerful to screen for molecular changes from different perspectives.

It will be interesting to determine if other aging-associated genes identified by scRNA-seq act in concert with Gas1 to suppress Ret signaling, or act to enhance Wnt (Brack et al., 2007), Tgfβ (Carlson et al., 2008), or FGF2 (Chakkalakal et al., 2012) signaling, to drive MuSC aging.

MATERIALS AND METHODS

Mice

The *Pax7*$^{cre\text{-}ERT2}$ (referred to as *Pax7*^{CE} in legends; B6;129-*Pax7*$^{tm2.1(cre/ERT2)}$*Fan*/J) mice (Lepper et al., 2009), and *Gas1*^{flox} mice (Jin et al., 2015) have been described. The *R26*^{YFP} (B6.129X1-*Gt*(*ROSA*)*26Sor*$^{tm1(EYFP)}$*Cos*/J) mice (Srinivas et al., 2001) was obtained from the Jackson Laboratory (JAX). Whenever YFP was included for assay, the *R26*^{YFP} allele was included in the background for Pax7^{+} MuSC lineage marking. The Gas1 conditional pan-expression (Gas1EX) allele, *R26*$^{CAG\text{-}Gas1}$, is generated for this work.

For young versus aged comparisons, mice were used at 2–3 month of age (young) or 18–24 month of age (aged). Sex was mixed. Animal experiments in this study were performed following the ethical regulations by Office of Laboratory Animal Welfare (OLAW), and in accordance with protocols approved by the Institutional Animal Care and Use Committee (IACUC) of the Carnegie Institution for Science (Permit number A3861-01).

Tamoxifen regimen

Tamoxifen was prepared and administered as described (Methods, Chapter 2).

MuSC isolation by FACS and myoblast culture

MuSCs were isolated as described (Methods, Chapter 2). For surface maker labeling, cell were incubated with DAPI and fluorophore-conjugated antibodies against CD45, CD31, Sca-1 and Vcam, at 4 °C for 0.5 h. After wash, cells were subjected to fluorescence-activated cell sorting (FACS) using the ARIA III (BD Biosciences).

Isolated mononuclear MuSCs were collected in Trizol (Thermo Fisher Scientific) for RNA-seq (see below), in F-10 with 10% horse serum (HS) for ChIP-seq (see below), cytospun for immunostaining.

Immunostaining

TA muscle sections or cytospun MuSCs were fixed for 10 min in 4% paraformaldehyde, permeabilized with 0.1% Triton X-100 (Sigma)/PBS for 10 min at room temperature (RT), rinsed with wash buffer (0.05% Triton-X 100/PBS), treated with blocking buffer (10% Normal Goat Serum (Genetex) and 1× carbo-free blocking solution(Vector)) for 1 h, prior to incubation with primary antibodies (see Supplementary Table) diluted in blocking buffer overnight at 4 °C. Cells were then washed with wash buffer and incubated with appropriate Alexa-Fluor-conjugated secondary antibodies (1:1,000, Life Technologies) and in blocking buffer for 1 h at RT. After wash and incubation with 4′,6-diamidino-2-phenylindole (DAPI) at 1 μg/ml for 5 min, samples were mounted with Fluoromount-G (SouthernBiotech) and coverslip (VWR).

RNA-seq and analysis

For each condition, 30,000 of fresh isolated MuSCs by FACS were lysed in Trizol reagent. RNA was isolated using the Direct-zol RNA Kit (Zymo). cDNA was generated and amplified using TruSeq RNA Library Preparation Kit v2 (Illunima) and amplified with ThruPLEX DNA-seq Kit (Takara).

Sequencing was carried out on an Illumina Nextseq-500 to generate single-ended 75 bp reads, which were aligned to the mouse genome (mm9) using TopHat (v2.1.0). Expression measurement of each gene was calculated from the resulting

alignment bam file by HTseq against the GENCODE annotation vm1. Differentially expressed genes were determined using edgeR with FDR cutoff of 0.05. MDS-plots were also generated using the edgeR package. GSEA (Subramanian et al., 2005) analysis was performed using ranked fold change values with hallmark gene sets database (h.all.v6.2.entrez.gmt).

ChIP-seq and analysis

Low-input ChIP-seq for fresh isolated MuSCs by FACS was performed following the previously described protocol (Zheng et al., 2015) with slight modifications. For each condition, 30,000 MuSCs were fixed with 1% formaldehyde/PBS for 10 min at RT, before quenching the reaction with 1/20 volume of 2.5 M glycine for 5 min at room temperature and mixing with ~5 × 10^8 DH5α *E.coli* (as carrier). Cell lysis, chromatin isolation and digestions were done using the EZ Nucleosomal DNA Prep Kit (Zymo) followed by further chromatin shearing and releasing using Bioruptor Pico (Diagenode) with 6 cycles of 30 s on/off sonication. The immunoprecipitations were performed using anti-H3K4me3 antibody (EMD Millipore, 07-473, 1:1,000) at 4 °C overnight. The immunoprecipitated DNA was then bound to Protein G Dynabeads (Thermo Fisher Scientific) for 2 h at 4 °C, followed by serial washes, proteinase K digestion, and purification by DNA Clean & Concentrator kit (Zymo). DNA libraries were prepared using ThruPLEX DNA-seq Kit (Takara) and sequenced on an Illumina Nextseq-500 to generate single-ended 75bp reads.

ChIP-seq reads were aligned to mouse genome (mm9) using Bowtie (version 1.1.2). 2 mismatches were allowed for the alignment and only uniquely mapped reads were allowed (parameters -v 2 -m 1). Promoter correlations for H3K4me3 enrichments are plotted as log2 of the average read density within 2 Kb up and downstream of TSS.

H3K4me3 peaks were called by MACS V1.4 with *p*-value threshold of 10^{-5}. The parameters are all default.

Single cell RNA-seq and analyses

Immediately following FACS isolation, young and aged MuSCs were counted by Countess II Automated Cell Counter (Thermo Fisher Scientific) and by hemocytometer manually for confirmation. GEMs were made using the Chromium Controller and libraries were made using the Chromium™ Single Cell 3' v2 Reagent Kit (10X Genomics) and sequenced on an Illumina NextSeq 500. The young and aged MuSCs were sequenced to a depth of 111 k reads/cell and 145 k reads/cell, respectively. Monocle (v2.6.3) (Qiu et al., 2017) was used for supervised machine learning and the generation of the distribution plots.

CHAPTER 4

Ret-GDNF Signaling in Muscle Stem Cell Aging

INTRODUCTION

Stem cell decline emerges as the integrative consequence of multiple types of damage, as well as the changes of different signaling pathways that govern normal biological processes. For instance, it is well known that stem cells lose self-renewal capacity with aging, and this contributes to their progressive decline over time. Maintenance at quiescence is one of the critical properties of MuSCs. Aberrant breaking of quiescence and spurious activation of dormant stem cell populations lead to their exhaustion. These abnormal cellular behavior could be attributed to the aging-related changes of important signaling pathways. The significance of stem cell quiescence for the long-term stability has been illustrated in MuSCs via investigating the fibroblast growth factor (FGF) signaling pathway. Brack's group showed that MuSC-specific deletion of Sprouty1, a FGF receptor inhibitor, in proliferating cells leads to constitutive activation of the extracellular-signal-regulated kinase/mitogen-activate protein kinase (ERK/MAPK) signaling pathway, which inhibit stem cell self-renewal (Shea et al., 2010). In line with this data, the same group further reported that aged MuSC niche has hyperactive FGF2 signaling, which gives rise to the breaking quiescence of stem cell and leads to the stem cell pool exhaustion, whereas targeted inhibition of this signaling pathway ameliorates the defects (Chakkalakal et al., 2012). Furthermore, Olwin's group showed that the aged MuSCs are desensitized to FGF2 signals under circumstances of muscle regeneration and have defects for proliferation or self-renewal, thus compromising the capacity for the muscle repair (Bernet et al., 2014).

On the other hand, extracellular signaling may affect other aspects of MuSC function including proliferation and differentiation. Age-related changes in local niche factors have been found to perturb regenerative capacity of MuSCs. In the aging skeletal muscle, increases in local TGF-β signaling have been reported to be coupled

with decreased expression of the Notch ligand Dl in the myofiber and decreases in deposition of the extracellular matrix protein fibronectin. These changes synergistically contribute to the loss of regenerative capacity, mostly by affecting musle stem cell function (Lukjanenko et al., 2016; Sousa-Victor et al., 2015). On the other hand, the p38 MAPK and the Janus kinase–Signal transducer and activator of transcription 3 (JAK/STAT3) signaling pathways have also been shown to lead to the loss of aging MuSCs after injury by affecting their proliferative expansion and self-renewal capacities (Cosgrove et al., 2014; Bernet et al., 2014; Tierney et al., 2014; Price et al., 2014). Altogether, signaling pathway differences result from niche alterations as well as cell-intrinsic changes are emerging as contributors that cause the age-dependent MuSC depletion and functional changes.

By conducting and analyzing my own RNA-seq and ChIP-seq datasets and comparing the young and aged control, and Gas1-genetically manipulated, MuSCs, I should be able to uncover Gas1-regulated pathway(s) that is crucial for MuSC aging and function. Indeed, I found that Ret, regulated by Gas1, is critical for MuSC self-renewal. Gas1 targets and represses Ret signaling across the aged stem cell population, thereby compromising their regenerative function. Importantly, GDNF, a ligand of Ret, can reverse the repression of Ret signaling by Gas1 to rejuvenate muscle regeneration and enhance MuSC renewal in aged muscles.

RESULTS

Ret is a downstream effector of Gas1 and required for MuSC self-renewal

Based on my RNA-seq and ChIP-seq data sets (Chapter 3), I identified Ret, a receptor tyrosine kinase (RTK) that mainly known as a neurotrophic factor sensor, to be negatively correlated with satellite cell aging, and negatively regulated by Gas1 pan-expression. Moreover, I was intrigued by reduced mRNA and H3K4me3 levels of *Ret* in aged control as well as young Gas1EX MuSCs (Figure 4.1A). *Ret* is a common signaling component for glial cell line-derived neurotrophic factor (GDNF) family of ligands, and plays many roles in the nervous system, including motor axon regeneration (Airaksinen et al., 2002). The role of Ret signaling in MuSC however has not been characterized.

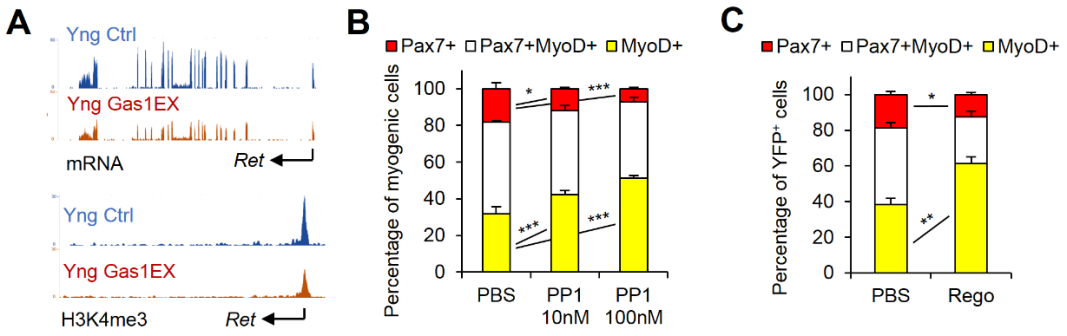

Figure 4.1. Ret is downstream of Gas1.

(A) RNA-seq (top) and H3K4me3 ChIP-seq (bottom) tracks from Yng Ctrl versus Gas1EX MuSCs at the *Ret* locus.

(B) Single myofibers isolated from Yng $Ret^{flox/flox}$ mice, cultured for 96 h with or without 1NM-PP1 (PP1, at specified concentrations), stained for Pax7 and MyoD, and quantified for their distributions (n = 3 mice; ≥ 20 myofibers per condition).

(C) Single myofibers from Yng Ctrl mice cultured for 96 h with or without Ret inhibitor Regorafenib (Rego, 10 nM), stained for Pax7 and MyoD, and quantified for myogenic

distributions (n = 3 mice; ≥ 20 myofibers per condition); PBS mock-treatment for control.

Data are mean ± s.d.; *$P < 0.05$; **$P < 0.01$; ***$P < 0.001$; by two-way ANOVA (B and C).

To elucidate the role of Ret in MuSC, I first utilized an engineered conditional Ret allele (Ret^{flox}) with a modification in the kinase domain that allows for selective binding and inhibition (Luo et al., 2007). Exons 14 and 15 are flanked by loxP sites in this Ret^{flox} targeted mutant strain. A V805A mutation in exon 15 is functionally silent, but sensitizes the protein to chemical inhibition of its kinase activity and the signaling could be blocked by 1NM-PP1. Cre-mediated excision of the floxed region results in a knockout allele. By applying 1NM-PP1 in the culture condition for single myofiber ex vivo assay, I examined the effect of inhibiting Ret signaling on myogenic cell fate of MuSCs from $Ret^{flox/flox}$ mice. The result showed that 1NM-PP1 decreased self-renewal and increased differentiation of MuSCs ex vivo via the single myofiber culture assay, compared to mock-treated controls (Figure 4.1B), according to the diminished $Pax7^{+}MyoD^{-}$ fraction and the expanded $Pax7^{-}MyoD^{+}$ population. Regorafenib (Wilhelm et al., 2011), a broad-spectrum RTK inhibitor which also targets Ret, yielded a similar result (Figure 4.1C). These data suggest Ret signaling has beneficial effect for MuSC normal function, and inhibiting this pathway may lead to compromised stem cell self-renewal and regeneration capacity.

To assess the role of Ret signaling in MuSCs in vivo, I inactivated *Ret* specifically in young $Pax7^{+}$ MuSCs by combining the $Pax7^{CE}$ allele with the conditional Ret allele Ret^{flox} (Luo et al., 2007), resulting in the compound conditional Ret knock-out mice $Pax7^{CE/+}Ret^{flox/flox}R^{YFP}$ (hereafter referred to as 'RetKO', Figure 4.2A). Similar to young Gas1EX, I observed a declined MuSC number from homeostatic young RetKO TA muscles after Tmx regimen. (Figure 4.2B and D). After muscle injury introduced by CTX, RetKO mice were defective in regeneration as reflected by reduced muscle fiber size (Figure 4.2E and F). Furthermore, both muscle injury and single myofiber culture assay revealed a reduction in $Pax7^{+}$ cells (Figure 4.2C and D; Figure

4.2G), indicating that knocking out Ret compromises satellite cell self-renewal. RNA-seq data from purified young RetKO MuSCs also manifested resemblance to aged control samples (Figure 4.2H). Altogether, these data showed that the RetKO phenotype is similar to that of the Gas1EX, and suggest that reduced level of *Ret* in Gas1EX MuSCs contributes to their dysfunction.

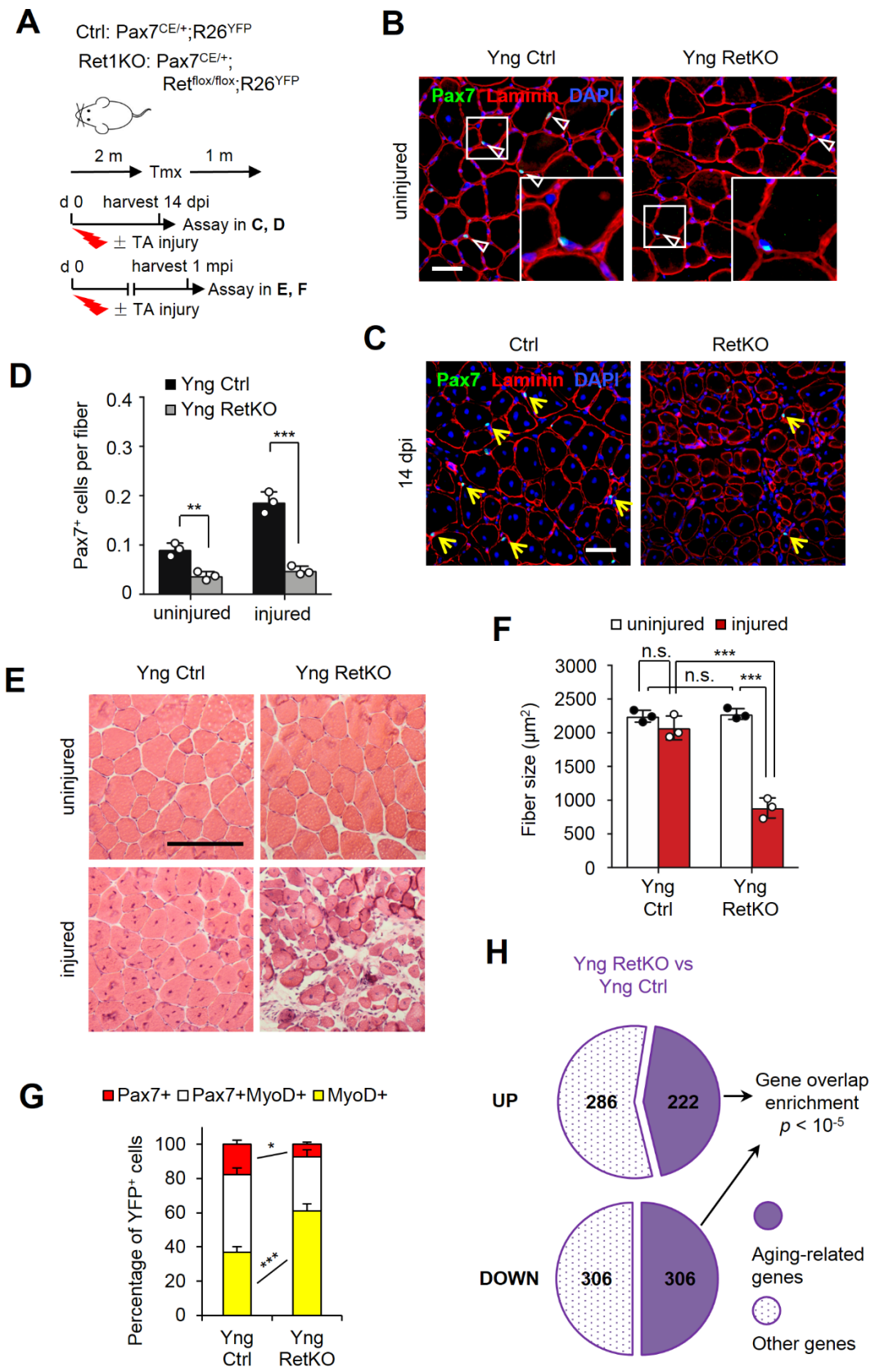
A
Ctrl: Pax7CE/+;R26YFP
Ret1KO: Pax7CE/+;
Retflox/flox;R26YFP
2 m
Tmx
1 m
d 0
harvest 14 dpi
Assay in C, D
± TA injury
d 0
harvest 1 mpi
Assay in E, F
± TA injury
B
Yng Ctrl
Yng RetKO
uninjured
Pax7 Laminin DAPI
C
Ctrl
RetKO
14 dpi
Pax7 Laminin DAPI
D
Yng Ctrl
Yng RetKO
Pax7+ cells per fiber
0.4
0.3
0.2
0.1
0
**
***
uninjured
injured
E
Yng Ctrl
Yng RetKO
uninjured
injured
F
uninjured
injured
Fiber size (µm2)
3000
2500
2000
1500
1000
500
0
n.s.
***
n.s.
***
Yng Ctrl
Yng RetKO
G
Pax7+
Pax7+MyoD+
MyoD+
Percentage of YFP+ cells
100
80
60
40
20
0
*
***
Yng Ctrl
Yng RetKO
H
Yng RetKO vs
Yng Ctrl
UP
286
222
Gene overlap
enrichment
p < 10-5
DOWN
306
306
Aging-related
genes
Other genes

Figure 4.2. Ret is required for MuSC self-renewal.

(A) Experimental schemes for Yng Ctrl and RetKO mice by $Pax7^{CE}$-directed, Tmx-induced expression; + and – indicate with and without injury, respectively, to the TA muscle. The $R26^{YFP}$ reporter allele was included for cell marking.

(B and C) Representative images of Pax7 (green) and Laminin (red) staining of Yng Ctrl and RetKO TA muscle sections under uninjured (B) and 14 days post injury (dpi) (C) status as specified in (A). Scale bar, 50 mm.

(D) Averaged $Pax7^{+}$ MuSCs per fiber for uninjured and injured muscles as specified in (B and C) (n = 3 mice per group; 10 sections per mouse).

(E) Representative images of muscle sections stained with H&E for Yng Ctrl and RetKO mice as specified in (A). Scale bar, 150 mm

(F) Averaged fiber size from data in (E) (n = 3 mice per group; 10 sections per mouse).

(G) Yng Ctrl and RetKO single myofibers cultured for 96 h, stained for Pax7 and MyoD, and quantified; myogenic cells are lineage-marked by YFP (n = 3 mice per group; ≥ 20 myofibers per mouse).

Data are mean ± s.d.; $*P < 0.05$; $**P < 0.01$; $***P < 0.001$; n.s., not significant; by two-way ANOVA (F and G) and multiple t-tests (D).

Gas1 negatively regulates Ret at the level of signaling

Gas1 was reported to bind to Ret and suppress its basal tyrosine (Y) phosphorylation level in two cell culture studies (Lopez-Ramirez et al., 2008; Biau et al, 2013), but not in another (Cabrera et al., 2006). In order to evaluate whether Gas1 regulate Ret signaling, I first confirmed that the Ret signaling was activated in endogenous MuSCs by probing for phosphorylation of RetY905 (catalytic phosphorylation site) on freshly isolated MuSCs from young and aged wild-type mice. pRetY905 signals could be detected in young MuSCs and the phosphorylation level was down-regulated in age MuSCs (Figure 4.3A and B). A side-by-side FACS sorted muscle fibro/adipogenic progenitors (FAPs) used as control showed no obvious changes in pRetY905 level between young and aged samples.

To further determine whether Gas1 regulates Ret signaling in MuSCs, I probed for phosphorylation of RetY1062 (auto-phosphorylation site) on MuSCs from isolated single myofibers by immunofluorescent staining. The result showed that approximately 40% young control MuSCs were pRetY1062^{+}. By contrast, most young Gas1EX or aged control MuSCs were pRetY1062^{-} (Figure 4.3C and D), suggesting that Gas1 plays a role in the suppression of Ret signaling in the aged MuSC population.

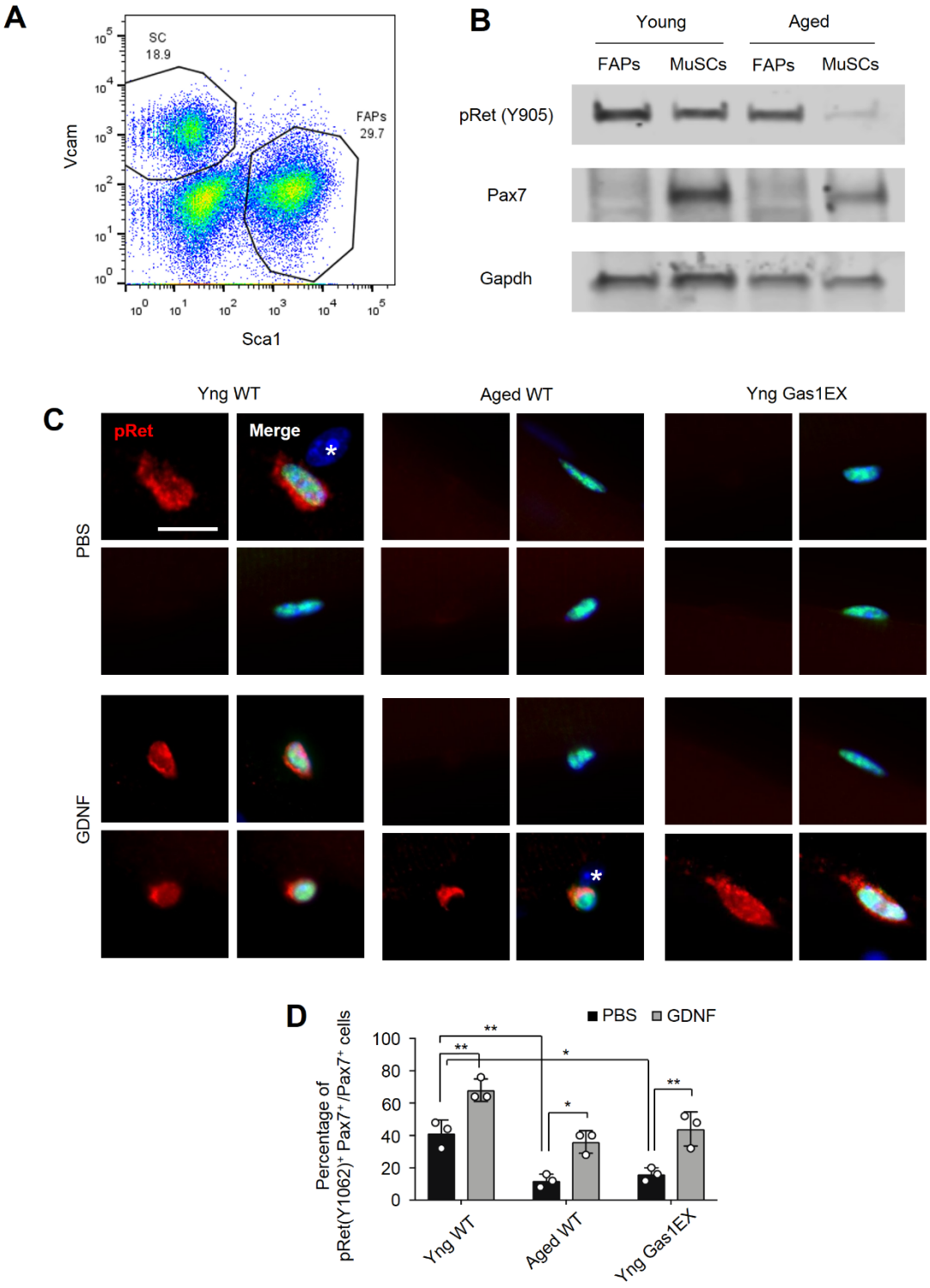

Figure 4.3. Ret is activated in young MuSCs and its signaling is dampened in aged MuSCs.

(A) FACS purification scheme of MuSCs and FAPs based on 4 surface markers ($CD45^-$ $CD31^-Sca1^-Vcam^+$) using wild type mice. Representative FACS plots from Yng wild

type (WT) are shown.

(B) Representative images of Western blotting showing protein expression of pRet (Y905) in MuSCs and FAPs from young and aged WT mice using strategy in (A).

(C) Representative images for MuSCs on single myofibers isolated from Yng WT, Aged WT, and Gas1EX mice, cultured for 24 h with PBS mock-treatment or GDNF (20 ng/ml), and stained for pRet (Y1062) (red), merged with Pax7 (green) and DAPI (blue). Two examples for each condition are shown; asterisk, myonuclei. Scale bar, 10 μm.

(D) Percentages of $Pax7^{+}pRet(Y1062)^{+}$ in total $Pax7^{+}$ MuSCs on SMs isolated from Yng or Aged wild-type (WT) or Gas1EX mice and cultured for 24 h with PBS or GDNF (20 ng/ml in PBS) (n = 3 mice per group; ≥ 20 myofibers per condition).

Data are mean ± s.d.; $*P < 0.05$; $**P < 0.01$; by two-way ANOVA (D).

Next, I went on to test whether Gas1 physically interacts with Ret. Proximity ligation assay (PLA) is a technique that allows for direct detection of protein-protein interactions with high specificity and sensitivity (Gullberg et al., 2004). Utilizing this approach, transient or weak protein-protein interactions can be visualized in situ. By PLA, close association between Gas1 and Ret was detected (as foci) in young and aged MuSCs and correlated with Gas1 expression (Figure 4.4A and B).

To further dissect the interactions between Gas1 and Ret, I generated a series of domain-deletion mutations of Gas1 to map the region that binds to Ret. Gas1 contains two cysteine-rich domains and a C-terminal region, and the domain-deletion mutants were designed accordingly (Figure 4.4C). Utilizing reciprocal co-immunoprecipitation, I confirmed that Gas1 can associate with Ret, and importantly, the association was abrogated only when the first cysteine-rich domain of Gas1 (domain 1) was deleted (Figure 4.4D). This result indicates that domain 1 is essential for Ret binding. It also implies that this domain, via binding to Ret, is necessary for Gas1 to impede MuSC self-renewal. To test this idea, I transiently transfected full-length Gas1 or the domain1-deleted mutant into MuSCs on young wildtype single myofibers and subjected them to ex vivo culture assay. Transient expression of full-length Gas1 in young MuSCs on the single myofibers was sufficient to reduce self-renewal and promote differentiation, similar to the young Gas1EX MuSCs phenotype. However, domain 1 deletion mutant of Gas1 had no obvious effect on myogenic cell fates (Figure 4.4E and F). Thus, these data indicate that Gas1's ability to reduce MuSC self-renewal relies on its Ret-interacting domain.

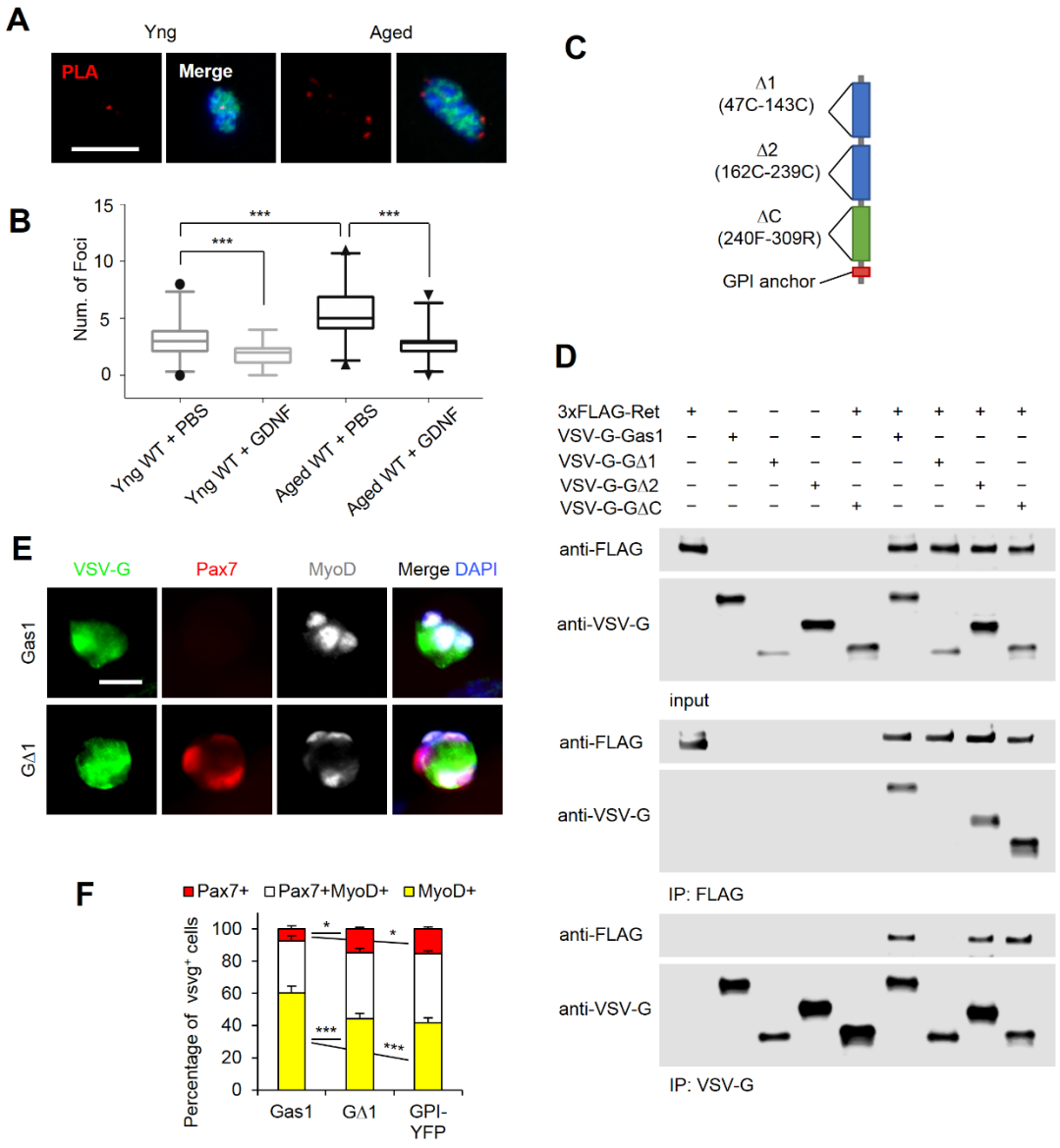

Figure 4.4. Gas1 binds Ret and inhibits its signaling.

(A) Representative images of Gas1:Ret PLA signals (red foci) for MuSCs on Yng or Aged SMs cultured for 24 h; Merge, PLA images merged with Pax7 (green) and DAPI (blue). Scale bar, 5 μm.

(B) Quantification of Gas1:Ret PLA foci number per MuSC in specified conditions (n = 3 mice per group; ≥ 20 myofibers per condition).

(C) Diagram for generating the serial domain-deletion mutations of Gas1.

(D) Reciprocal co-immunoprecipitations (co-IP) between 3xFLAG-tagged Ret and

VSV-G-tagged full-length and 3 domain-deleted Gas1s (diagrammed at bottom right) expressed in HEK293T cells. Input lysates and FLAG-IPed and VSV-G-IPed fractions are indicated.

(E and F) MuSCs on Yng WT single myofibers transfected with Gas1, Gas1 domain 1-deleted mutant (GΔ1), or GPI-YFP cultured for 96 h and stained for VSV-G tag (green), Pax7 (red), MyoD (gray), and DAPI (blue) (E), and quantified for their distribution (F) (n = 3 mice per group; ≥ 20 myofibers per condition). VSV-G-tagged GPI-YFP served as a control. Scale bar, 10 μm.

Data are mean ± s.d.; *$P < 0.05$; ***$P < 0.001$; by Kruskal-Wallis test (B) and two-way ANOVA (F).

GDNF can reverse the effect of Gas1 by activating Ret signaling

I next asked whether it is possible to reverse the negative effect of Gas1 on Ret signaling. GDNF is a natural ligand for the Ret-GFRα1 dimer (Airaksinen et al., 2002) and GFRα1 is the highest expressed GFRα member in MuSCs by RNA-seq. I first administered GDNF in the culture for isolated myofibers from young and aged $Pax7^{CE/+}R26^{YFP}$ control mice. Strikingly, for both young and aged single myofibers, application of GDNF resulted in a considerable increase of the $Pax7^{+}MyoD^{-}$ self-renewed fraction, at the expense of the $Pax7^{-}MyoD^{+}$ proportion that are destined for differentiation (Figure 4.5A and B). Importantly, Persephin (PSPN), a ligand for the Ret-GFRα4 dimer (Airaksinen et al., 2002), was used as a specificity control and showed no effect on myogenic cell fate of MuSCs on cultured single myofibers (Figure 4.5C), demonstrating the selectivity of GDNF in this context.

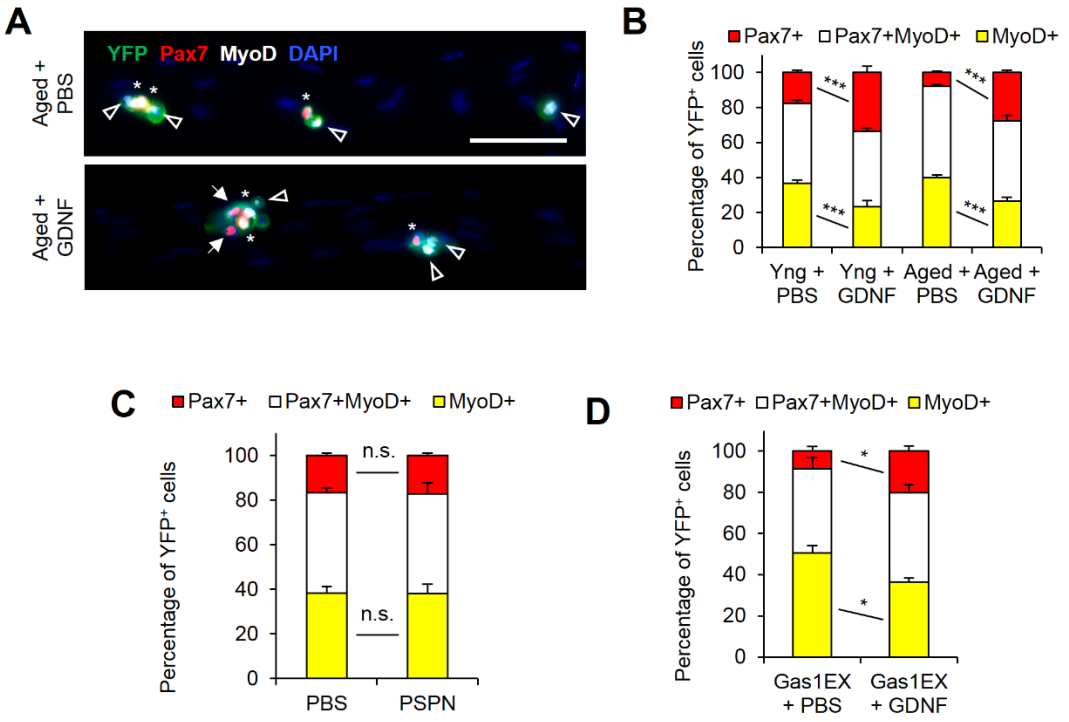

Figure 4.5. GDNF can improve MuSCs self-renewal

(A) Representative images of Aged Ctrl MuSCs on single myofibers cultured for 96 h

with PBS or GDNF (20 ng/ml in PBS) and stained for Pax7 (red) and MyoD (gray), myogenic cells are lineage-marked by YFP (green). Arrows, $Pax7^+$ cells; asterisks, $Pax7^+MyoD^+$ cells; open arrowheads, $MyoD^+$ cells. Scale bar, 25 μm.

(B) Myogenic distribution for Yng and Aged groups using the assay in (A) (n = 3 mice per group; ≥ 20 myofibers per condition).

(C) single myofibers from Yng Ctrl mice were cultured for 96 h with PBS or Persephin (PSPN) (20 ng/ml), stained for Pax7 and MyoD, and quantified for myogenic distributions (n = 3 mice; ≥ 20 myofibers per condition).

(D) single myofibers from Yng Gas1EX mice cultured for 96 h with PBS or GDNF (20 ng/ml), stained for Pax7 and MyoD, and quantified for myogenic distributions (n = 3 mice; ≥ 20 myofibers per condition).

Data are mean ± s.d.; $*P < 0.05$; $***P < 0.001$; n.s., not significant; by two-way ANOVA (B) and multiple t-tests (C and D).

Consistently, GDNF increased the fractions of young and aged control MuSCs with detectable pRetY1062 (Figure 4.3C and D). If young Gas1EX mimicked the satellite cell aging and took effects through regulating Ret signaling, I reasoned that administration of GDNF could also rescue the defects caused by forced expression of Gas1. Indeed, GDNF was also sufficient to stimulate pRetY1062 signal in MuSCs of young Gas1EX mice (Figure 4.3C and D). Moreover, GDNF raised the self-renewed $Pax7^{+}MyoD^{-}$ population on cultured myofibers from young Gas1EX animals (Figure 4.5D), indicating a reversal of Gas1-mediated inhibition of Ret. Further, GDNF could reduce Gas1-Ret PLA foci in young and aged MuSCs (Figure 4.4B). Based on all these data, I propose that GDNF competitively displaces Gas1 from Ret to relieve signaling inhibition.

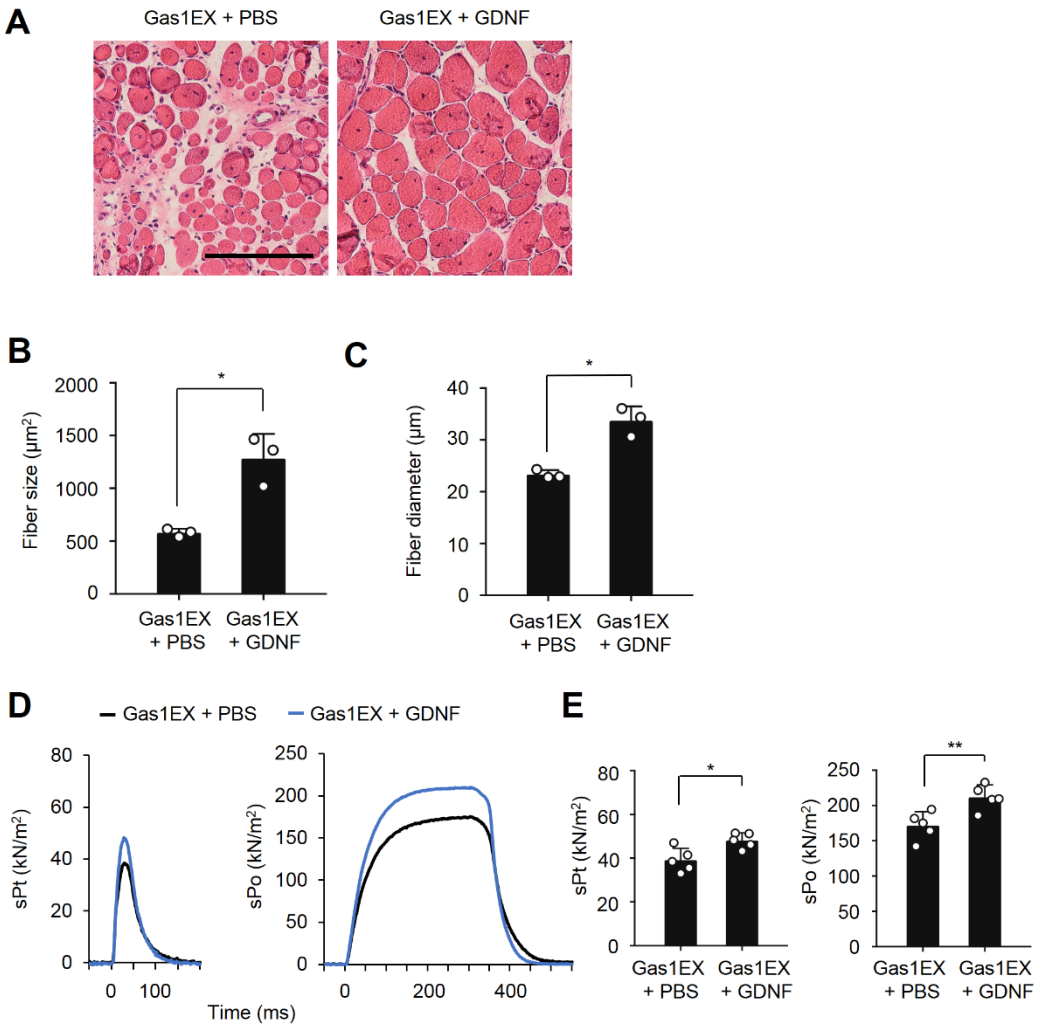

Figure 4.6. GDNF enhances Muscle regeneration in Yng Gas1EX mice

(A) Representative images of Yng Gas1EX TA muscle sections with intramuscular injections of PBS or GDNF (500 ng; at 2, 4 and 14 dpi) at 1 mpi, stained with H&E. Scale bar, 150 μm.

(B and C) Averaged fiber sizes (B) and fiber diameters (C) from data in (A) (n = 3 mice per group; 10 sections per mouse).

(D and E) Representative traces of normalized s*P*t and s*P*o (D) and quantifications (E) of Yng Gas1EX TA muscles treated with PBS or GDNF (as described in C) (n = 5 muscles per condition).

Data are mean ± s.d.; **P* < 0.05; ***P* < 0.01; by two-sided unpaired t-test (B, C and E).

Because GDNF stimulated pRet in Gas1EX MuSCs ex vivo, I tested whether intramuscular administration of GDNF could rescue the defects in the Gas1EX model. Indeed, I observed improvements in regenerative myofiber size and muscle forces in GDNF-treated young Gas1EX muscles (Figure 4.6A to E). As a control, I showed that young RetKO failed to respond to GDNF treatment, both ex vivo and in vivo, indicating that Ret constituted an essential mediator of the GDNF signal in MuSCs (Figure 4.7A to F). The hypothesis that MuSCs aging is driven by Gas1's inhibitory effect on Ret signaling makes a clear prediction that GDNF should also be able to overcome Gas1, stimulate Ret signaling, and enhance the function of MuSCs in naturally aged mice. I was pleased to find that not only aged muscle regeneration and regenerated muscle forces were improved by intramuscular GDNF injection (Figure 4.8A and B; Figure 4.8E and F), but also the number of $Pax7^{+}$ MuSCs was increased (Figure 4.8C and D). I conclude that GDNF can reverse dampened Ret signaling caused by homogenized Gas1 in aged MuSCs, thereby enhancing regeneration of aged muscle.

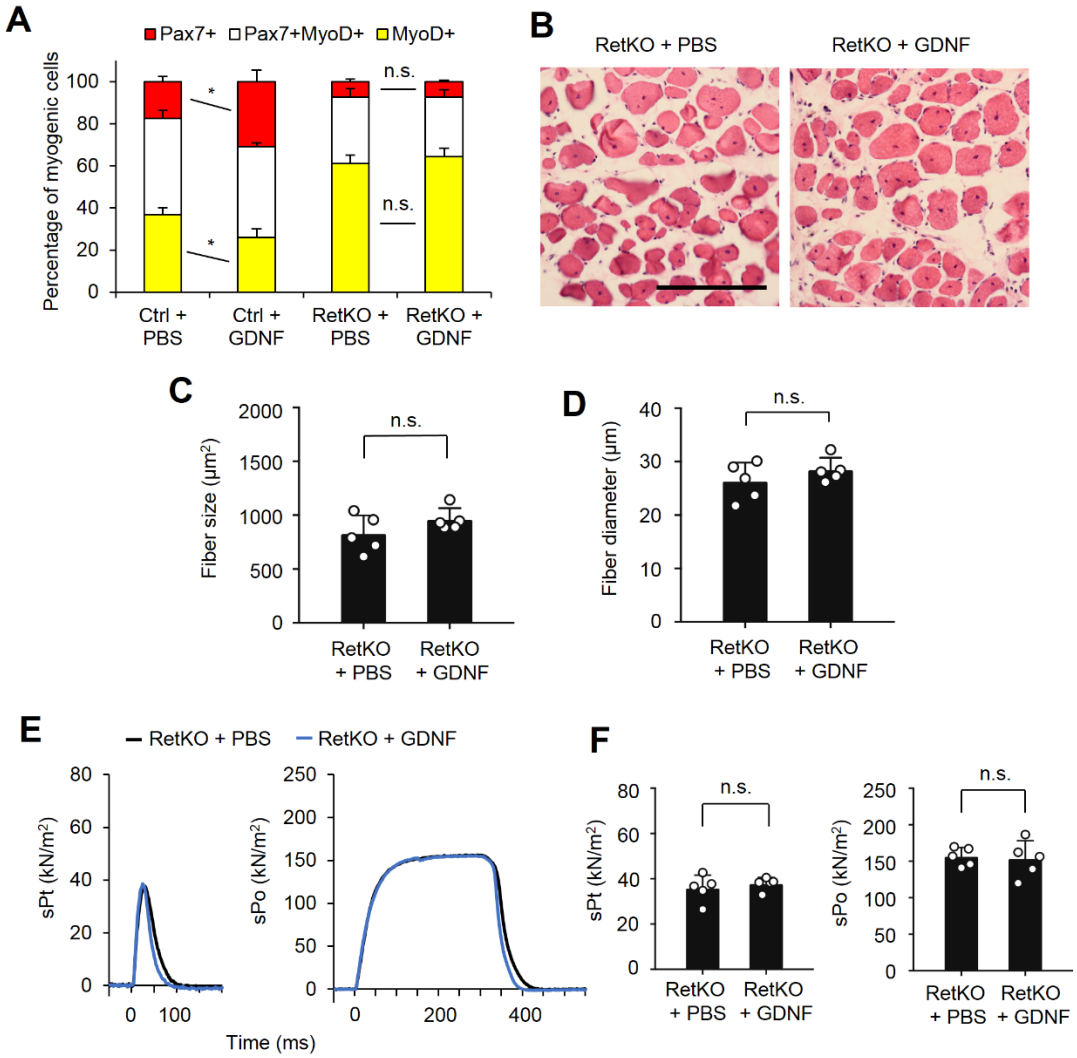

Figure 4.7. GDNF does not alter MuSCs self-renewal and muscle regeneration in young RetKO Mice

(A) Single myofibers from Yng Ctrl or RetKO mice cultured for 96 h with or without GDNF (20 ng/ml), stained for Pax7 and MyoD, and quantified for myogenic distributions (n = 3 mice; ≥ 20 myofibers per condition).

(B) Representative images of Yng RetKO TA muscle sections with intramuscular injections of PBS or GDNF (500 ng; at 2, 4 and 14 dpi) at 1 mpi, stained with H&E. Scale bar, 150 μm.

(C and D) Averaged fiber sizes (C) and fiber diameters (D) from data in (B) (n = 5 mice

per group; 10 sections per mouse).

(E and F) Representative traces of normalized s*P*t and s*P*o (E) and quantifications (F) of Yng RetKO TA muscles treated with PBS or GDNF at 1 mpi as above (n = 5 muscles per condition).

Data are mean ± s.d.; n.s., not significant; by two-way ANOVA (A) and two-sided unpaired t-test (C, D and F).

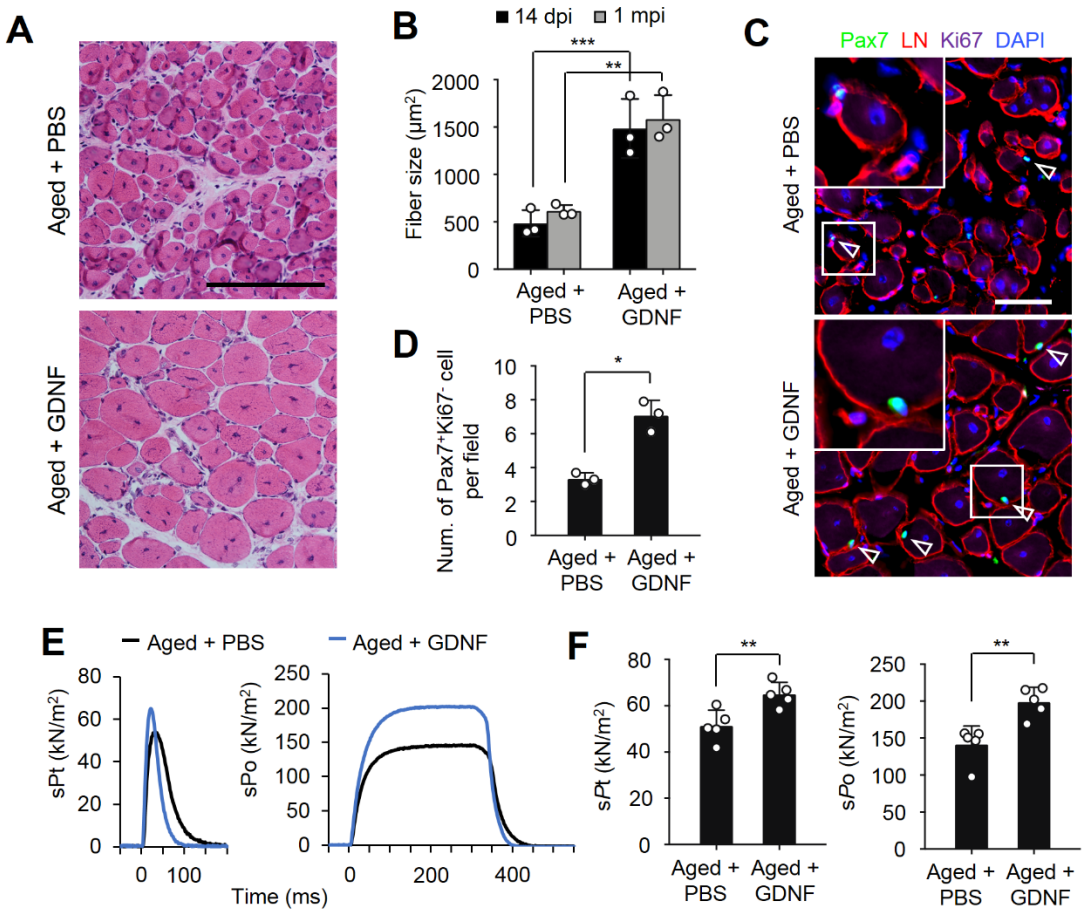

Figure 4.8. GDNF enhances MuSCs self-renewal and muscle regeneration in aged Mice

(A) Representative images of Aged wild-type (WT) TA muscles at 1 month-post-injury (mpi) after intramuscular injections of PBS or GDNF (500 ng; at 2, 4 and 14 day-post-injury (dpi)) and stained with H&E. Scale bar, 150 μm.

(B) Averaged fiber size from data in (A) (n = 3 mice per group; 10 sections per mouse).

(C) Immunostained sections from Aged WT TA muscles treated with PBS or GDNF (500 ng; at 2, 4 dpi) at 14 dpi with CTX. Scale bar, 50 μm.

(D) Averaged $Pax7^{+}Ki67^{-}$ (quiescent) MuSCs per field (1.074 mm^2) from data in (C) (n = 3 mice per group; 10 sections per mouse).

(E–F) Representative traces of normalized s*P*t and s*P*o (E) and quantifications (F) of

Aged WT TA muscles treated with PBS or GDNF at 1 mpi (n = 5 muscles per condition). Data are mean ± s.d.; *$P < 0.05$; **$P < 0.01$; ***$P < 0.001$; by two-way ANOVA (B) and two-sided unpaired t-test (D and F).

GDNF could rescue the dysregulated p38 activation in aged control and young Gas1EX MuSCs

Aged MuSCs harbor persistently active p38α/β signaling that gives rise to increased myogenic commitment and differentiation (Cosgrove et al., 2014). Further, higher p38α/β signaling alteres the polarization of phospho-p38α/β (p-p38) specifically in the committed daughter cell, thus limiting MuSC self-renewal (Bernet et al., 2014). Consistent with these data, partial inhibition of p38α/β signaling help to re-establish the asymmetric p-p38 segregation in aged MuSCs, which enhances self-renewal, muscle regeneration, and force generation after repair (Bernet et al., 2014; Cosgrove et al., 2014).

Based on the fact that the dysfunction of aged MuSCs are correlated with the pervasively activated p-p38 signaling, I wondered whether the Gas1 manipulated mouse model would have changes in p-p38 signaling corresponding to aging phenotype. First, I stained the freshly isolated (t0) single myofibers from young control and Gas1EX mice with p-p38. The result showed that, similar to the aged MuSCs, young Gas1EX MuSCs have higher proportion of activated p-p38 signaling (Figure 4.9A). In addition, more young MuSCs from RetKO mice, compared to MuSCs from young control mice, have p-p38 pathway activated (Figure 4.9B). In contrast, by comparing immunostaining of p-p38 in MuSCs on single myofibers from aged control and aged Gas1KO mice, the latter showed lower percentage of activated p38 (Figure 4.9C). These data suggests that the Gas1-Ret interaction affects MuSCs function, at least in part, through influencing the phosphorylation of p38.

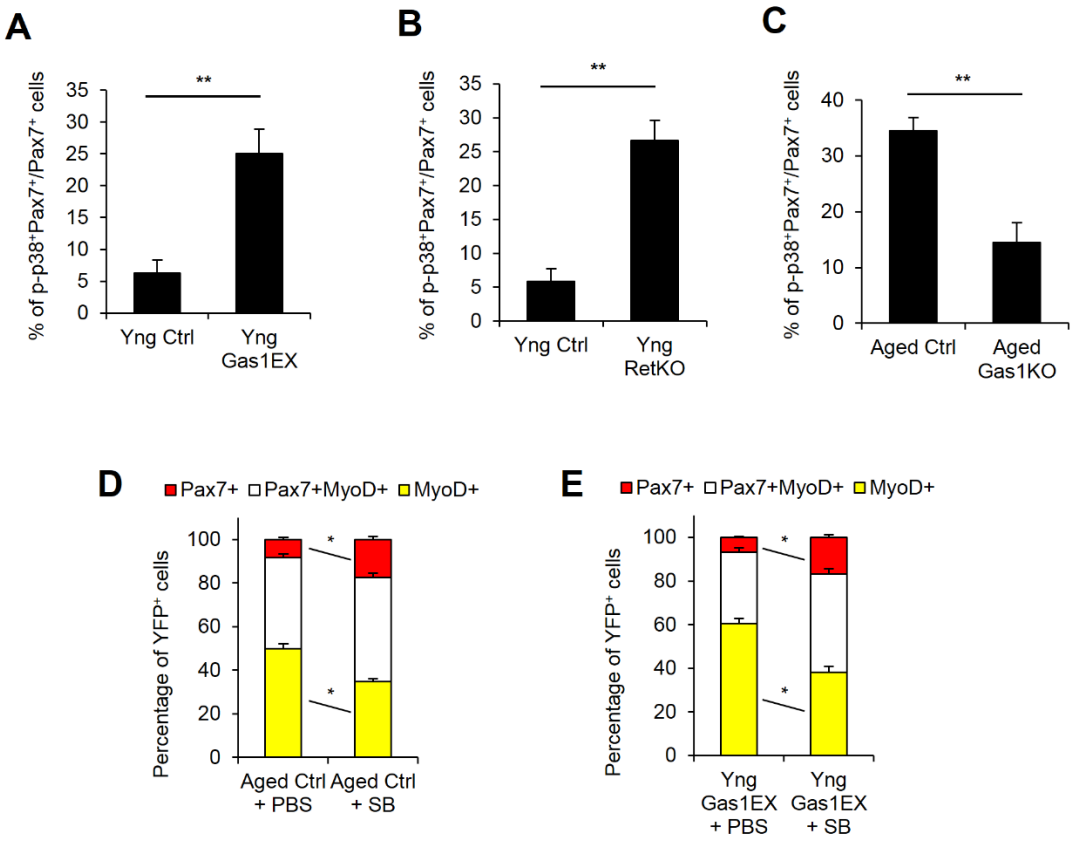

Figure 4.9. Dysregulated p-p38 signaling is correlated to the defects in young Gas1EX MuSCs

(A) Quantification of phosphorylated p38α/β MAPK (p-p38) in Pax7$^+$ MuSCs from Yng Ctrl and Yng Gas1EX mice (n = 3 mice per group; ≥ 20 myofibers per condition).

(B) Quantification of p-p38 in Pax7$^+$ MuSCs from Yng Ctrl and Yng RetKO mice (n = 3 mice per group; ≥ 20 myofibers per condition).

(C) Quantification of p-p38 in Pax7$^+$ MuSCs from Aged Ctrl and Aged Gas1KO mice (n = 3 mice per group; ≥ 20 myofibers per condition).

(D) Single myofibers from Aged Ctrl mice cultured for 96 h with or without p-p38 inhibitor SB202190 (SB) (10 mM), stained for Pax7 and MyoD, and quantified for myogenic distributions (n = 3 mice; ≥ 20 myofibers per condition).

(E) Single myofibers from Yng Gas1EX Ctrl mice cultured for 96 h with or without p-

p38 inhibitor SB (10 mM), stained for Pax7 and MyoD, and quantified for myogenic distributions (n = 3 mice; ≥ 20 myofibers per condition).

Data are mean ± s.d.; *$P < 0.05$; **$P < 0.01$; by two-sided unpaired t-test (A, B and C) and multiple t-tests (D and E).

According to these results, and the previously reported data that partial inhibition of p-p38 could restore the self-renewal and muscle repair after injury in aged animals in vivo and in vitro, I asked whether the self-renewal defect of MuSCs from aged mice could be rescued by applying p-p38 inhibitor ex vivo. I applied p-p38 inhibitor SB202190 or PBS as control in the culture media and found that indeed the inhibitor increased the $Pax7^{+}$ self-renewal population and decreased the $MyoD^{+}$ population (Figure 4.9D). Importantly, application of p-p38 inhibitor also gave similar result using the young Gas1EX MuSCs (Figure 4.9E). These data indicate that the partial inhibition of p-p38 can enhance the self-renewal of naturally aged MuSCs. Moreover, the young Gas1EX MuSCs, mimicking the naturally aged MuSCs, can also be rescued by reducing p38 signaling.

Furthermore, based on the results that GDNF could rescue the functions of aged control and young Gas1EX MuSCs, I next asked whether GDNF treatment could alleviate activated p38 signaling in these cells. Single myofibers were isolated with GDNF addition to the media in every step. After isolation, myofibers were incubated in the media contacting GDNF for another one hour, following by immunostaining with Pax7 and p-p38. The data showed that on the aged control single myofibers, fewer MuSCs displayed p-p38 with GDNF treatment (Figure 4.10A and B). The young Gas1EX single myofibers showed similar results, further suggested that pan-expression of Gas1 in the MuSC mimic the naturally aged MuSCs (Figure 4.10C). As a control, GDNF had no obvious effects on the myogenic cell fates changes of MuSCs from young RetKO single myofibers (Figure 4.10D), corroborating that GDNF role in the MuSC depends on Ret.

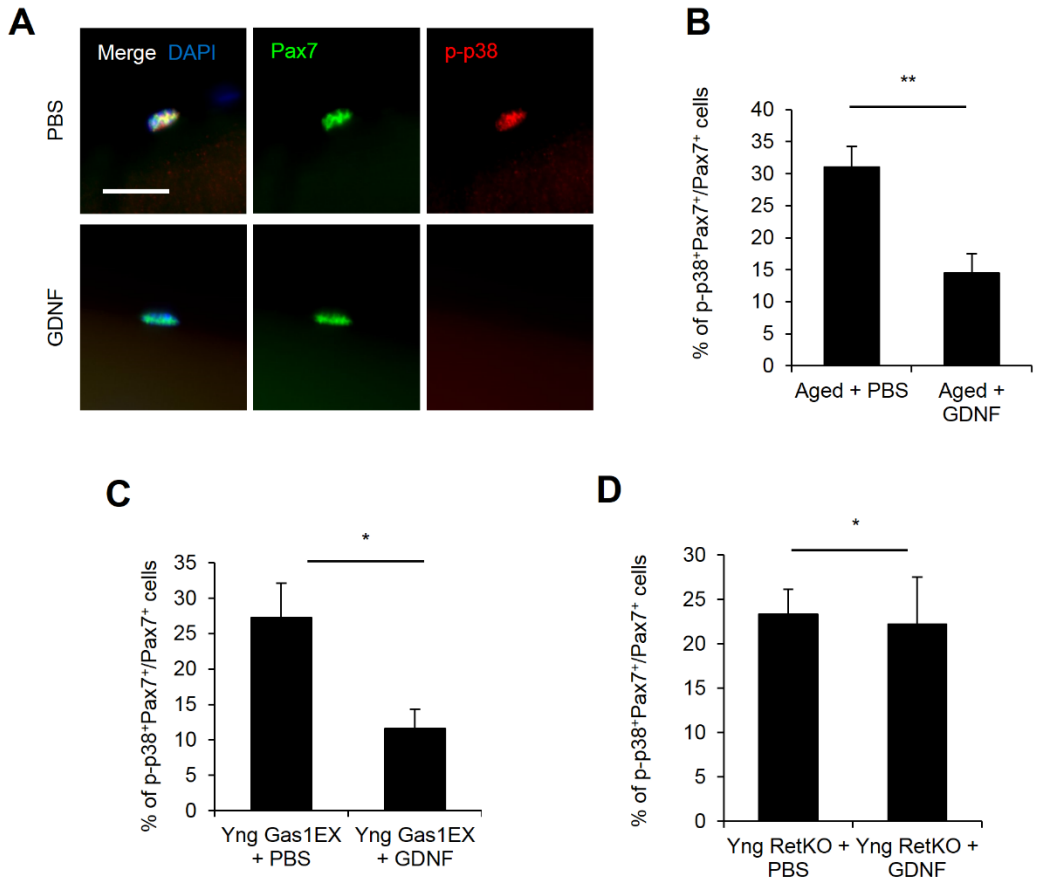

Figure 4.10. GDNF could rescue the dysregulated p-p38 signaling in Aged Ctrl and Yng Gas1EX MuSCs

(A) Representative images of MuSCs on Aged Ctrl single myofibers with or without GDNF treatment and stained for Pax7 (green) and p-p38 (red). Scale bar, 20 μm.

(B) Quantification of p-p38 in $Pax7^+$ MuSCs on Aged Ctrl single myofibers with or without GDNF treatment using data in (A) (n = 3 mice per group; ≥ 20 myofibers per condition).

(C) Quantification of p-p38 in $Pax7^+$ MuSCs on Yng Gas1EX single myofibers with or without GDNF treatment (n = 3 mice per group; ≥ 20 myofibers per condition).

(D) Quantification of p-p38 in $Pax7^+$ MuSCs on Yng RetKO single myofibers with or without GDNF treatment (n = 3 mice per group; ≥ 20 myofibers per condition).

Data are mean ± s.d.; $*P < 0.05$; $**P < 0.01$; by two-sided unpaired t-test (B, C and D).

DISCUSSION

Here I provide multiple lines of evidence that support Gas1 drives intrinsic MuSC aging and regenerative decline. Gas1 reduces MuSC self-renewal by reducing Ret activity at two levels, biochemically and transcriptionally. Previous work reached different conclusions for how Gas1 modulated Ret signaling in different cell lines/types (Cabrera et al., 2006; Lopez-Ramirez et al., 2008; Biau et al., 2013). In MuSCs, Gas1 exists in a complex with Ret and suppresses Ret phosphorylation, and Ret-binding is required for Gas1 to inhibit MuSC renewal. The kinetics of $Gas1^{+}$ cell fraction leads us to propose that the direct and primary role of Gas1 is to suppress Ret signaling via physical interaction, whereas transcriptional repression of Ret is a long-term feedforward mechanism. During this feedforward process, the competition between Gas1 and GDNF for Ret signaling eventually tilts in favor of Gas1 and leads to homogenized reduction of Ret signaling and transcription in aged MuSCs.

The ability of Gas1 to induce G0 cell cycle arrest in cell lines depends on p53 (Ruaro et al., 1997). I show here that Gas1 pan-expression in young MuSCs induces instead, breaking of G0 quiescence. Loss, rather than dependence, of p53 function, recapitulates a mitotic defect of aged MuSCs (Liu et al., 2018). It is thus unlikely that Gas1 cooperates with p53 for MuSC aging. Gas1 is also known as a sonic hedgehog (Shh) co-receptor during embryonic development (Martinelli and Fan, 2007a, b). However, neither scRNA-seq nor bulk-RNA-seq identified Shh pathway genes or downstream targets, such as Patched1 or Smoothened, to be differentially expressed in MuSCs of aged mice and mouse models described herein. By contrast, not only the molecular and biochemical evidence discussed above supports a Gas1-Ret regulatory axis in the MuSC, but also RetKO and Gas1EX mice share the same defects. Together these threads indicate that Gas1 acts through Ret in the MuSC.

While I show the role of Ret and GDNF in MuSC self- renewal and muscle regeneration, other RTKs and their ligands have also been implicated in aspects of adult myogenesis. FGF2 is a potent growth factor for MuSC and myoblast proliferation in vitro. The requirement of FGF receptors in muscle regeneration however needs clarification in vivo (Yablonka-Reuveni et al., 2015). HGF can stimulate myoblast proliferation and migration in vitro, and genetic data reveal that its receptor c-Met mainly mediates myoblast migration and fusion during regeneration (Webster and Fan, 2013). It is worth noting that Ret is critical for motor axon regeneration (Fontana et al., 2012) and synaptic maturation (Baudet et al., 2008) after lesion. GDNF secreted by the muscle fiber is proposed to guide these processes. GDNF expression is also elevated in newly regenerated muscle fibers (Suzuki et al., 1998). It seems that motor axons/synapses and MuSCs depend on muscle-derived GDNF for homeostatic maintenance, and that after injury, newly regenerated muscle fibers deploy GDNF to direct re-innervation and stem cell renewal. This common usage of the Ret-GDNF pathway may underlie how muscle structure and function are maintained and restored coordinately. Lastly, I present intramuscular injection of GDNF, a natural biological factor, as a proof of principle method to improve aged muscle regeneration. This contrasts to most studies to date using technically demanding in vitro manipulations to improve MuSC for transplantation. I envision that methods to increase GDNF levels, either endogenously or exogenously, can also be considered to boost MuSC number and function in other degenerative muscle conditions.

MATERIALS AND METHODS

Mice

The *Pax7*$^{cre\text{-}ERT2}$ (referred to as *Pax7*^{CE} in legends; B6;129-*Pax7*$^{tm2.1(cre/ERT2)}$*Fan*/J) mice (Lepper et al., 2009), and *Gas1*^{flox} mice (Jin et al., 2015) have been described. The *R26*^{YFP} (B6.129X1-*Gt*(*ROSA*)*26Sor*$^{tm1(EYFP)}$*Cos*/J) mice (Srinivas et al., 2001) and *Ret*^{flox} (STOCK Ret<tm1.2Ddg>/J) mice (Luo et al., 2007) were obtained from the Jackson Laboratory (JAX). Whenever YFP was included for assay, the *R26*^{YFP} allele was included in the background for Pax7^{+} MuSC lineage marking. The Gas1 conditional pan-expression (Gas1EX) allele, *R26*$^{CAG\text{-}Gas1}$, is generated for this work. C57BL/6 mice were used as wild-type (WT) mice.

For young versus aged comparisons, mice were used at 2–3 month of age (young) or 18–24 month of age (aged). Sex was mixed. Animal experiments in this study were performed following the ethical regulations by Office of Laboratory Animal Welfare (OLAW), and in accordance with protocols approved by the Institutional Animal Care and Use Committee (IACUC) of the Carnegie Institution for Science (Permit number A3861-01).

GDNF administration

For in vivo GNDF treatment, TA muscles received 2 × 10 μl GDNF (50 ng/μl in PBS, PeproTech) at 2 and 4 dpi and were harvested at 14 dpi. For TA muscles harvested at 1 mpi, an extra dosage was administrated at 14 dpi. Phosphate buffered saline (PBS) was used for mock-injection for control.

Muscle sample processing

TA muscles were harvested, fixed for 10 min in ice cold 4%

paraformaldehyde (EMS) in PBS, sequentially changed through 10%, 20% and 30% sucrose/PBS overnight, embedded in OCT, frozen in isopentane (Sigma)/liquid nitrogen, and stored at –80 °C freezer until cryo-sectioning. Cross-sections (10 μm) of the muscle mid-belly region were stained with Hematoxylin and Eosin (H&E; Surgipath), or used for immunostaining.

MuSC isolation by FACS and myoblast culture

MuSCs were isolated following the previously described protocol (Liu et al., 2015) with slight modifications. For MuSC preparation, skeletal muscles were dissected and incubated in 0.2% Collagenase Type I (Thermo Fisher Scientific) in Ham's F-10 Nutrient Mix (F-10; Gibco) at 37 °C with gentle shaking for 1.5 h followed by centrifugation and wash. Tissues were then incubated in 0.2% Dispase (Gibco) in F-10 at 37 °C with gentle shaking for 0.5 h. Cells were then gone through 20-gauge needles for dissociation and filtered through 40 μm cell strainer (VWR) and wash.

For surface maker labeling, cell were incubated with DAPI and fluorophore-conjugated antibodies against CD45, CD31, Sca-1 and Vcam, at 4 °C for 0.5 h. After wash, cells were subjected to fluorescence-activated cell sorting (FACS) using the ARIA III (BD Biosciences). Isolated mononuclear MuSCs were collected in Trizol (Thermo Fisher Scientific) for RNA-seq, in F-10 with 10% horse serum (HS) for ChIP-seq.

Single myofiber (SM) isolation, transfection, and culture

SMs with associated MuSCs were isolated from extensor digitorum longus (EDL) muscles (Zammit et al., 2004) by 1.5 h digestion in 0.2% Collagenase Type I in DMEM at 37 °C. The digested EDL muscle was then transferred to petri dishes

containing DMEM, 1% Pen/Strep, and 1% Glutamax for mechanical dissociation to release individual myofibers. Isolated myofibers were subjected to direct fixation for immunostaining, or transferred to serum-coated Petri dishes for culture (SM culture medium: 10% FBS, 1% Pen/Strep, 1% Glutamax in DMEM). Pending on the assays, myofibers were cultured for different lengths of time before fixation and downstream assays. For pRet analysis and PLA assay (see below), myofibers were cultured for 24 h. Protease and Phosphatase Inhibitor Cocktail (Thermo Fisher Scientific) was used as directed during fixation. For self-renewal assays with Pax7 and MyoD expression, 96 h cultures were used. For SM transfection, isolated myofibers were transfected with VSV-G-tagged full-length Gas1, Gas1-domain 1-truncation mutant, or GPI-anchored-YFP using TransfeX (ATCC) at 1:3 DNA(μg):TransfeX(μl) ratio. Twelve h after transfection, fresh SM culture medium was added and myofibers were cultured for total of 96 h at 37 °C, 5% CO_2 for self-renewal assays. For Ret signaling inhibition, 1NM-PP1 (10 nM and 100 nM, EMD Millipore) and Regorafenib (10 nM, Selleckchem) was added to SM culture medium for samples from $Ret^{flox/flox}$ mice and control mice, respectively. GDNF (20 ng/ml; PeproTech) or PSPN (as specificity control, 20 ng/ml; ProSpec) was directly added to the culture. Medium was changed daily with the same concentration of inhibitors or recombinant factors until assay.

Immunostaining

TA muscle sections, SMs or cytospun MuSCs were fixed for 10 min in 4% paraformaldehyde, permeabilized with 0.1% Triton X-100 (Sigma)/PBS for 10 min at room temperature (RT), rinsed with wash buffer (0.05% Triton-X 100/PBS), treated with blocking buffer (10% Normal Goat Serum (Genetex) and 1× carbo-free blocking solution(Vector)) for 1 h, prior to incubation with primary antibodies (see

Supplementary Table) diluted in blocking buffer overnight at 4 °C. Samples were then washed with wash buffer and incubated with appropriate Alexa-Fluor-conjugated secondary antibodies (1:1,000, Life Technologies) and in blocking buffer for 1 h at RT. After wash and incubation with 4′,6-diamidino-2-phenylindole (DAPI) at1 μg/ml for 5 min, samples were mounted with Fluoromount-G (SouthernBiotech) and coverslip (VWR). For EdU detection, the Click-iT reaction kit (Life Technologies) was used prior to incubation in DAPI according to manufacturer's recommendations.

Force measurement

In situ force measurements of TA muscles were conducted as previously described (Hakim et al., 2013, Rozo et al., 2016), and the data were analyzed using the 1300A Whole Animal System (Aurora Scientific). Mice were anaesthetized with isoflurane and placed on isothermal stage. Intact TA muscles were dissected and constantly immersed in Ringer's solution (homemade). Single twitch or tetanic contractions were elicited with electrical stimulations applied by two electrodes placed on either side of the muscle. In all experiments 0.2 ms pulses at 10 V supramaximal voltage were used. Muscle optimal length (Lo) that allows a maximum isometric twitch force (*P*t) was determined by a series of twitch contractions with small variations of the muscle tension. To obtain maximum isometric tetanic force (*P*o), muscles were stimulated for 300 ms at different frequencies from 50 to 200 Hz. A 1 min recovery period was allowed between stimulations. Muscle wet weight and Lo were used to calculate the cross-sectional area (CSA) of the TA muscle for normalization to obtain specific isometric twitch force s*P*t (kN/mm^2) and s*P*o (kN/mm^2).

RNA-seq and analysis

For each condition, 30,000 of fresh isolated MuSCs by FACS were lysed in Trizol reagent. RNA was isolated using the Direct-zol RNA Kit (Zymo). cDNA was generated and amplified using TruSeq RNA Library Preparation Kit v2 (Illunima) and amplified with ThruPLEX DNA-seq Kit (Takara).

Sequencing was carried out on an Illumina Nextseq-500 to generate single-ended 75 bp reads, which were aligned to the mouse genome (mm9) using TopHat (v2.1.0). Expression measurement of each gene was calculated from the resulting alignment bam file by HTseq against the GENCODE annotation vm1. Differentially expressed genes were determined using edgeR with FDR cutoff of 0.05. MDS-plots were also generated using the edgeR package. GSEA (Subramanian et al., 2005) analysis was performed using ranked fold change values with hallmark gene sets database (h.all.v6.2.entrez.gmt).

ChIP-seq and analysis

Low-input ChIP-seq for fresh isolated MuSCs by FACS was performed following the previously described protocol (Zheng et al., 2015) with slight modifications. For each condition, 30,000 MuSCs were fixed with 1% formaldehyde/PBS for 10 min at RT, before quenching the reaction with 1/20 volume of 2.5 M glycine for 5 min at room temperature and mixing with ~5×10^8 DH5α *E.coli* (as carrier). Cell lysis, chromatin isolation and digestions were done using the EZ Nucleosomal DNA Prep Kit (Zymo) followed by further chromatin shearing and releasing using Bioruptor Pico (Diagenode) with 6 cycles of 30 s on/off sonication. The immunoprecipitations were performed using anti-H3K4me3 antibody (EMD Millipore, 07-473, 1:1,000) at 4 °C overnight. The immunoprecipitated DNA was then bound to Protein G Dynabeads (Thermo Fisher Scientific) for 2 h at 4 °C, followed by serial

washes, proteinase K digestion, and purification by DNA Clean & Concentrator kit (Zymo). DNA libraries were prepared using ThruPLEX DNA-seq Kit (Takara) and sequenced on an Illumina Nextseq-500 to generate single-ended 75bp reads.

ChIP-seq reads were aligned to mouse genome (mm9) using Bowtie (version 1.1.2). 2 mismatches were allowed for the alignment and only uniquely mapped reads were allowed (parameters -v 2 -m 1). Promoter correlations for H3K4me3 enrichments are plotted as log2 of the average read density within 2 Kb up and downstream of TSS. H3K4me3 peaks were called by MACS V1.4 with *p*-value threshold of 10^{-5}. The parameters are all default.

Proximity ligation assay (PLA)

PLA for Gas1 and Ret on MuSCs were performed with Duolink In Situ Red kit (Sigma) following the manufacturer's guidelines. SM were fixed for 10 min in 4% paraformaldehyde, permeabilized with 0.1% Triton-X-100/PBS for 10 min at RT, and blocked with Duolink Blocking Solution for 2 h. Myofibers were then incubated with primary antibodies against Gas1 (goat, R&D, AF2644, 1:50) and Ret (rabbit, Alomone, ANT-025, 1:50) diluted in Duolink Blocking Solution at 4 °C overnight. Omitting either primary antibody resulted in no signal. PLA reactions were subsequently carried out using Duolink PLA probes for goat and rabbit and Duolink In Situ Detection Reagents Red. After washes, myofibers were stained for Pax7 using the moncoloncal Ab (DSHB), followed by an Alex-488 anti-mouse IgG1 secondary antibody (Invitrogen) and DAPI, and then mounted in ProLong Diamond Antifade Mountant (Thermo Fisher Scientific). Quantification of PLA was performed by counting PLA foci number per MuSC.

Co-immunoprecipitation

HEK293T cells (ATCC, tested negative for mycoplasma contamination by MycoProbe Mycoplasma Detection Kit (R&D Systems)) were transfected with pcDNA3-3xFLAG-Ret and/or pAP-VSV-G-Gas1/Gas1-domain-truncated mutants by lipofectamine2000 (Invitrogen) for 24 h according to manufacturer's guidelines. Cells were lysed in lysis buffer (50mM Tris pH 8.0, 150mM NaCl, 0.5% Digitonin (Sigma), and protease inhibitors) for 1 h at RT. Cell lysates were cleared by centrifugation, and subjected to immunoprecipition by either anti-FLAG M2 Affinity Gel (Sigma) or anti-VSV-G Agarose Conjugate (Sigma) for 2 h at 4 °C. Affinity matrixes were washed and eluted in 2X SDS-PAGE sample buffer for Western blotting using anti-FLAG (Sigma) and anti-VSV-G antibodies (Invitrogen).

Western Blot

4X SDS sample buffer was added to the supernatant to reach 1 X concentration. Samples were boiled for 5 min before subjected to 7.5% SDS-PAGE. Kaleidoscope wide-range molecular weight marker (Bio-Rad) was used for size. Western transfer was performed with transfer buffer to nitrocellulose membrane (Amersham) via Biorad semi-dry transfer system for 1 hour at constant current condition per guidance of manufacturer. Membrane was blocked in 5% low fat milk powder in TBS for 30 min, incubated with primary antibody in blocking solution for overnight at 4°C, washed in TBS, 3X, 10 min each, incubated with secondary antibody in blocking solution for 1 hour, washed in TBS, 3X, 10 min each, and then subjected to ECL reaction using the kit from Amersham (ECL Western Blotting Detection Reagents) and subjected to membrane scanning using LI-COR ODYSSEY® Fc Dual- Mode Imaging System.

CHAPTER 5

Targeting β1-integrin signaling enhances regeneration in aged and dystrophic muscle in mice

This chapter contains literature previously published in:

Rozo, M., Li, L., and Fan, C.M. (2016). Targeting beta1-integrin signaling enhances regeneration in aged and dystrophic muscle in mice. Nature medicine 22, 889-896.

INTRODUCTION

Sarcopenia, the slow progressive loss of skeletal muscle mass concomitant with advancing age, affects elderly people. Age-related muscle wasting is characterized by loss of muscle quantity and quality due to changes in muscle metabolism, function and regeneration (Ryall et al., 2008). The poor regeneration of aged muscle is not attributed solely to the loss of MuSCs (Chakkalakal et al., 2012), although MuSC numbers decline during aging in mice and humans. Instead, the impaired regeneration is linked to aged-related changes in both extrinsic systemic and local environments as well as intrinsic defects (Brack et al., 2007; Cosgrove et al., 2014; Conboy et al., 2003; Shea et al., 2010; Carlson et al., 2008; Bernet et al., 2014).

A well-studied niche signal, fibroblast growth factor-2 (FGF-2), has important roles in driving MuSC proliferation. MuSCs are maintained in a quiescent state by repressing FGF-2 signals (Shea et al., 2010). Aging increases the level of FGF-2 in skeletal muscle and decreases the level of FGF signaling inhibitor Spry1 in the MuSC, which results in loss of a portion of MuSCs due to breaking quiescence (Chakkalakal et al., 2012). Paradoxically, aged MuSCs are non-responsive to FGF-2 (Bernet et al., 2014) for proliferation and self-renewal. Inhibiting FGF signaling in aged MuSCs rescues the quiescent phenotype at the expense of regeneration (Chakkalakal et al., 2012), while ectopically activating FGF receptor 1 (FGFR1) rescues the proliferative capacity of aged MuSCs (Bernet et al., 2014). It is unclear what underlies the differential requirement for FGF and what causes the desensitization of FGFR1, but changes in interactions with other cell surface proteins may contribute.

Integrins adhere to the extra cellular matrix (ECM) to cooperate with different growth factor signaling pathways depending on cell-type and context (Assoian et al., 2001). Integrins are heterodimers comprised of an α and a β chain that function to link

the ECM to the actin cytoskeleton (Hynes et al., 2002). There are 18 α and eight β chains, which can form at least 28 isoforms. Of particular relevance to skeletal muscles are α7 and α5 integrins and laminin α2 for their mutations cause muscular dystrophies (Helbling-Leclerc et al., 1995; Hynes et al., 2002). Inactivation of *Itgb1* (encoding β1-integrin) in the embryonic muscle lineage causes defects in muscle cell migration, fusion, and sarcomere assembly, but not progenitor proliferation (Schwander et al., 2003). Although β1-integrin is conspicuously expressed by adult MuSCs, its role has not been examined, especially in regards to modulating FGF signaling. The former member in our lab Michelle showed that β1-integrin is the sensor of the MuSC niche that maintains quiescence during homeostasis, and sustains their expansion and self-renewal during regeneration. Together with her work, I showed that β1-integrin also cooperates with FGF-2 to synergistically activate their common downstream effectors Erk and Akt. We further demonstrate that activating β1-integrin signaling restores FGF sensitivity in aged MuSCs and improves muscle regeneration. Activating β1-integrin in the *mdx* mouse (Bulfield et al., 1984), a model for Duchenne muscular dystrophy, can also promote MuSC expansion and improve function. We propose that β1-integrin is a potential therapeutic target of muscle pathological conditions in which the MuSC niche is compromised.

RESULTS

MuSCs without β1-integrin cannot maintain quiescence and sustain proliferation upon injury

To define the function of β1-integrin in adult MuSCs, we employed a *Pax7*$^{Cre\text{-}ERT2(CE)}$ driver (Lepper et al., 2009) for tamoxifen (tmx) inducible gene inactivation of a *Itgb1* conditional allele (*Itgb1*^{f}; Raghavan et al., 2000) in MuSCs. To assess whether β1-integrin loss affected MuSCs niche occupancy, previous lab member Michelle followed lineage-marked cells up to 180 d and found that the number of *Itgb1*$^{-/-}$ MuSCs declined over time. Via immunostaining for BrdU and MyoD, she showed that MuSCs loss is due to spurious activation and differentiation. And I further showed that polarity proteins m-cadherin and Par3 were not localized appropriately in *Itgb1*$^{-/-}$ MuSCs (Figure 5.1), suggesting mutant MuSC loss is associated with polarity defects. We conclude β1-integrin senses quiescent MuSC-niche to maintain polarity and prevent spurious activation and differentiation.

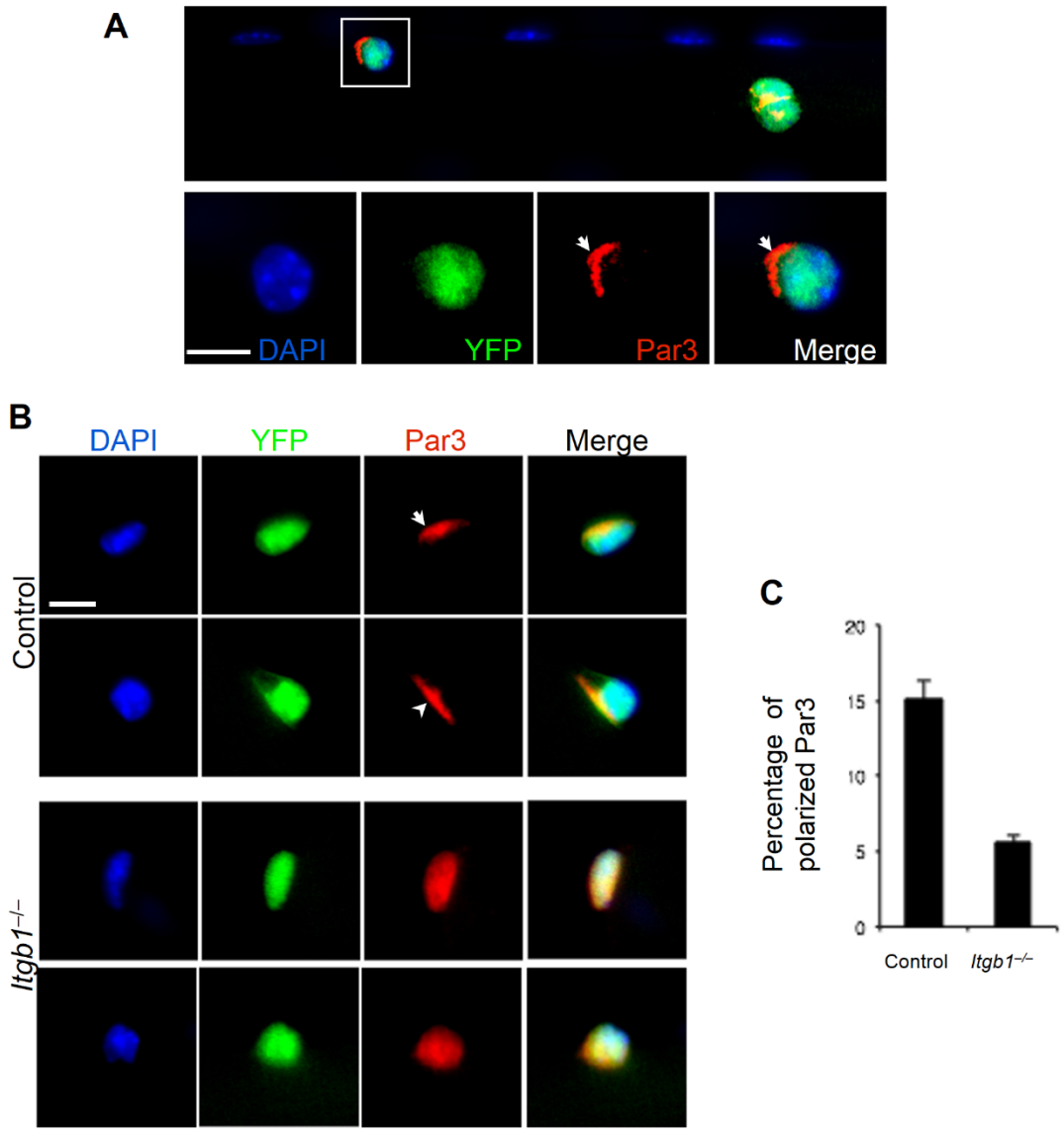

Figure 5.1. *Itgb1*$^{-/-}$ cells show defective expression of polarity marker Par3

(A) Two control MuSCs on myofiber stained for Par3, YFP and DAPI 30 h after isolation, show heterogeneity; enlarged images of the inset are below. Scale bars, 10 μm.

(B) More examples of single control and mutant MuSCs stained as in (A); arrowheads, polarized Par3. Scale bars, 10 μm.

(C) Percentage of control and *Itgb1*$^{-/-}$ cells with polarized Par3. More than 20 fibers and 50 cells were scored for each group; Student's t-test: $*P < 0.05$.

Next, Michelle used the *Itgb1* conditional knockout mice to conduct the injury assay to assess whether *Itgb1*$^{-/-}$ MuSCs could support regeneration. She showed that the regenerated fiber numbers is drastically reduced in mutant, suggesting a MuSC expansion defect. Also, consistent with embryonic studies (Schwander et al., 2003), adult *Itgb1*$^{-/-}$ myoblasts migrated and fused poorly *in vitro*, which explains the reduced diameter of regenerated fibers. Furthermore, she observed that Pax7^{+} cell numbers were significantly reduced in the regenerative area of muscles from *Itgb1*$^{-/-}$ mice indicating that *Itgb1*$^{-/-}$ MuSCs turned off Pax7 and failed to self-renew. Thus, β1-integrin is required for MuSC proliferation and self-renewal to drive muscle regeneration.

β1-integrin crosstalks with FGF signaling in MuSCs

Activation of integrins by the ECM cooperates with receptor tyrosine kinases (RTKs), including FGFR, to activate Erk MAP kinases and drive proliferation in many cell types (Assoian et al., 2001; Miyamoto et al., 1996; Polanska et al., 2009). FGF-2 stimulates myoblast proliferation via the same effectors (Jones et al., 2001), which may involve integrin signaling. I therefore examined whether *Itgb1*$^{-/-}$ myoblasts were defective in FGF-2 responsiveness with or without fibronectin, an ECM molecule originally used to demonstrate integrin-RTK crosstalk (Roovers et al., 1999; Miyamoto et al., 1996). The phosphorylation levels of their common downstream effectors, Erk and Akt (pErk1, pErk2 and pAkt) were assessed (Figure 5.2A and B). Control cells responded better to FGF-2 in the presence of fibronectin; low levels of FGF-2 was sufficient to phosphorylate Erk and, to a lesser extent Akt. In contrast, fibronectin or high levels of FGF-2 alone only weakly activated Erk and Akt. Mutant cells were indeed defective in responding to FGF-2 in the presence of fibronectin. Importantly, high levels of FGF-2 could partially restore cooperativity, likely due to compensation

by other fibronectin-binding integrins in *Itgb1*$^{-/-}$ cells.

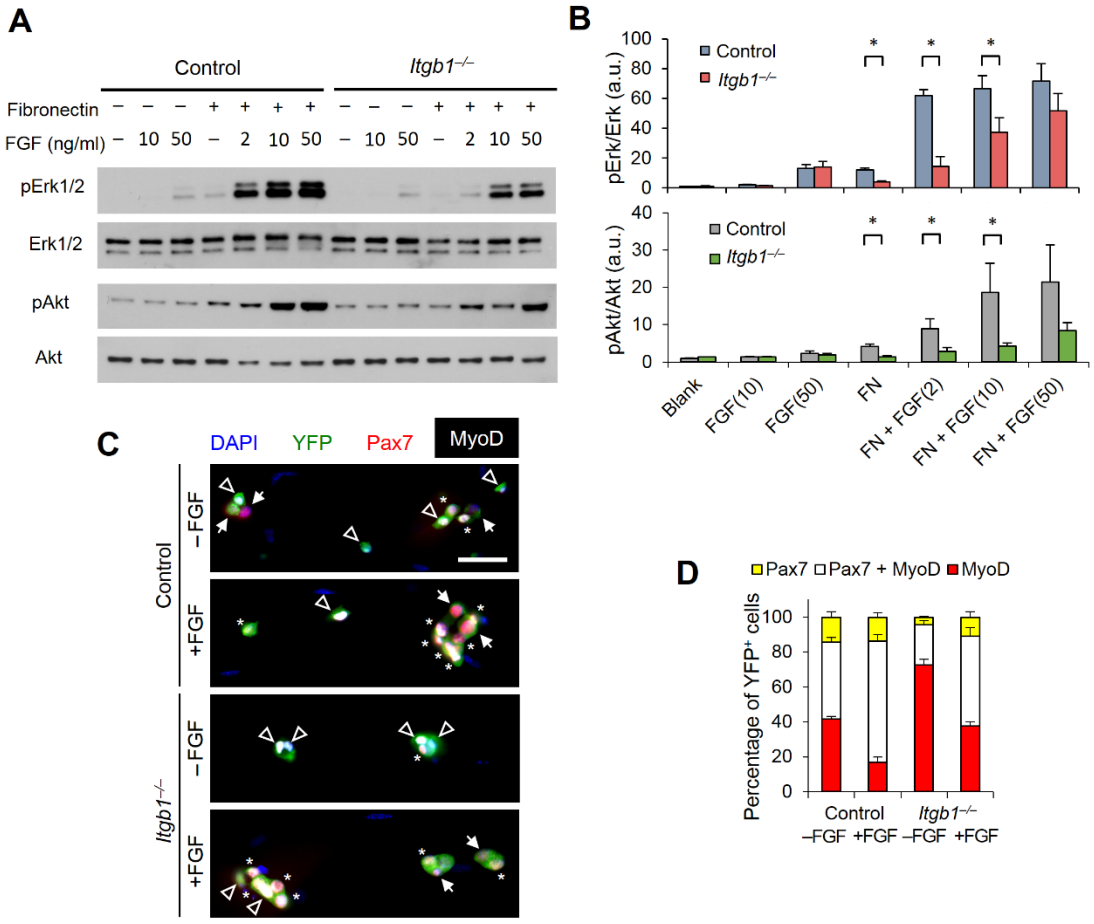

Figure 5.2. *Itgb1*$^{-/-}$ MuSCs show a compromised response to FGF-2 that can be partially restored by exogenous FGF-2

(A) Western blots for pErk1 and pErk2, Erk1 and Erk2, pAkt, and Akt of control and *Itgb1*$^{-/-}$ cells. Fibronectin addition (+) and FGF-2 concentrations (FGF (ng/ml)) are indicated.

(B) Fold induction from data in (**c**), normalized to control cells without fibronectin and FGF-2 (set at 1 arbitrary unit (a.u.)); n = 4 parallel sets of myoblasts. Paired comparisons with significant differences are indicated; data are expressed as mean ± s.e.m.; two-way ANOVA: *$P < 0.05$.

(C) Control and *Itgb1*$^{-/-}$ MuSCs cultured for 96 h with or without 10 ng/ml FGF-2 were stained for YFP, Pax7, MyoD, and DAPI; arrows, Pax7^{+} cells, asterisks, Pax7^{+}MyoD^{+}

cells, and triangles, $MyoD^+$ cells; scale bar: 25 mm.

(D) Percentage distribution of various cell populations from data in (C); $n = 3$ animals; ≥ 20 myofibers per condition; two-way ANOVA: $P < 0.01$ for $Pax7^+MyoD^+$ and $MyoD^+$, –FGF vs. +FGF (control and $Itgb1^{-/-}$), control vs. $Itgb1^{-/-}$ (–FGF and +FGF); $P < 0.05$ for $Pax7^+$, control vs. $Itgb1^{-/-}$ (–FGF).

Data were compared by two-way ANOVA: $*P < 0.05$ and n.s., not significant.

I next assessed the relevance of the cooperativity between integrin and FGF signaling in the MuSC. Using the single myofiber assay to examine MuSC fates, I determined that the majority of control MuSCs maintained Pax7 expression ($Pax7^{+}MyoD^{-}$ and $Pax7^{+}MyoD^{+}$). Addition of FGF increased the $Pax7^{+}MyoD^{+}$ expanding population but did not alter the $Pax7^{+}MyoD^{-}$ self-renewed fraction (Figure 5.2C and D). In contrast, the majority of mutant MuSCs were committed to differentiate, expressing only MyoD, at the expense of $Pax7^{+}MyoD^{+}$ and $Pax7^{+}MyoD^{-}$ fractions. The latter two populations were partially rescued by FGF-2 addition, again suggesting compensation by other integrins. MuSC self-renewal has been associated with FGF stimulation of asymmetric p38α/β MAPK phosphorylation (Bernet et al., 2014; Troy et al., 2012). Michelle showed that fewer *Itgb1*$^{-/-}$ MuSCs displayed polarized pp38, relative to controls, and FGF-2 could increase the fraction of mutant MuSCs with polarized pp38. Together, we have uncovered a mechanism for β1-integrin in sustaining MuSC expansion and self-renewal.

Aged MuSCs are defective in integrin activity

The characteristics of *Itgb1*$^{-/-}$ MuSCs are similar to aged MuSCs; both are gradually lost from the niche (Chakkalakal et al., 2012), cannot sustain proliferation (Conboy et al., 2005), are committed to differentiation (Cosgrove et al., 2014), and are defective in self-renewal (Bernet et al., 2014). Given that ECM composition (Kragstrup et al., 2001) and stiffness (Wood et al., 2014) change in aged muscles, we wondered whether the aged environment impacts β1-integrin or overall integrin activity, thereby desensitizing aged MuSCs to FGF-2 (Bernet et al., 2014). To probe for changes in integrin activity in aged MuSCs, Michelle first used an antibody (9EG7) that recognizes the "high-affinity" ligand-bound active β1-integrin (Bazzoni et al., 1995; Takagi et al., 2002) on young

and aged MuSCs. The majority of young myofiber-associated MuSCs displayed well-aligned basal membrane-bound β1-integrin in its active conformation, mirroring total β1-integrin. Despite a basally localized pattern of total β1-integrin (Figure 5.3A), more aged MuSCs displayed active β1-integrin in abnormal patterns: in disorganized puncta or undetectable.

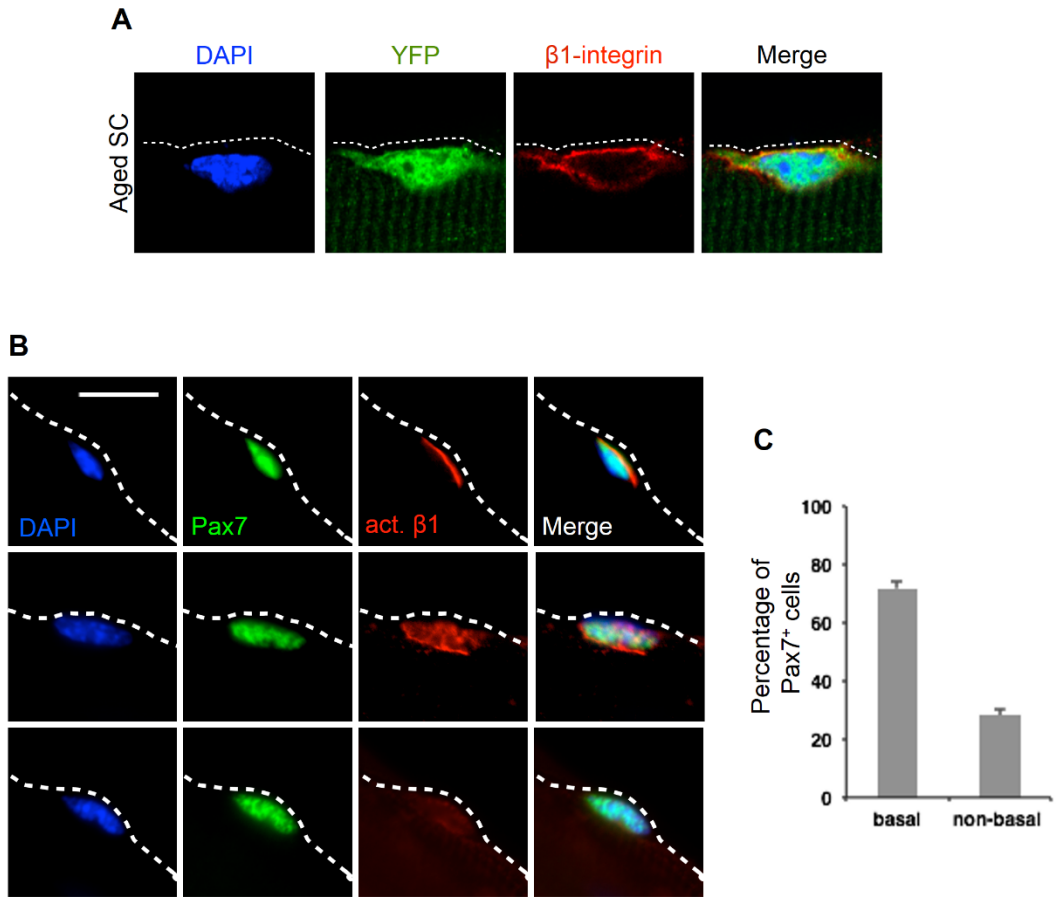

Figure 5.3. Distribution of β1-integrin in aged and dystrophic MuSCs

(A) Aged MuSCs show laminar-localized pan β1-integrin. YFP^+ myofiber-associated MuSCs of aged mice at 1 h after isolation stained for pan β1-integrin. Localization pattern mirrors young control MuSCs stained for pan-β1 integrin; dashed lines outline the basal side of the myofiber; scale bar: 10 mm.

(B and C) MuSCs on *mdx* myofibers have dysregulated β1-integrin activity: (B) $Pax7^+$ MuSCs on myofibers after isolation from *mdx* mice show basally restricted (top) and

non-basally restricted (middle and bottom) activated β1-integrin (act. β1) patterns (same exposure time), compared to control (young SC). (C) Percentages of act. β1 displaying basal and non-basal pattern in the $Pax7^+$ SC population.

If dysregulated integrin signaling underlies the dysfunction of aged MuSCs, activating β1-integrin alone may be sufficient for rescue. To test this, Michelle injected injured muscles with a β1-integrin-activating antibody TS2/16 (Hintermann et al., 2001). And she observed that TS2/16 did not enhance the already robust regeneration in young animals, but it improved regeneration in aged mice to a level comparable to the young. To determine whether TS2/16 improves MuSC function, we applied it to myofiber-associated aged MuSCs and assessed their expansion and Pax7 expression. Neither the IgG control, nor TS2/16 or FGF-2 treatment alone showed an effect. TS2/16 and FGF-2 together increased the fraction of $Pax7^{+}$ cells (not shown), the number of fiber-associated myogenic cells, and the fraction of MuSCs displaying polarized pp38 (Figure 5.4).

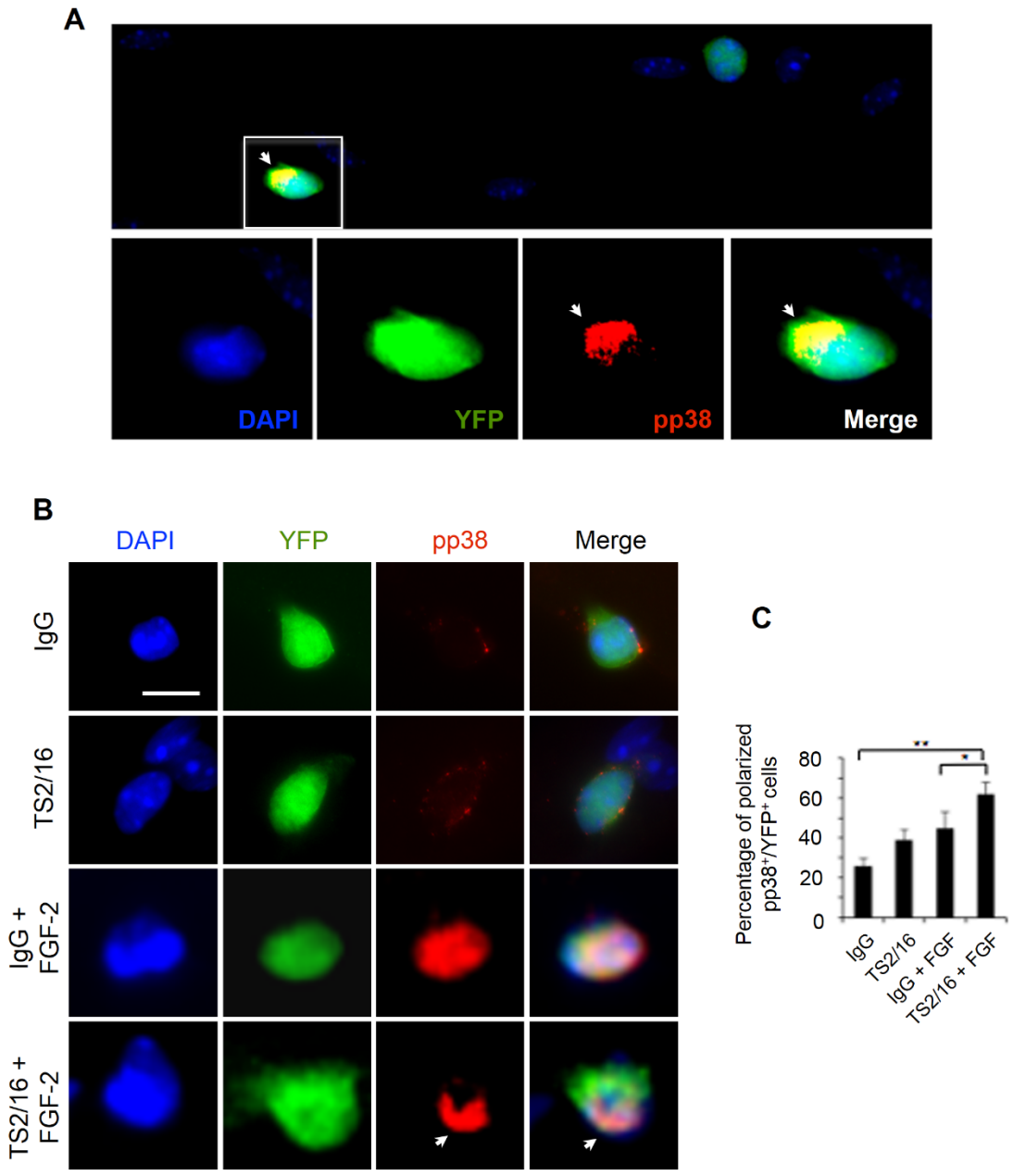

Figure 5.4. TS2/16 and FGF-2 increase the fraction of aged MuSCs displaying polarized pp38

(A and B) Myofiber-associated aged MuSCs cultured for 24 h with IgG or TS2/16 and stained for Pax7 and FGFR1. (A) Representative images (from 20); scale bar: 10 µm. (B) Percentage of FGFR1$^+$ cells within the Pax7$^+$ population; mean ± s.d., n = 3 experiments, ≥ 20 myofibers per condition; Student's t-test: *$P < 0.05$.

(A) Two cells on a single myofiber show heterogeneity of pp38 staining between YFP-

marked MuSCs. The cell in the inset shows polarized pp38, while the other shows none-to-minimal pp38 signal; scale bars: 10 mm.

(B) Additional single cell examples of various patterns of pp38 distribution in aged myofiber-associated lineage-marked YFP^+ MuSCs cultured for 30 h with control IgG or TS2/16 (10 μg/ml), with or without FGF-2 (10 ng/ml); scale bar: 10 mm.

(C) Percentages of MuSCs with polarized pp38 (arrowhead in A and B); those with only a few puncta of pp38 signal were not counted as polarized; $n = 3$ experimental replicates, ≥ 25 myofibers each condition per replicate; Student's *t*-test paired comparison: $*P < 0.05$, $**P < 0.01$.

Since TS2/16 alone is sufficient *in vivo,* we surmise that muscle damage releases a sufficient amount of FGF-2 to cooperate with TS2/16-activated β1-integrin in aged MuSCs. Mechanistically, I found that TS2/16 increased the fraction of aged MuSCs on myofibers with detectable FGFR1, relative to control IgG (Figure 5.5A and B). Although not sufficient to enhance expansion, TS2/16 alone increased the proportion of aged MuSCs with detectable phosphorylated FGFR (pFGFR). TS2/16 and FGF-2 together stimulated pFGFR in almost all aged MuSCs (Figure 5.5C and D), consistent with their dual requirement for enhancing aged MuSC expansion. Associations between FGFR and α-integrins (Calderwood et al., 2000) or αvβ3-integrin (Hintermann et al., 2001) were suggested to underlie FGF-integrin cooperativity. I showed that, via reciprocal co-immunoprecipitation, FGFR1 can associate with β1-integrin, and that TS2/16 enhances their association (Figure 5.5E). These data indicate that TS2/16 operates at multiple layers to enhance FGF signaling and restore the responsiveness in aged MuSCs.

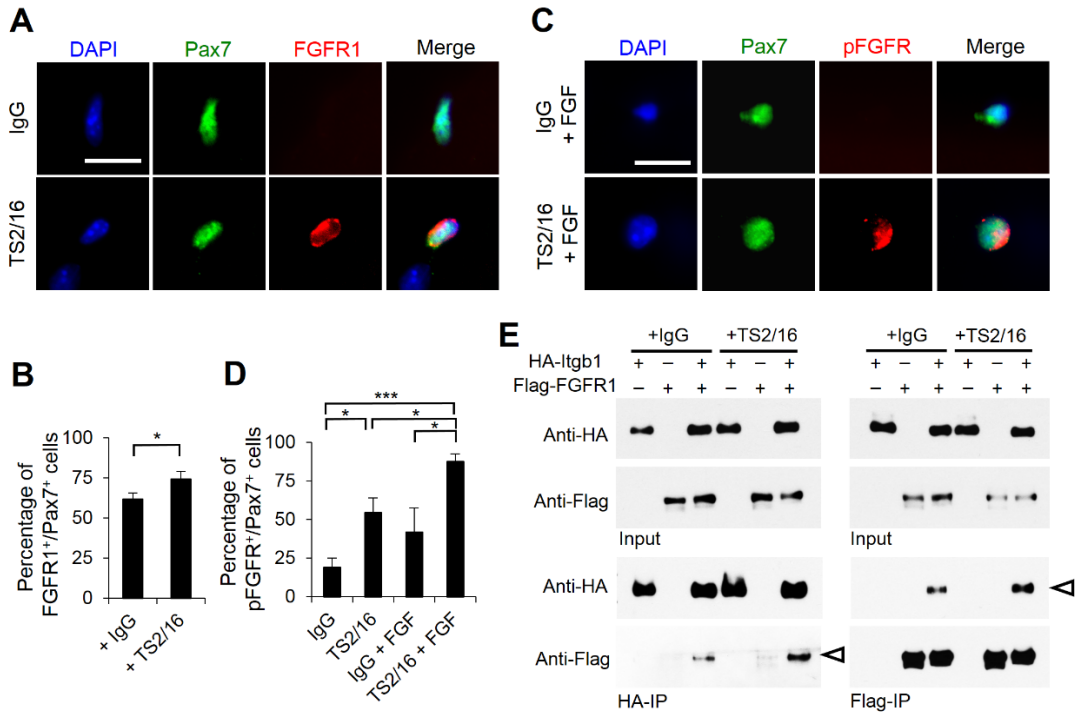

Figure 5.5. Activating β1-integrin in aged MuSCs enhances FGF signaling to

promote MuSC expansion

(A and B) Myofiber-associated aged MuSCs cultured for 24 h with IgG or TS2/16 and stained for Pax7 and FGFR1. (A) Representative images (from 20); scale bar: 10 μm. (B) Percentage of $FGFR1^+$ cells within the $Pax7^+$ population; mean ± s.d., $n = 3$ experiments, ≥ 20 myofibers per condition; Student's *t*-test: $*P < 0.05$.

(C and D) Aged MuSCs cultured with IgG or TS2/16, and with or without FGF-2, were stained for phospho-FGFR (pFGFR) and Pax7. (C) Representative images of IgG + FGF-2 and TS2/16 + FGF-2 (from 20 images of each group); scale bar: 10 μm. (D) Percentage of $pFGFR^+$ cells within the $Pax7^+$ SC population; mean ± s.d.; $n = 3$ experiments, ≥ 20 myofibers scored per condition; Student's *t*-test: $*P < 0.05$, $***P < 0.001$.

(E) Reciprocal co-immunoprecipitation (co-IP) between HA-tagged Itgb1 and Flag-tagged FGFR1 in HEK293T cells, with IgG or TS2/16 added, followed by Western blot; input lysates, top two rows; IPed fractions, bottom two rows; antibodies for IP, labeled at bottom, and for Western blots, left. Open arrowheads indicate co-IPed Flag-FGFR1 (left) and HA-Itgb1 (right).

Activating β1-integrin improves dystrophic muscles

The positive effect of TS2/16 on regeneration in aged environment led us consider whether it might be beneficial in another context of impaired muscle regeneration: muscular dystrophy. For this, we employed the *mdx* mouse model, which lacks dystrophin expression due to a nonsense mutation (Bulfield et al., 1984). As the *mdx* muscle contains disorganized ECM, we anticipated more $Pax7^+$ MuSCs residing outside of the myofiber lamina, relative to those in the control (C57BL/10). Additionally, *mdx* MuSCs associated with myofibers displayed abnormal patterns of active β1-integrin (Figure 5.3B and C). Michelle administered TS2/16 into the TA muscle of *mdx* mice and found that a single dose was sufficient to promote the expansion of myogenic cells, as shown by increased EdU incorporation 3 d after treatment (not shown). She extended TS2/16 treatment to 4 weekly injections (Figure 5.6A) and found cross-sectional area and muscle fiber diameter were increased, relative to those treated with control IgG (Figure 5.6A to C). As α7β1-integrin binds to laminin, the ECM component that engages with the dystrophin complex, activating β1-integrin likely also enhances muscle fiber integrity in *mdx* mice via improved connection to the ECM.

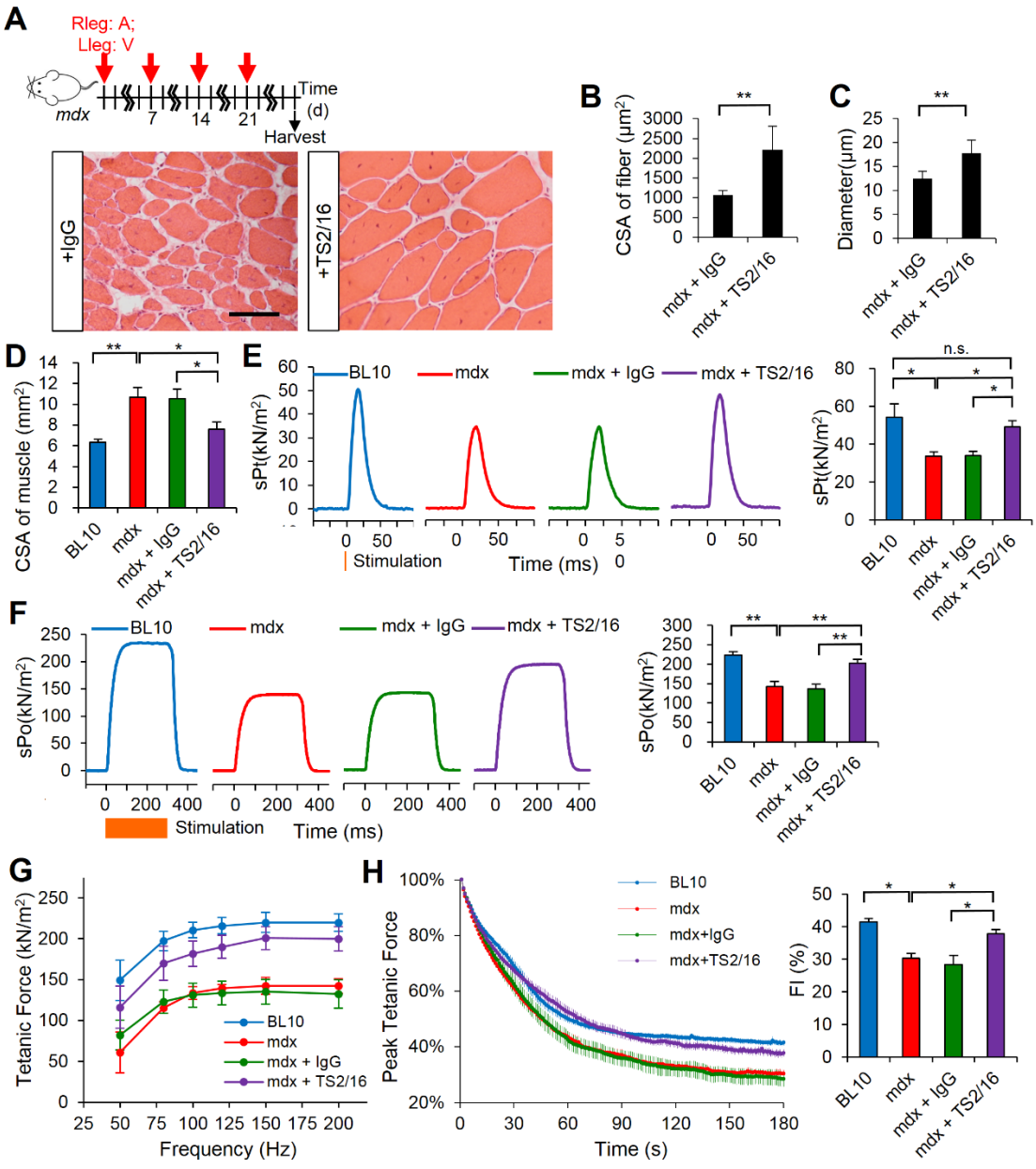

Figure 5.6. Activating β1-integrin in *mdx* mice ameliorates dystrophic pathology and restores muscle strength

(A) Schematic of long-term IgG or TS2/16 treatment and images of H&E stained muscle sections (courtesy of Michelle Rozo) of treated *mdx* mice at 28 d; scale bar = 25 μm.

(B and C) Cross-sectional area (CSA) (B) and diameter (C) of myofbers from data in (A); $n = 3$ animals per treatment, ten sections per animal; mean ± s.d.; Student's *t*-test: $*P < 0.05$, $**P < 0.01$.

(D) CSA of TA muscles from 4 groups of 3 month old mice: C57BL/10 (BL10, untreated), *mdx* (untreated), *mdx* + IgG (IgG treated), *mdx* + TS2/16 (TS2/16-treated); the latter two groups were treated by regimen in (A).

(E to H) Contractile properties of TA muscles were measured *in situ*:

(E) Representative traces of normalized specific twitch force (sPt) and quantifications; orange vertical line, time of stimulation.

(F) Representative traces for specific maximum tetanic forces (sPo) and quantifications; orange bar, duration of stimulation (300 ms).

(G) Normalized tetanic force to stimulation frequency relationship.

(H) Fatigue traces (left) over 180 s and fatigue indices (FI = tetanic $force_{t0}$ / tetanic $force_{t180}$) for all groups. Numerical data are expressed as mean ± s.d.; $n = 5$ for each group; Student's *t*-test: $*P < 0.05$, $**P < 0.01$, and n.s., not significant.

To determine whether the above long-term regimen resulted in functional rescue, I used the same paradigm to compare the contractile properties of IgG- and TS2/16-treated *mdx* TA muscles *in situ*; WT and untreated *mdx* TA muscles were done in parallel for references (Figure 5.6D to H). TS2/16-treated *mdx* muscles had reduced cross sectional areas than those of *mdx* and IgG-treated *mdx* muscles, consistent with a reversal from hypertrophic pathology. Significantly, TS2/16-treated muscles showed strength improvements in a variety of measurements, including single twitch force, maximum isometric tetanic force, force-frequency relationship, time to fatigue, and fatigue index. Activating β1-integrin may therefore be a viable therapeutic means to improve muscle repair and function in diseased conditions.

DISCUSSION

Our results frame a model in which β1-integrin acts as a sensor of the MuSC niche that declines in function upon aging. Because *Itgb1*$^{-/-}$ cells show compromised pErk induction by FGF-2, their quiescence breaking is more likely due to cell polarity defects than overt FGF-Erk signaling (Chakkalakal et al., 2012). In the regenerative context, β1-integrin has a distinct role in cooperating with FGF-2 to drive MuSC proliferation and renewal. In aged muscle, changes in ECM (Kragstrup et al., 2011; Wood et al., 2014) impose physiological relevant alterations in integrin activity (Lukjanenko et al., 2016), which likely contribute to the decline of MuSC's FGF sensitivity. The current view regarding FGF and aging MuSCs is puzzling. Aging MuSCs are sensitive to increased FGF-Erk signaling, causing quiescence break and loss (Chakkalakal et al., 2012), and yet aged MuSCs are insensitive to FGF-2 for expansion *in vitro* (Bernet et al., 2014). Our study provides a potential explanation: A fraction of aging MuSCs with sufficient integrin activity cooperates with increasing FGF-2 to break quiescence and becomes lost, while those with dysregulated integrin activity insufficient to support FGF signaling, remain. As such the remaining aged MuSCs cannot support robust regeneration after injury, unless integrin activity is re-established, e.g. by TS2/16, to restore FGF signaling.

While activating β1-integrin alone can improve regeneration in both aged and dystrophic muscles, it may prove more effective to target all integrins relevant to MuSC expansion and FGF-sensitivity, e.g. RGD-binding integrins. There are minimally eight integrins (three of which contain β1-integrin) that bind to the RGD motif, which is the integrin binding site of many ECM molecules, including fibronectin (Hynes et al., 2002). While β1-integrin and fibronectin cooperate with FGF-2, we cannot exclude contributions by other RGD-containing ECM components. Conversely, as MuSCs

express almost all α- and β-integrins (Siegel et al., 2009), defining the contribution of each integrin in this context may take considerable efforts. Despite the complexity, our findings help to explain why ECM implantation can enhance muscle regeneration (Sicari et al., 2014). Future investigation into how the integrin-FGF axis intersects with other pathways, e.g. Stat3, to regulate MuSC function, is important. Although *Stat3* expression is not changed in *Itgb1*$^{-/-}$ MuSCs, *Stat3* is up-regulated in activated MuSCs (Fukada et al., 2007) and inhibiting Stat3 enhances regeneration in aging and dystrophic contexts (Price et al., 2014; Tierney et al., 2014). It would be remiss if we do not mention that other than FGF-2, integrins can cooperative with many growth factors that may also contribute to MuSC function. We provide here a proof of principle study that may be broadly applicable to muscle diseases involving MuSC niche dysfunction, but further refinement is needed for this method to become a viable treatment. Given the role of integrin in other stem cells (Raghavan et al., 2000; Tanentzapf et al., 2007), knowledge derived from our study likely have implications for aging and decline of function in other stem cells.

MATERIALS AND METHODS

Mice

Animal experiments in this study were performed in accordance with protocols approved by the Institutional Animal Care and Use Committee (IACUC) of the Carnegie Institution for Science (Permit number A3861-01). The *Pax7*$^{\text{cre-ERT2(CE)}}$ allele (B6;129-*Pax7*$^{\text{tm2.1(cre/ERT2)}}$*Fan*/J) has been described (Lepper et al., 2009). The *Itgb1*$^{\text{f}}$ allele (B6;129-Itgb1tm1Efu/J) (Raghavan et al., 2000) and *R26R*$^{\text{YFP}}$ (B6.129X1-*Gt*(*ROSA*)*26Sor*$^{\text{tm1(EYFP)}}$*Cos*/J) (Srinivas et al., 2001) reporter mice were obtained from the Jackson Laboratory. *Pax7*$^{\text{CE/+}}$; *Itgb1*$^{\text{f/f}}$ is referred to as *Itgb1*$^{-/-}$. Controls used were *Pax7*$^{\text{CE/+}}$; *R26R*$^{\text{YFP/YFP}}$. For young versus aged comparisons, mice were used at 3 - 6 month of age (young) or 18 - 24 month of age (aged). For non-lineage marked MuSC studies, aged C56/BL6 mice were used (JAX and NIH). Sex was mixed. For dystrophic muscle studies, control and *mdx* male mice of C57BL/10 background (JAX) were used at 3 - 4 months of age.

Mice were given tamoxifen (tmx, 20 mg/ml in corn oil (Sigma)) at 3 mg per 40 g body weight per intraperitoneal injection, once a day consecutively for 5 days. All experiments except where noted were conducted 3 d after the final injection. For injury, mice were anesthetized using 2,2,2-Tribromoethanol (Sigma), which was dissolved in 2-methyl-2-butanol (Sigma) as 100% (w/v) stock solution, diluted 1:80 in PBS, and injected intraperitoneally at 10 µl per g body weight. For *Itgb1*$^{-/-}$ vs. control injury, 50 µl of 10 µM cardiotoxin (CTX; Sigma) was injected using an insulin syringe (U-100; Becton Dickinson) into TA muscles. Animals were then harvested at post injury time points stated in the text and legends.

For needle tract injury, TA muscles were injured as described previously. Two d post injury, TA muscles received 6 X 10 µl anti-TLR2 [TS2/16] (10 µg/ml), 60

μl vehicle control (mouse IgG, 10 μg/ml), RGD peptide (10 μg/ml), or scrambled peptide (10 μg/ml) by intramuscular injections. Muscles were harvested 3 d after these injections for analysis. For *mdx* mice, 10 μg (in 25 ul) of vehicle control IgG or TS2/16 were injected to each TA muscles, either by single injection or repeated 4 times weekly.

Muscle sample processing

TA muscles were harvested, fixed for 8 min in ice cold 4 paraformaldehyde (EMS) in phosphate buffered saline (PBS), incubated sequentially in 10% and 20% sucrose/PBS overnight, frozen in isopentane (Sigma)/liquid nitrogen, and stored at –80 °C freezer until cryosectioning. Cross-sections (10 μm) were stained with Haematoxylin and Eosin (H&E, Surgipath) or used for immunostaining.

Myofiber isolation and myoblast culture.

Myofibers with associated MuSCs were isolated from extensor digitorum longus (EDL) muscles by 1.5 h digestion in 0.2% Collagenase Type I in DMEM at 37 °C. The digested muscle was then transferred to tissue culture dishes containing DMEM, 1% Pen/Strep, and 1% Glutamax. Live myofibers were isolated with a fire polished glass pipette. Isolation of individual myofibers by pipette was repeated to remove dead myofibers and cellular debris. They were either immediately fixed for assay (e.g. probe for activated β1-integrin) or placed in DMEM, 10% Horse Serum, 1% Penn/Strep, and 1% Glutamax with daily medium and reagent changes. Please note that this minimal growth medium contains no additional additives. Pending on the assays, myofibers were cultured for different amount of time before fixation. For Par3, pp38, FGFR1, and pFGFR analysis, myofibers were cultured for 36 h. For self-renewal assays with Pax7 and MyoD expression, 48 - 96 h cultures were used (specified in text or

figure legend). They were either cultured with or without FGF-2 (10 ng/ml), and with or without IgG or TS2/16 (10 μg/ml). Phosphatase Inhibitor Cocktail Set II (Calbiochem) was used as directed during fixation.

For FGF and fibronectin stimulation, we modified the condition described previously for other cell types (Roovers et al., 1999; Miyamoto et al., 1996). The day of experiment, control and *Itgb1*$^{-/-}$ myoblasts were detached by 2mM EDTA in serum-free base-media (SFBM, high glucose DMEM, 0.5% BSA, Pen/Strep), washed twice and cultured in SFBM on petri-dish as suspension for 2 h to minimize residual effect of growth factors and contact-dependent signaling from prior culture condition. 50,000 cells were then transferred to each well of a 12-well dish containing SFBM with or without fibronectin (10 μg/ml) for 20 min. The wells were either coated with Sigma-cote (to prevent attachment) or pre-coated with fibronectin (10 μg/ml overnight). Specified concentrations of FGF-2 were then added and cells were harvested 10 min later for Western blots (see below for detailed procedure). Blots were first probed with anti-pErk1/2 and anti-pAkt, followed by HRP-conjugated secondary Ab and ECL detection (Amershame). Blots were then stripped and re-probed with anti-Erk1/2 and anti-Akt. Fold of stimulation is presented as pErk/Erk and pAkt/Akt ratios relative to pErk/Ekr and pAkt/Akt ratios, respectively, of control cells in SFBM. The pErk/Ekr and pAkt/Akt ratios of control cells in SFBM are used as the normalization denominator and set at an arbitrary unit of 1-fold.

Immunostaining

Cells or muscle sections were fixed for 10 min in 4% paraformaldehyde, permeabilized with 0.1% Triton-X-100 (Sigma)/PBS for 15 min at room temperature (RT), rinsed with wash buffer (0.05% Triton-X 100/PBS), treated with blocking buffer

(10% Normal Goat Serum (Genetex) and 1% Blocking powder (Perkin Elmer) in wash buffer) for 1 - 2 hr, prior to incubation with primary antibodies diluted in blocking buffer overnight at 4 °C. Primary antibodies were applied. Cells or muscle sections were washed with wash buffer and incubated with appropriate Alexa-Fluor-conjugated secondary antibodies with various fluorescent wavelengths in blocking buffer for 1 h at RT. After wash and incubation with DAPI (1 μg/ml for 5 min), slides were then mounted with Fluoromount-G (SouthernBiotech) and coverslips (VWR).

Western blot

For protein extraction, cells were lysed in T-Per Tissue Protein Extraction Reagent (Thermo), 1 mM PMSF (Sigma), 1× Halt Phosphatase Inhibitor Cocktail (Thermo), and Complete Protease Inhibitor Tablet (Roche). Total protein extract was resolved by SDS-PAGE on precast gels (Bio-Rad) and then transferred to Immuno-blot PVDF Membranes (Bio-Rad) using a Bio-Rad mini-Protein II Transfer system. Membranes were rinsed in 0.1% Tween (Sigma)/TBS (20 mM Tris-HCl pH 7.5, 150 mM NaCl), blocked for 1 h at RT in 5% low-fat milk (Carnation)/0.1% Tween/TBS (blocking buffer), then incubated with primary antibodies in blocking buffer overnight at 4 °C. Primary antibodies against following antigens were used at specified dilutions: β1-integrin, 1:1000 (Millipore); pErk, Erk, pAkt, and Akt, all at 1:1000. After washing in 0.1% Tween/TBS, appropriate secondary antibodies (Amersham, Invitrogen, and Bio-rad) were diluted 1:10,000 in blocking buffer and incubated for 1 h at RT.

Co-immunoprecipitation

HEK293T cells (Clontech, tested negative for mycoplasma contamination by MycoProbe Mycoplasma Detection Kit (R&D Systems)) were plated on fibronectin-

coated 6-well dishes and transfected with pcDNA3-FGFR1-flag and/or pcDNA3-Itgb1-HA by lipofectamine2000 (Invitrogen) overnight according to manufacturer's manual. Next day, they were incubated in media containing 5 μg/ml of IgG or TS2/16 for 1 h at 4 °C. Cells were washed with cold PBS and lysed in 1% NP40 (50mM HEPES, 150mM NaCl, 10% glycerol, protease inhibitors (Thermo)) for 30 min at 4 °C. Lysates were clarified by centrifugation, and subjected to immunoprecipition by anti-HA affinity matrix (Pierce) or anti-Flag affinity matrix (Sigma) for 2 h at 4 °C. Affinity matrix were washed and proteins were eluted in 2X SDS-PAGE sample buffer for Western blotting using anti-Flag and anti-HA antibodies (Sigma).

Force measurements and fatigue analysis

In situ force measurements of TA muscles were conducted as done previously, and the data were analyzed using the 1300A Whole Animal System (Aurora Scientific). Mice were anaesthetized with isoflurane and placed on isothermal stage. Intact TA muscles were dissected and constantly immersed in Ringer's solution. Single twitch or tetanic contractions were elicited with electrical stimulations applied by two electrodes placed on either side of the muscle. In all experiments we used 0.2 ms pulses at 10 V supramaximal voltage. Muscle optimal length (Lo) that allows a maximum isometric twitch force (Pt) was determined by a series of twitch contractions with small variations of the muscle tension. To obtain maximum isometric tetanic force (Po), muscles were stimulated for 300 ms at different frequencies from 50 to 200 Hz. A 1 min recovery period was allowed between stimulations. The muscles were then fatigued at 150 Hz with one contraction per second for 180 s. Muscle wet weight and Lo were used to calculate the cross-sectional area (CSA) of the TA muscle for normalization to obtain specific isometric twitch force sPt (kN/mm^2) and sPo (kN/mm^2).

REFERENCES

Airaksinen, M.S., and Saarma, M. (2002). The GDNF family: signalling, biological functions and therapeutic value. Nature reviews Neuroscience *3*, 383-394.

Altschuler, S.J., and Wu, L.F. (2010). Cellular heterogeneity: do differences make a difference? Cell *141*, 559-563.

Anders, S., Pyl, P.T., and Huber, W. (2015). HTSeq--a Python framework to work with high-throughput sequencing data. Bioinformatics *31*, 166-169.

Assoian, R.K., and Schwartz, M.A. (2001). Coordinate signaling by integrins and receptor tyrosine kinases in the regulation of G1 phase cell-cycle progression. Curr Opin Genet Dev *11*, 48-53.

Baudet, C., Pozas, E., Adameyko, I., Andersson, E., Ericson, J., and Ernfors, P. (2008). Retrograde signaling onto Ret during motor nerve terminal maturation. The Journal of neuroscience : the official journal of the Society for Neuroscience *28*, 963-975.

Bazzoni, G., Shih, D.T., Buck, C.A., and Hemler, M.E. (1995). Monoclonal antibody 9EG7 defines a novel beta 1 integrin epitope induced by soluble ligand and manganese, but inhibited by calcium. The Journal of biological chemistry *270*, 25570-25577.

Beauchamp, J.R., Heslop, L., Yu, D.S., Tajbakhsh, S., Kelly, R.G., Wernig, A., Buckingham, M.E., Partridge, T.A., and Zammit, P.S. (2000). Expression of CD34 and Myf5 defines the majority of quiescent adult skeletal muscle satellite cells. The Journal of cell biology *151*, 1221-1234.

Bentzinger, C.F., Wang, Y.X., and Rudnicki, M.A. (2012). Building muscle: molecular regulation of myogenesis. Cold Spring Harb Perspect Biol *4*.

Bernet, J.D., Doles, J.D., Hall, J.K., Kelly Tanaka, K., Carter, T.A., and Olwin, B.B.

(2014). p38 MAPK signaling underlies a cell-autonomous loss of stem cell self-renewal in skeletal muscle of aged mice. Nature medicine *20*, 265-271.

Biau, S., Jin, S., and Fan, C.M. (2013). Gastrointestinal defects of the Gas1 mutant involve dysregulated Hedgehog and Ret signaling. Biology open *2*, 144-155.

Blanco-Bose, W.E., Yao, C.C., Kramer, R.H., and Blau, H.M. (2001). Purification of mouse primary myoblasts based on alpha 7 integrin expression. Experimental cell research *265*, 212-220.

Bosnakovski, D., Xu, Z., Li, W., Thet, S., Cleaver, O., Perlingeiro, R.C., and Kyba, M. (2008). Prospective isolation of skeletal muscle stem cells with a Pax7 reporter. Stem cells *26*, 3194-3204.

Brack, A.S., Conboy, M.J., Roy, S., Lee, M., Kuo, C.J., Keller, C., and Rando, T.A. (2007). Increased Wnt signaling during aging alters muscle stem cell fate and increases fibrosis. Science *317*, 807-810.

Brack, A.S., and Munoz-Canoves, P. (2016). The ins and outs of muscle stem cell aging. Skelet Muscle *6*, 1.

Bulfield, G., Siller, W.G., Wight, P.A., and Moore, K.J. (1984). X chromosome-linked muscular dystrophy (mdx) in the mouse. Proc Natl Acad Sci U S A *81*, 1189-1192.

Cabrera, J.R., Sanchez-Pulido, L., Rojas, A.M., Valencia, A., Manes, S., Naranjo, J.R., and Mellstrom, B. (2006). Gas1 is related to the glial cell-derived neurotrophic factor family receptors alpha and regulates Ret signaling. The Journal of biological chemistry *281*, 14330-14339.

Calderwood, D.A., Shattil, S.J., and Ginsberg, M.H. (2000). Integrins and actin filaments: reciprocal regulation of cell adhesion and signaling. The Journal of biological chemistry *275*, 22607-22610.

Carlson, B.M. (1973). The regeneration of skeletal muscle. A review. Am J Anat *137*,

119-149.

Carlson, M.E., Conboy, M.J., Hsu, M., Barchas, L., Jeong, J., Agrawal, A., Mikels, A.J., Agrawal, S., Schaffer, D.V., and Conboy, I.M. (2009). Relative roles of TGF-beta1 and Wnt in the systemic regulation and aging of satellite cell responses. Aging Cell *8*, 676-689.

Carlson, M.E., Hsu, M., and Conboy, I.M. (2008). Imbalance between pSmad3 and Notch induces CDK inhibitors in old muscle stem cells. Nature *454*, 528-532.

Chakkalakal, J.V., Jones, K.M., Basson, M.A., and Brack, A.S. (2012). The aged niche disrupts muscle stem cell quiescence. Nature *490*, 355-360.

Cheung, T.H., Quach, N.L., Charville, G.W., Liu, L., Park, L., Edalati, A., Yoo, B., Hoang, P., and Rando, T.A. (2012). Maintenance of muscle stem-cell quiescence by microRNA-489. Nature *482*, 524-528.

Collins, C.A., Olsen, I., Zammit, P.S., Heslop, L., Petrie, A., Partridge, T.A., and Morgan, J.E. (2005). Stem cell function, self-renewal, and behavioral heterogeneity of cells from the adult muscle satellite cell niche. Cell *122*, 289-301.

Conboy, I.M., Conboy, M.J., Smythe, G.M., and Rando, T.A. (2003). Notch-mediated restoration of regenerative potential to aged muscle. Science *302*, 1575-1577.

Conboy, I.M., Conboy, M.J., Wagers, A.J., Girma, E.R., Weissman, I.L., and Rando, T.A. (2005). Rejuvenation of aged progenitor cells by exposure to a young systemic environment. Nature *433*, 760-764.

Cornelison, D.D., Filla, M.S., Stanley, H.M., Rapraeger, A.C., and Olwin, B.B. (2001). Syndecan-3 and syndecan-4 specifically mark skeletal muscle satellite cells and are implicated in satellite cell maintenance and muscle regeneration. Dev Biol *239*, 79-94.

Cosgrove, B.D., Gilbert, P.M., Porpiglia, E., Mourkioti, F., Lee, S.P., Corbel, S.Y.,

Llewellyn, M.E., Delp, S.L., and Blau, H.M. (2014). Rejuvenation of the muscle stem cell population restores strength to injured aged muscles. Nature medicine *20*, 255-264.

Del Sal, G., Ruaro, M.E., Philipson, L., and Schneider, C. (1992). The growth arrest-specific gene, gas1, is involved in growth suppression. Cell *70*, 595-607.

Dhawan, J., and Rando, T.A. (2005). Stem cells in postnatal myogenesis: molecular mechanisms of satellite cell quiescence, activation and replenishment. Trends Cell Biol *15*, 666-673.

Elsasser, W.M. (1984). Outline of a theory of cellular heterogeneity. Proc Natl Acad Sci U S A *81*, 5126-5129.

Fonseca-Pereira, D., Arroz-Madeira, S., Rodrigues-Campos, M., Barbosa, I.A., Domingues, R.G., Bento, T., Almeida, A.R., Ribeiro, H., Potocnik, A.J., Enomoto, H.*, et al.* (2014). The neurotrophic factor receptor RET drives haematopoietic stem cell survival and function. Nature *514*, 98-101.

Fontana, X., Hristova, M., Da Costa, C., Patodia, S., Thei, L., Makwana, M., Spencer-Dene, B., Latouche, M., Mirsky, R., Jessen, K.R.*, et al.* (2012). c-Jun in Schwann cells promotes axonal regeneration and motoneuron survival via paracrine signaling. The Journal of cell biology *198*, 127-141.

Franceschi, C., Bonafe, M., Valensin, S., Olivieri, F., De Luca, M., Ottaviani, E., and De Benedictis, G. (2000). Inflamm-aging. An evolutionary perspective on immunosenescence. Ann N Y Acad Sci *908*, 244-254.

Fukada, S., Uezumi, A., Ikemoto, M., Masuda, S., Segawa, M., Tanimura, N., Yamamoto, H., Miyagoe-Suzuki, Y., and Takeda, S. (2007). Molecular signature of quiescent satellite cells in adult skeletal muscle. Stem cells *25*, 2448-2459.

Gilbert, P.M., Havenstrite, K.L., Magnusson, K.E., Sacco, A., Leonardi, N.A., Kraft, P.,

Nguyen, N.K., Thrun, S., Lutolf, M.P., and Blau, H.M. (2010). Substrate elasticity regulates skeletal muscle stem cell self-renewal in culture. Science *329*, 1078-1081.

Gobeil, S., Zhu, X., Doillon, C.J., and Green, M.R. (2008). A genome-wide shRNA screen identifies GAS1 as a novel melanoma metastasis suppressor gene. Genes & development *22*, 2932-2940.

Gullberg, M., Gustafsdottir, S.M., Schallmeiner, E., Jarvius, J., Bjarnegard, M., Betsholtz, C., Landegren, U., and Fredriksson, S. (2004). Cytokine detection by antibody-based proximity ligation. Proc Natl Acad Sci U S A *101*, 8420-8424.

Hakim, C.H., Wasala, N.B., and Duan, D. (2013). Evaluation of muscle function of the extensor digitorum longus muscle ex vivo and tibialis anterior muscle in situ in mice. J Vis Exp.

Hayashi, K., de Sousa Lopes, S.M.C., Tang, F., Lao, K., and Surani, M.A. (2008). Dynamic equilibrium and heterogeneity of mouse pluripotent stem cells with distinct functional and epigenetic states. Cell stem cell *3*, 391-401.

Helbling-Leclerc, A., Zhang, X., Topaloglu, H., Cruaud, C., Tesson, F., Weissenbach, J., Tome, F.M., Schwartz, K., Fardeau, M., Tryggvason, K., *et al.* (1995). Mutations in the laminin alpha 2-chain gene (LAMA2) cause merosin-deficient congenital muscular dystrophy. Nat Genet *11*, 216-218.

Hintermann, E., Bilban, M., Sharabi, A., and Quaranta, V. (2001). Inhibitory role of alpha 6 beta 4-associated erbB-2 and phosphoinositide 3-kinase in keratinocyte haptotactic migration dependent on alpha 3 beta 1 integrin. The Journal of cell biology *153*, 465-478.

Holzenberger, M., Dupont, J., Ducos, B., Leneuve, P., Geloen, A., Even, P.C., Cervera, P., and Le Bouc, Y. (2003). IGF-1 receptor regulates lifespan and resistance to

oxidative stress in mice. Nature *421*, 182-187.

Howarth, M., Takao, K., Hayashi, Y., and Ting, A.Y. (2005). Targeting quantum dots to surface proteins in living cells with biotin ligase. Proc Natl Acad Sci U S A *102*, 7583-7588.

Huang da, W., Sherman, B.T., and Lempicki, R.A. (2009). Systematic and integrative analysis of large gene lists using DAVID bioinformatics resources. Nat Protoc *4*, 44-57.

Hynes, R.O. (2002). Integrins: bidirectional, allosteric signaling machines. Cell *110*, 673-687.

Jin, S., Martinelli, D.C., Zheng, X., Tessier-Lavigne, M., and Fan, C.M. (2015). Gas1 is a receptor for sonic hedgehog to repel enteric axons. Proc Natl Acad Sci U S A *112*, E73-80.

Jones, N.C., Fedorov, Y.V., Rosenthal, R.S., and Olwin, B.B. (2001). ERK1/2 is required for myoblast proliferation but is dispensable for muscle gene expression and cell fusion. J Cell Physiol *186*, 104-115.

Jung, Y., and Brack, A.S. (2014). Cellular mechanisms of somatic stem cell aging. Curr Top Dev Biol *107*, 405-438.

Kann, M., Bae, E., Lenz, M.O., Li, L., Trannguyen, B., Schumacher, V.A., Taglienti, M.E., Bordeianou, L., Hartwig, S., Rinschen, M.M.*, et al.* (2015). WT1 targets Gas1 to maintain nephron progenitor cells by modulating FGF signals. Development *142*, 1254-1266.

Kragstrup, T.W., Kjaer, M., and Mackey, A.L. (2011). Structural, biochemical, cellular, and functional changes in skeletal muscle extracellular matrix with aging. Scand J Med Sci Sports *21*, 749-757.

Langmead, B., Trapnell, C., Pop, M., and Salzberg, S.L. (2009). Ultrafast and memory-

efficient alignment of short DNA sequences to the human genome. Genome Biol *10*, R25.

Lepper, C., Conway, S.J., and Fan, C.M. (2009). Adult satellite cells and embryonic muscle progenitors have distinct genetic requirements. Nature *460*, 627-631.

Lepper, C., Partridge, T.A., and Fan, C.M. (2011). An absolute requirement for Pax7-positive satellite cells in acute injury-induced skeletal muscle regeneration. Development *138*, 3639-3646.

Liu, L., Charville, G.W., Cheung, T.H., Yoo, B., Santos, P.J., Schroeder, M., and Rando, T.A. (2018). Impaired Notch Signaling Leads to a Decrease in p53 Activity and Mitotic Catastrophe in Aged Muscle Stem Cells. Cell stem cell *23*, 544-556 e544.

Liu, L., Cheung, T.H., Charville, G.W., Hurgo, B.M., Leavitt, T., Shih, J., Brunet, A., and Rando, T.A. (2013). Chromatin modifications as determinants of muscle stem cell quiescence and chronological aging. Cell reports *4*, 189-204.

Liu, L., Cheung, T.H., Charville, G.W., and Rando, T.A. (2015). Isolation of skeletal muscle stem cells by fluorescence-activated cell sorting. Nat Protoc *10*, 1612-1624.

Liu, L., and Rando, T.A. (2011). Manifestations and mechanisms of stem cell aging. The Journal of cell biology *193*, 257-266.

Liu, N., Garry, G.A., Li, S., Bezprozvannaya, S., Sanchez-Ortiz, E., Chen, B., Shelton, J.M., Jaichander, P., Bassel-Duby, R., and Olson, E.N. (2017). A Twist2-dependent progenitor cell contributes to adult skeletal muscle. Nature cell biology *19*, 202-213.

Liu, Y., Liu, C., Yamada, Y., and Fan, C.M. (2002). Growth arrest specific gene 1 acts as a region-specific mediator of the Fgf10/Fgf8 regulatory loop in the limb. Development *129*, 5289-5300.

Lo Celso, C., Fleming, H.E., Wu, J.W., Zhao, C.X., Miake-Lye, S., Fujisaki, J., Cote,

D., Rowe, D.W., Lin, C.P., and Scadden, D.T. (2009). Live-animal tracking of individual haematopoietic stem/progenitor cells in their niche. Nature *457*, 92-96.

Lopez-Otin, C., Blasco, M.A., Partridge, L., Serrano, M., and Kroemer, G. (2013). The hallmarks of aging. Cell *153*, 1194-1217.

Lopez-Ramirez, M.A., Dominguez-Monzon, G., Vergara, P., and Segovia, J. (2008). Gas1 reduces Ret tyrosine 1062 phosphorylation and alters GDNF-mediated intracellular signaling. International journal of developmental neuroscience : the official journal of the International Society for Developmental Neuroscience *26*, 497-503.

Lukjanenko, L., Jung, M.J., Hegde, N., Perruisseau-Carrier, C., Migliavacca, E., Rozo, M., Karaz, S., Jacot, G., Schmidt, M., Li, L.*, et al.* (2016). Loss of fibronectin from the aged stem cell niche affects the regenerative capacity of skeletal muscle in mice. Nature medicine *22*, 897-905.

Luo, W., Wickramasinghe, S.R., Savitt, J.M., Griffin, J.W., Dawson, T.M., and Ginty, D.D. (2007). A hierarchical NGF signaling cascade controls Ret-dependent and Ret-independent events during development of nonpeptidergic DRG neurons. Neuron *54*, 739-754.

Madisen, L., Mao, T., Koch, H., Zhuo, J.M., Berenyi, A., Fujisawa, S., Hsu, Y.W., Garcia, A.J., 3rd, Gu, X., Zanella, S.*, et al.* (2012). A toolbox of Cre-dependent optogenetic transgenic mice for light-induced activation and silencing. Nat Neurosci *15*, 793-802.

Martinelli, D.C., and Fan, C.M. (2007a). Gas1 extends the range of Hedgehog action by facilitating its signaling. Genes & development *21*, 1231-1243.

Martinelli, D.C., and Fan, C.M. (2007b). The role of Gas1 in embryonic development and its implications for human disease. Cell Cycle *6*, 2650-2655.

Mauro, A. (1961). Satellite cell of skeletal muscle fibers. J Biophys Biochem Cytol *9*, 493-495.

McCarthy, J.J., Mula, J., Miyazaki, M., Erfani, R., Garrison, K., Farooqui, A.B., Srikuea, R., Lawson, B.A., Grimes, B., Keller, C.*, et al.* (2011). Effective fiber hypertrophy in satellite cell-depleted skeletal muscle. Development *138*, 3657-3666.

Merkle, F.T., Mirzadeh, Z., and Alvarez-Buylla, A. (2007). Mosaic organization of neural stem cells in the adult brain. Science *317*, 381-384.

Mikkelsen, T.S., Ku, M., Jaffe, D.B., Issac, B., Lieberman, E., Giannoukos, G., Alvarez, P., Brockman, W., Kim, T.K., Koche, R.P.*, et al.* (2007). Genome-wide maps of chromatin state in pluripotent and lineage-committed cells. Nature *448*, 553-560.

Miyamoto, S., Teramoto, H., Gutkind, J.S., and Yamada, K.M. (1996). Integrins can collaborate with growth factors for phosphorylation of receptor tyrosine kinases and MAP kinase activation: roles of integrin aggregation and occupancy of receptors. The Journal of cell biology *135*, 1633-1642.

Montarras, D., Morgan, J., Collins, C., Relaix, F., Zaffran, S., Cumano, A., Partridge, T., and Buckingham, M. (2005). Direct isolation of satellite cells for skeletal muscle regeneration. Science *309*, 2064-2067.

Murphy, M.M., Lawson, J.A., Mathew, S.J., Hutcheson, D.A., and Kardon, G. (2011). Satellite cells, connective tissue fibroblasts and their interactions are crucial for muscle regeneration. Development *138*, 3625-3637.

Neves, J., Demaria, M., Campisi, J., and Jasper, H. (2015). Of flies, mice, and men: evolutionarily conserved tissue damage responses and aging. Dev Cell *32*, 9-18.

Oh, J., Lee, Y.D., and Wagers, A.J. (2014). Stem cell aging: mechanisms, regulators and therapeutic opportunities. Nature medicine *20*, 870-880.

Parker, M.H., Seale, P., and Rudnicki, M.A. (2003). Looking back to the embryo: defining transcriptional networks in adult myogenesis. Nat Rev Genet *4*, 497-507.

Patel, A.P., Tirosh, I., Trombetta, J.J., Shalek, A.K., Gillespie, S.M., Wakimoto, H., Cahill, D.P., Nahed, B.V., Curry, W.T., Martuza, R.L., *et al.* (2014). Single-cell RNA-seq highlights intratumoral heterogeneity in primary glioblastoma. Science *344*, 1396-1401.

Polanska, U.M., Fernig, D.G., and Kinnunen, T. (2009). Extracellular interactome of the FGF receptor-ligand system: complexities and the relative simplicity of the worm. Dev Dyn *238*, 277-293.

Price, F.D., von Maltzahn, J., Bentzinger, C.F., Dumont, N.A., Yin, H., Chang, N.C., Wilson, D.H., Frenette, J., and Rudnicki, M.A. (2014). Inhibition of JAK-STAT signaling stimulates adult satellite cell function. Nature medicine *20*, 1174-1181.

Qiu, X., Mao, Q., Tang, Y., Wang, L., Chawla, R., Pliner, H.A., and Trapnell, C. (2017). Reversed graph embedding resolves complex single-cell trajectories. Nat Methods *14*, 979-982.

Raghavan, S., Bauer, C., Mundschau, G., Li, Q., and Fuchs, E. (2000). Conditional ablation of beta1 integrin in skin. Severe defects in epidermal proliferation, basement membrane formation, and hair follicle invagination. The Journal of cell biology *150*, 1149-1160.

Robinson, M.D., McCarthy, D.J., and Smyth, G.K. (2010). edgeR: a Bioconductor package for differential expression analysis of digital gene expression data. Bioinformatics *26*, 139-140.

Rocheteau, P., Gayraud-Morel, B., Siegl-Cachedenier, I., Blasco, M.A., and Tajbakhsh, S. (2012). A subpopulation of adult skeletal muscle stem cells retains all template DNA strands after cell division. Cell *148*, 112-125.

Roovers, K., Davey, G., Zhu, X., Bottazzi, M.E., and Assoian, R.K. (1999). Alpha5beta1 integrin controls cyclin D1 expression by sustaining mitogen-activated protein kinase activity in growth factor-treated cells. Mol Biol Cell *10*, 3197-3204.

Rosen, G.D., Sanes, J.R., LaChance, R., Cunningham, J.M., Roman, J., and Dean, D.C. (1992). Roles for the integrin VLA-4 and its counter receptor VCAM-1 in myogenesis. Cell *69*, 1107-1119.

Rozo, M., Li, L., and Fan, C.M. (2016). Targeting beta1-integrin signaling enhances regeneration in aged and dystrophic muscle in mice. Nature medicine *22*, 889-896.

Ruaro, E.M., Collavin, L., Del Sal, G., Haffner, R., Oren, M., Levine, A.J., and Schneider, C. (1997). A proline-rich motif in p53 is required for transactivation-independent growth arrest as induced by Gas1. Proc Natl Acad Sci U S A *94*, 4675-4680.

Sacco, A., Doyonnas, R., Kraft, P., Vitorovic, S., and Blau, H.M. (2008). Self-renewal and expansion of single transplanted muscle stem cells. Nature *456*, 502-506.

Sambasivan, R., Yao, R., Kissenpfennig, A., Van Wittenberghe, L., Paldi, A., Gayraud-Morel, B., Guenou, H., Malissen, B., Tajbakhsh, S., and Galy, A. (2011). Pax7-expressing satellite cells are indispensable for adult skeletal muscle regeneration. Development *138*, 3647-3656.

Schneider, C., King, R.M., and Philipson, L. (1988). Genes specifically expressed at growth arrest of mammalian cells. Cell *54*, 787-793.

Schultz, E., Gibson, M.C., and Champion, T. (1978). Satellite cells are mitotically quiescent in mature mouse muscle: an EM and radioautographic study. J Exp Zool *206*, 451-456.

Schwander, M., Leu, M., Stumm, M., Dorchies, O.M., Ruegg, U.T., Schittny, J., and

Muller, U. (2003). Beta1 integrins regulate myoblast fusion and sarcomere assembly. Dev Cell *4*, 673-685.

Schworer, S., Becker, F., Feller, C., Baig, A.H., Kober, U., Henze, H., Kraus, J.M., Xin, B., Lechel, A., Lipka, D.B.*, et al.* (2016). Epigenetic stress responses induce muscle stem-cell ageing by Hoxa9 developmental signals. Nature *540*, 428-432.

Seale, P., Sabourin, L.A., Girgis-Gabardo, A., Mansouri, A., Gruss, P., and Rudnicki, M.A. (2000). Pax7 is required for the specification of myogenic satellite cells. Cell *102*, 777-786.

Seppala, M., Depew, M.J., Martinelli, D.C., Fan, C.M., Sharpe, P.T., and Cobourne, M.T. (2007). Gas1 is a modifier for holoprosencephaly and genetically interacts with sonic hedgehog. J Clin Invest *117*, 1575-1584.

Shavlakadze, T., McGeachie, J., and Grounds, M.D. (2010). Delayed but excellent myogenic stem cell response of regenerating geriatric skeletal muscles in mice. Biogerontology *11*, 363-376.

Shea, K.L., Xiang, W., LaPorta, V.S., Licht, J.D., Keller, C., Basson, M.A., and Brack, A.S. (2010). Sprouty1 regulates reversible quiescence of a self-renewing adult muscle stem cell pool during regeneration. Cell stem cell *6*, 117-129.

Sherwood, R.I., Christensen, J.L., Conboy, I.M., Conboy, M.J., Rando, T.A., Weissman, I.L., and Wagers, A.J. (2004). Isolation of adult mouse myogenic progenitors: functional heterogeneity of cells within and engrafting skeletal muscle. Cell *119*, 543-554.

Sicari, B.M., Rubin, J.P., Dearth, C.L., Wolf, M.T., Ambrosio, F., Boninger, M., Turner, N.J., Weber, D.J., Simpson, T.W., Wyse, A.*, et al.* (2014). An acellular biologic scaffold promotes skeletal muscle formation in mice and humans with volumetric muscle loss. Sci Transl Med *6*, 234ra258.

Siegel, A.L., Atchison, K., Fisher, K.E., Davis, G.E., and Cornelison, D.D. (2009). 3D timelapse analysis of muscle satellite cell motility. Stem cells *27*, 2527-2538.

Smythe, G.M., Shavlakadze, T., Roberts, P., Davies, M.J., McGeachie, J.K., and Grounds, M.D. (2008). Age influences the early events of skeletal muscle regeneration: studies of whole muscle grafts transplanted between young (8 weeks) and old (13-21 months) mice. Exp Gerontol *43*, 550-562.

Sousa-Victor, P., Garcia-Prat, L., Serrano, A.L., Perdiguero, E., and Munoz-Canoves, P. (2015). Muscle stem cell aging: regulation and rejuvenation. Trends Endocrinol Metab *26*, 287-296.

Sousa-Victor, P., Gutarra, S., Garcia-Prat, L., Rodriguez-Ubreva, J., Ortet, L., Ruiz-Bonilla, V., Jardi, M., Ballestar, E., Gonzalez, S., Serrano, A.L.*, et al.* (2014). Geriatric muscle stem cells switch reversible quiescence into senescence. Nature *506*, 316-321.

Spagnuolo, R., Corada, M., Orsenigo, F., Zanetta, L., Deuschle, U., Sandy, P., Schneider, C., Drake, C.J., Breviario, F., and Dejana, E. (2004). Gas1 is induced by VE-cadherin and vascular endothelial growth factor and inhibits endothelial cell apoptosis. Blood *103*, 3005-3012.

Srinivas, S., Watanabe, T., Lin, C.S., William, C.M., Tanabe, Y., Jessell, T.M., and Costantini, F. (2001). Cre reporter strains produced by targeted insertion of EYFP and ECFP into the ROSA26 locus. BMC Dev Biol *1*, 4.

Subramanian, A., Tamayo, P., Mootha, V.K., Mukherjee, S., Ebert, B.L., Gillette, M.A., Paulovich, A., Pomeroy, S.L., Golub, T.R., Lander, E.S.*, et al.* (2005). Gene set enrichment analysis: a knowledge-based approach for interpreting genome-wide expression profiles. Proc Natl Acad Sci U S A *102*, 15545-15550.

Suzuki, H., Hase, A., Kim, B.Y., Miyata, Y., Nonaka, I., Arahata, K., and Akazawa, C.

(1998). Up-regulation of glial cell line-derived neurotrophic factor (GDNF) expression in regenerating muscle fibers in neuromuscular diseases. Neurosci Lett *257*, 165-167.

Takagi, J., and Springer, T.A. (2002). Integrin activation and structural rearrangement. Immunol Rev *186*, 141-163.

Tedesco, F.S., Dellavalle, A., Diaz-Manera, J., Messina, G., and Cossu, G. (2010). Repairing skeletal muscle: regenerative potential of skeletal muscle stem cells. J Clin Invest *120*, 11-19.

Tierney, M.T., Aydogdu, T., Sala, D., Malecova, B., Gatto, S., Puri, P.L., Latella, L., and Sacco, A. (2014). STAT3 signaling controls satellite cell expansion and skeletal muscle repair. Nature medicine *20*, 1182-1186.

Trapnell, C., Pachter, L., and Salzberg, S.L. (2009). TopHat: discovering splice junctions with RNA-Seq. Bioinformatics *25*, 1105-1111.

Troy, A., Cadwallader, A.B., Fedorov, Y., Tyner, K., Tanaka, K.K., and Olwin, B.B. (2012). Coordination of satellite cell activation and self-renewal by Par-complex-dependent asymmetric activation of p38alpha/beta MAPK. Cell stem cell *11*, 541-553.

Webster, M.T., and Fan, C.M. (2013). c-MET regulates myoblast motility and myocyte fusion during adult skeletal muscle regeneration. PLoS One *8*, e81757.

Whalen, R.G., Harris, J.B., Butler-Browne, G.S., and Sesodia, S. (1990). Expression of myosin isoforms during notexin-induced regeneration of rat soleus muscles. Dev Biol *141*, 24-40.

Wilhelm, S.M., Dumas, J., Adnane, L., Lynch, M., Carter, C.A., Schutz, G., Thierauch, K.H., and Zopf, D. (2011). Regorafenib (BAY 73-4506): a new oral multikinase inhibitor of angiogenic, stromal and oncogenic receptor tyrosine kinases with

potent preclinical antitumor activity. International journal of cancer *129*, 245-255.

Wood, L.K., Kayupov, E., Gumucio, J.P., Mendias, C.L., Claflin, D.R., and Brooks, S.V. (2014). Intrinsic stiffness of extracellular matrix increases with age in skeletal muscles of mice. J Appl Physiol (1985) *117*, 363-369.

Yablonka-Reuveni, Z., Danoviz, M.E., Phelps, M., and Stuelsatz, P. (2015). Myogenic-specific ablation of Fgfr1 impairs FGF2-mediated proliferation of satellite cells at the myofiber niche but does not abolish the capacity for muscle regeneration. Front Aging Neurosci *7*, 85.

Yin, H., Price, F., and Rudnicki, M.A. (2013). Satellite cells and the muscle stem cell niche. Physiol Rev *93*, 23-67.

Yu, G., Wang, L.G., Han, Y., and He, Q.Y. (2012). clusterProfiler: an R package for comparing biological themes among gene clusters. OMICS *16*, 284-287.

Zammit, P.S., Golding, J.P., Nagata, Y., Hudon, V., Partridge, T.A., and Beauchamp, J.R. (2004). Muscle satellite cells adopt divergent fates: a mechanism for self-renewal? The Journal of cell biology *166*, 347-357.

Zammit, P.S., Relaix, F., Nagata, Y., Ruiz, A.P., Collins, C.A., Partridge, T.A., and Beauchamp, J.R. (2006). Pax7 and myogenic progression in skeletal muscle satellite cells. J Cell Sci *119*, 1824-1832.

Zamorano, A., Lamas, M., Vergara, P., Naranjo, J.R., and Segovia, J. (2003). Transcriptionally mediated gene targeting of gas1 to glioma cells elicits growth arrest and apoptosis. J Neurosci Res *71*, 256-263.

Zhang, Y., Liu, T., Meyer, C.A., Eeckhoute, J., Johnson, D.S., Bernstein, B.E., Nusbaum, C., Myers, R.M., Brown, M., Li, W.*, et al.* (2008). Model-based analysis of ChIP-Seq (MACS). Genome Biol *9*, R137.

Zhao, P., and Hoffman, E.P. (2004). Embryonic myogenesis pathways in muscle

regeneration. Dev Dyn *229*, 380-392.

Zheng, X., Yue, S., Chen, H., Weber, B., Jia, J., and Zheng, Y. (2015). Low-Cell-Number Epigenome Profiling Aids the Study of Lens Aging and Hematopoiesis. Cell reports *13*, 1505-1518.

Curriculum Vitae

Liangji Li

D.O.B.:08/25/1988 Nationality: P. R. China

EDUCATION

2019 **Ph.D.**, Cell, Molecular, Developmental Biology and Biophysics PhD program
Department of Biology, **Johns Hopkins University**
Area of Concentration: Developmental Biology and Regeneration

2012 Graduate Program for Master's Degree on Cell Biology
School of Life Sciences, **Sun Yat-sen University**, Guangzhou, China

2011 **B.S.**, Biotechnology,
School of Life Sciences, **Sun Yat-sen University**, Guangzhou, China Overall GPA: 3.96/4.0 Rank: 1/139

RESEARCH EXPERIENCE

2013-present Doctoral thesis research
Department of Biology, Johns Hopkins University;
Carnegie Institution for Science, Department of Embryology, MD
Advisor: Dr. Chen-Ming Fan
Title: "Characterizing the function of Gas1 in muscle stem cells aging"
Summary: ● I used various approaches including genetics, next generation sequencing, biochemistry, cell biology, and functional assays to study the role of Gas1 in muscle stem cells (MuSCs).
● I showed that *Growth arrest-specific gene 1* (*Gas1*) is expressed in a small subset of young, progressively in larger fractions of adult, and eventually in almost all of aged MuSCs in mice.
● I found that Gas1 reduces stem cell self-renewal via pan-expression of *Gas1* in young MuSCs and inactivation of *Gas1* in aged MuSCs.
● I defined the mechanism of Gas1 directing MuSC aging via reducing the activity of Ret, which is required for MuSC self-renewal.
● I uncovered Ret-ligand, GDNF, can restore Ret signaling and enhance MuSC self-renewal and regenerated muscle function in aged mice.

2015-2016 Collaborative research
Carnegie Institution for Science, Department of Embryology, MD
Advisor: Dr. Chen-Ming Fan
Summary: I demonstrated how β1-integrin acts as a muscle stem cell niche sensor and how it regulates MuSCs functions in the context of aging and muscular dystrophy via cell biology, biochemistry, and muscle functional approaches.

2011-2012 Master program research
School of Life Sciences, Sun Yat-sen University
Advisor: Dr. Zhou (Sunny) Songyang
Summary: ● I screened for key candidate genes which play important roles in the primordial germ cells specification from mouse ESCs via transfection.
● I obtained differentiated cells driven by the overexpression of differentiation associated candidate genes and characterize their identity via analyzing expression profiles by qPCR.
● I constructed the conditional knockout mouse embryonic stem cells of a differentiation associated candidate gene.

2010-2011 Undergraduate research
School of Life Sciences, Sun Yat-sen University
Advisor: Dr. Zhou (Sunny) Songyang
Title: "The Construction of Targeting Vectors for the Conditional Knockout of an Important Stem Cell-Differentiation Associated Gene in Mice"
Summary: I designed and constructed a targeting vector for the conditional knockout of a differentiation associated candidate gene.

TEACHING EXPERIENCE

2017-2019 Research assistance
Guide lab members and rotation student to learn techniques in the field including next-generation sequencing (RNA-seq; ChIP-seq; Ribo-seq); isolation and culture of muscle stem cells and myofibers; FACS technique; mouse surgery
Post-doc: Yun Bai; Jiaxiang Tao, Anwen Shao; Nathalie Gerassimov
Rotation student: Haolong Zhu
Carnegie Institution for Science, Department of Embryology

2013-2014 Teaching assistance
Genetics (1st term 2013)
Developmental Biology (2nd term 2014)
Department of Biology, Johns Hopkins University

2010-2011 Teaching assistance
Principles of Biological Investigation (1st term 2010)
School of Life Sciences, Sun Yat-sen University

HONORS & AWARDS

2011 Excellent Undergraduate Student in Sun Yat-sen University

2011 Excellent Graduation Thesis in Sun Yat-sen University

2010 First Grade Scholarship of Sun Yat-sen University

2009 National Scholarship (highest-level scholarship in China)

2009	First Grade Scholarship of Sun Yat-sen University
2008	Yingcai Scholarship of Sun Yat-sen University
2008	First Grade Scholarship of Sun Yat-sen University

ACADEMIC ACTIVITIES

2010	3rd Guangzhou International Conference on Stem Cell and Regenerative Medicine, Guangzhou, China
2011	13th Society of Chinese Bioscientists in America International Symposium, Guangzhou, China
2016	Keystone Symposia on Molecular and Cellular Biology: Epigenetic and Metabolic Regulation of Aging and Aging-Related Diseases, Santa Fe, NM
	Poster presentation: "Coordination of β1-Integrin and FGF Drives Muscle Stem Cell Expansion: Implications for Aging and Muscular Dystrophy"
2017	19th Annual Johns Hopkins University CMDB PhD retreat, Hershey, PA
	Poster presentation: "Characterizing the function of Gas1 in muscle stem cells aging"

PUBLICATIONS

1. **Li, L.**, Rozo, M., Yue, S., Zheng, X., Tan, F., Lepper, C., Fan, C. M. (2019). "Muscle stem cell renewal suppressed by Gas1 can be reversed by GDNF in mice" ***Nature Metabolism*** *(Accepted)* (first author)
2. Rozo, M.*, **Li, L.***, and Fan, C. M. (2016). Targeting beta1-integrin signaling enhances regeneration in aged and dystrophic muscle in mice. ***Nature medicine*** *22*, 889-96. (co-first author)
3. Lukjanenko, L., Jung, M. J., Hegde, N., Perruisseau-Carrier, C., Migliavacca, E., Rozo, M., Karaz, S., Jacot, G., Schmidt, M., **Li, L.**, Metairon, S., Raymond, F., Lee, U., Sizzano, F., Wilson, D. H., Dumont, N. A., Palini, A., Fassler, R., Steiner, P., Descombes, P., Rudnicki, M. A., Fan, C. M., von Maltzahn, J., Feige, J. N., and Bentzinger, C. F. (2016). Loss of fibronectin from the aged stem cell niche affects the regenerative capacity of skeletal muscle in mice. ***Nature medicine*** *22*, 897-905.
4. Kann, M., Bae, E., Lenz, M. O., **Li, L.**, Trannguyen, B., Schumacher, V. A., Taglienti, M. E., Bordeianou, L., Hartwig, S., Rinschen, M. M., Schermer, B., Benzing, T., Fan, C. M., and Kreidberg, J. A. (2015). WT1 targets Gas1 to maintain nephron progenitor cells by modulating FGF signals. ***Development*** *142*, 1254-66.